NASA CR-135093
AIRESEARCH 75-211789

# ADVANCED ACOUSTIC AND AERODYNAMIC 20-INCH FAN PROGRAM

FINAL REPORT



by J R Erwin and R W Heldenbrand

AIRESEARCH MANUFACTURING COMPANY OF ARIZONA
A DIVISION OF THE GARRETT CORPORATION
PHOENIX, ARIZONA



prepared for

NATIONAL AERONAUTICS AND SPACE ADMINISTRATION
NASA Lewis Research Center
Contract NAS3-18533

| 1 Report No | 2 Government Accession No | 3 Recipient's Catalog No |
|---|---|---|
| NASA CR-135093 | | |

| 4 Title and Subtitle | 5 Report Date |
|---|---|
| Advanced Acoustic and Aerodynamic 20-Inch Fan Program | February 15, 1977 |
| | 6 Performing Organization Code |
| 7 Author(s) | 8 Performing Organization Report No |
| J. R. Erwin and R. W. Heldenbrand | 75-211789 |
| | 10 Work Unit No |
| 9 Performing Organization Name and Address | 11 Contract or Grant No |
| AiResearch Manufacturing Company of Arizona<br>Sky Harbor Airport, 402 S 36th Street<br>P.O Box 5217<br>Phoenix, Arizona 85034 | NAS3-18533 |
| | 13 Type of Report and Period Covered |
| 12 Sponsoring Agency Name and Address | Contractor Final Report |
| National Aeronautics and Space Administration<br>NASA Lewis Research Center<br>21000 Brookpark Road<br>Cleveland, Ohio 44135 | 14 Sponsoring Agency Code<br>NASA LeRC |

15 Supplementary Notes

Project Manager, James G. Lucas, V/STOL and Noise Division, NASA Lewis Research Center, Cleveland, Ohio

16 Abstract

This is a final report covering the aerodynamic analyses and the mechanical analyses, and stress tests of a 20-inch diameter advanced fan design intended for acoustic investigation by NASA-LeRC. A high-tip-speed transonic fan rotor was scaled directly to 20 0 inches (0 508 m) from a 28.74-inch (0.73-m) diameter rotor that was designed and tested under a previous NASA-LeRC program. A new stator was designed and fabricated for the fan and incorporated with a test rig housing and adapter hardware for installation in the NASA-LeRC Jet Noise Facility for acoustic evaluation The stator was designed to allow mounting at three axial locations, and the fan, housing, and adapters are reversible so that either the inlet or the exhaust ends of the assembly face the open room of the test facility Excellent aerodynamic performance is predicted, and a low noise signature is expected since the unique aerodynamic design features of this fan are directly conducive to producing minimum sound power

| 17 Key Words (Suggested by Author(s)) | 18 Distribution Statement |
|---|---|
| Low-Noise, High Efficiency Transonic Fan | |

| 19 Security Classif (of this report) | 20 Security Classif (of this page) | 21 No of Pages | 22 Price |
|---|---|---|---|
| Unclassified | Unclassified | | |

* For sale by the National Technical Information Service, Springfield, Virginia 22151

NASA-C-168 (Rev 6-71)

# CONTENTS

# SUMMARY

A high-tip-speed transonic fan rotor was scaled directly to 20.0 inches (0.508 m) from a 28.74-inch (0.73-m) diameter rotor that was designed and tested under a previous NASA-LeRC program. The objective of this design was the provision of a rotor design that could deliver good efficiency with low noise generation at low work input through the elimination of strong shock losses and shock-induced separation in the high-Mach-number tip region. In the rotor blade tip region, the design incorporates weak oblique shocks only, with supersonic relative outlet velocities. Although the rotor relative velocities were well into the supersonic range, the stator velocities were at modest, subsonic levels. Hence, the stator design is conventionally subsonic, and has the primary role of turning the flow back to the axial direction. A new stator was designed and fabricated for the fan, and incorporated with a test rig housing and adapter hardware for installation in the NASA-LeRC Engine Fan and Jet Noise Facility for acoustic evaluation. A low noise signature is expected, since the unique aerodynamic design features of this fan are directly conducive to producing minimum sound power. The stator was designed to allow mounting at three axial locations, and the fan, housing, and adapters are reversible so that either the inlet or the exhaust ends of the assembly face the open room of the test facility.

The transonic fan has the following values of stage design parameters:

| | |
|---|---|
| Overall pressure ratio | 1.5 |
| Adiabatic efficiency | 0.88 |
| Equivalent total flow | 71.7 lb/s (32.5 kgm/s) |
| Flow per unit annulus area | 42.0 lb/s/ft$^2$ (205.1 kgm/s/m$^2$) |
| Equivalent tip speed | 1600 ft/s (487.7 m/s) |
| Inlet hub-to-tip radius ratio | 0.46 |
| Tip diameter | 20.0 inches (0.508 m) |

# INTRODUCTION

The recent need for power plants to propel large transport aircraft capable of long-range flights has spurred the development of very-high-bypass-ratio turbofan engines (bypass ratios between 8 and 12 or even higher are being explored). The fan component of these high-bypass-ratio engines, in general, controls the engine diameter and requires large drive-turbine work. In addition, the engine configurational constraints restrict the direct-drive turbine diameter to a fraction of that of the fan, leading to low turbine wheel speeds. Consequently, the resulting fan turbine usually consists of a large number of highly-loaded stages and/or compromised turbine efficiency. Alternatively, the fan may be run at tip speeds substantially above those for which good efficiency has been achieved for the fan pressure ratios commonly used in high-bypass-ratio engines. Such fans have, in the past, employed strong shock waves at the rotor leading edge, which resulted in the production of additional front-end noise. The ultimate engine design usually includes a combination of fan and fan-turbine penalties. However, such penalties could be reduced or conceivably eliminated by use of a fan capable of high efficiency at high rotative speeds and the low-pressure ratios compatible with high-bypass ratios. The purpose of the program reported herein was to provide a 20-inch (0.508-m) diameter high-tip-speed axial-flow fan stage, having the potential for reduced noise, for test in the NASA-LeRC Engine Fan and Jet Noise Facility.

The rotor selected for this program was scaled directly from the 28.74-inch fan stage designed, built, and tested successfully under NASA Contract NAS3-13498, and reported in NASA CR-121095 (Ref. 1) and CR-121263 (Ref. 2). This rotor provides good efficiency at low work input by the elimination of strong shock losses and shock induced separation in the high-Mach-number tip region. These factors should also tend to reduce the noise generated by the rotor and the stator. The design conditions for the fan were a tip speed of 1600 ft/s (487.7 m/s) and a stage total pressure ratio of 1.50. The details of the rotor aerodynamic design are included in Reference 1; however, the principal design features are summarized herein for reference. The only change made for the 20-inch scaled version of the fan rotor, increasing the contour tolerance band, is discussed herein.

The stator was changed from the previously tested design in two major respects. The aerodynamic design was changed to provide a better match for the flow conditions actually measured at the discharge of the larger rotor. The solidity was increased slightly, with a greater variation from hub to tip, in an effort to reduce the diffusion factor, and thus, reduce the stator losses. Exit area was reduced with a consequent increase in exit Mach

number and an accompanying reduction in diffusion factor. Other aerodynamic changes incorporated to match the measured flow conditions, with the use of NASA 65-series blade sections, result in a three-dimensional stator design that is expected to provide an increase in stage efficiency of one to two points over the original, larger design.

The second change to the stator was to allow for variations in axial spacing between the stator and the rotor. Provision was made in the housing assembly to locate the stator one, two, or three rotor chord lengths aft of the rotor blade trailing-edge plane. Full details of the stator design are provided.

Subsequent sections of this report include descriptions of the rig hardware required to adapt to the NASA test facility, the results of tests conducted to verify predicted fan blade vibration characteristics, and a discussion of the potential benefits and penalties associated with the use of this type of fan in a turbofan engine.

The contract required that the rotor be instrumented with strain gauges, and that a stress measurement plan (Appendix A, herein) be prepared for use by NASA in developing test plans. Since the instrumented rotor was available, permission was requested, and granted, to use the rotor for a part of a verification test series to be conducted under USAF Aero Propulsion Laboratory Contract F33615-74-C-2012. Use of the rotor would be a convenience to AiResearch and of mutual benefit to NASA and the Air Force. The test consisted of spinning the rotor in a whirl pit and recording the strain gauge outputs. The results of this test are included herewith as they were presented to the Air Force.

## ROTOR DESIGN

### Rotor Aerodynamic Design

Several new rotor aerodynamic concepts influenced the design of this transonic rotor. A design objective was to avoid tip normal shock losses by substitution of oblique shocks in the high-Mach-number tip region. In addition, the strengths of the oblique shocks were restricted to values for which the static pressure rise would not exceed the separation criteria generally accepted for turbulent boundary layers on flat plates. The static pressure rise and the total pressure ratio values were kept below the maximum values obtainable from rotors of 1600 fps (487.7 m/s) tip speed to make them consistent with near-optimum hub potential. Lower losses and an improved stall margin were anticipated to result from this design approach. Another feature essential to this approach was the calculation of the rotor design outlet velocity diagrams that satisfied radial equilibrium with supersonic rotor-tip relative leaving velocities. In spite of the excess tip speed (for the design pressure ratio), the design value of rotor-tip static density rise was small enough so that axial velocity did not incur a significant reduction. Accordingly, the use of negative camber at the rotor tip proved to be unnecessary for the radially constant stage pressure ratio.

To terminate the necessary supersonic waves at the blade trailing edges, a characteristic procedure allowing for change in radius and stream filament thickness was used for the wholly supersonic sections. The locations of the points for expansions and compressions and their points of impingement on opposite surfaces were carefully controlled to cancel all oblique shocks inside the blade passage. The shocks were also spaced apart to prevent the accumulating effect from causing separation. The strength of the shocks that originate at the blade leading edges was minimized (in the high-Mach-number outboard region) by utilizing small leading-edge thicknesses and wedge angles. At the design condition, no tip waves propagated upstream from the rotor. An important design consideration involved the magnitude of the speed at which supersonic flow could be initiated in the tip region (i.e., the starting Mach number). The contraction ratio was prescribed to be sufficiently small to permit tip starting at a speed somewhere below design speed, including an area allowance for boundary layer blockage.

The principle design objectives were:

| | |
|---|---|
| Overall total pressure ratio | 1.5 |
| Flow per unit annulus area | 42.0 lb/s/ft$^2$ (205.1 kgm/s/m$^2$) |
| Equivalent tip speed | 1600 ft/s (487.7 m/s) |
| Rotor and stator aspect ratios | 3.0 (originally) |
| Rotor inlet hub-to-tip radius ratio | 0.50 maximum |
| Rotor tip solidity | 1.4 (approximately) |
| Objective adiabatic efficiency | 0.88 |
| Equivalent total flow | 71.7 lb/s (32.5 kgm/s) |
| Rotor inlet hub-to-tip radius ratio | 0.462 |
| Tip diameter | 20.0 inch (0.508 m) |

The rotor aerodynamic design is identical with that described in NASA CR-121095. The rotor is scaled from a 28.74-inch design to a 20-inch tip (inlet) diameter with only one exception; the scaled blade tolerance band was biased such that the scaled minimum tolerance matched the larger blades nominal tolerance value.

## Rotor Mechanical Design

The 20-inch transonic scaled fan assembly was analyzed for stress and vibration. Fan blade analysis was accomplished with the use of finite-element programs ISOBOSS and ISOVIBE for stress and vibration. The disk and spinner assembly was analyzed with use of finite-element program ISOPDQ. The mechanical design point was 110-percent speed (20,240 rpm).

The blade stresses are the same as the original 28.74-inch fan blade, and no problems are expected (see Figure 1). In order to avoid a potential flutter problem with the first torsional mode such as occurred on the initial full-scale blade design, and to be as good as or better than the final full-scale design, several changes in addition to simple dimensional scaling were implemented. This was done to prevent a decrease in the scaled-blade natural frequency. The nominal blueprint blade section coordinates were scaled from the full-size blade. However, the tolerances are biased to make this the minimum blade condition, thus, a thicker nominal blade condition is provided. The disk is made of steel rather than titanium as used on the 28.74-inch fan, thus providing a stiffer base and subsequently higher frequencies.

Blade Analysis. The fan blade effective stress distribution shown in Figure 1 is the same as for the original unscaled blade. Maximum effective stress at 110-percent speed is 565 x $10^6$ N/m$^2$ (82 ksi) on the suction side at the root. The yield strength is 689 x $10^6$ N/m$^2$ (100 ksi), giving a margin of safety of 0.22.

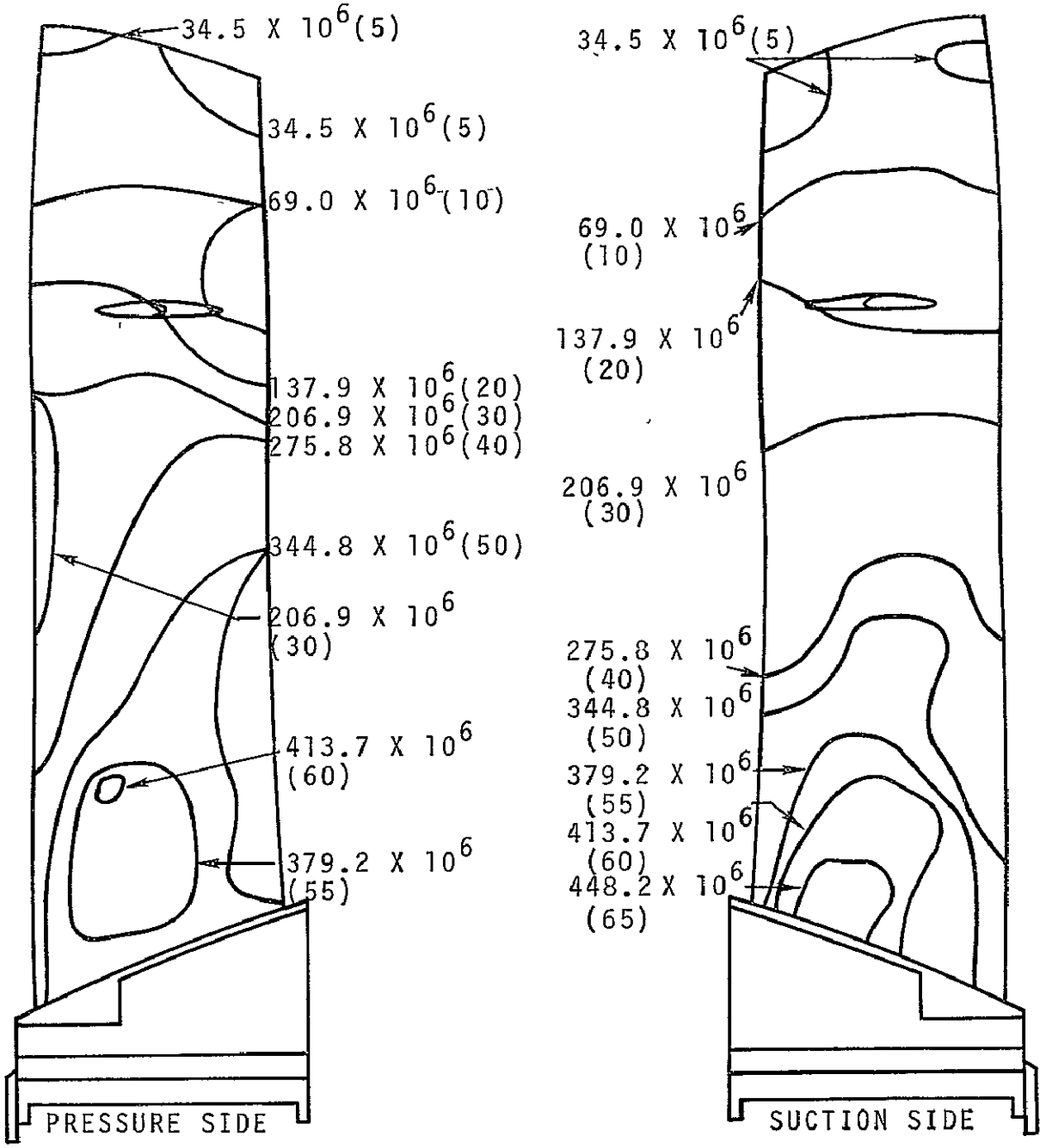


STRESSES IN $N/M^2$ (KSI)
AERODYNAMIC DESIGN POINT LOADS INCLUDED
AT THE AERODYNAMIC DESIGN SPEED (18,400 RPM)

Figure 1. NASA 20-Inch Fan Blade Effective Stress.

Disk-Spinner Analysis. - Disk and spinner weight and inertia properties are shown in Table 1. The disk design criteria are summarized in Table 2, and the stress results are summarized in Table 3 and Figure 2. The average tangential stress is 295 x $10^6$ $N/m^2$ (42.8 ksi), which gives a high burst speed of 34,400 rpm (170 percent). A large margin is desirable since holes were required in the disk web to be compatible with the NASA installation. The maximum radial stress is at these drive shaft bolt holes. The holes are in accordance with the NASA guidelines not to exceed twice the yield strength at the local hole area.

The blade-to-disk attachment stresses and shedding speeds are summarized in Table 4. The maximum dovetail fillet stress (including its stress concentration factor) has a margin of safety of minus 0.03, based on general engine low-cycle-fatigue design practice. Because of the short-life requirement for the NASA rig, a negative margin of safety can be tolerated.

The mid-span damper stress is shown in Figure 3. Maximum effective stress at 110 percent is 551 x $10^6$ $N/m^2$ (80 ksi), with a margin of safety of 0.25. The blade untwist, at 100-percent speed, shown in Figure 4, is the same as for the original unscaled blade.

Salt-pattern tests on the full-scale blade were performed with the mid-span damper free and fixed. Results are shown in Table 5 and Figures 5 and 6. Calculated mode shapes and frequencies for the scaled blade, shown in Figure 7, can be compared with the salt patterns pictured in Figure 5 with the mid-span damper constrained. The differences between the calculated and salt-pattern frequencies in the constrained condition are due primarily to the more rigid fixity of the salt-pattern fixture.

The fan blade interference diagram shown in Figure 8 includes salt-pattern results and the calculated operating conditions. The effective mid-span damper spring rates at operation were determined by the full-scale blade responses measured during the rig strain-gauge testing. The tolerance effect is included, which gives the possible band of frequencies based on airfoil geometry. Blade flutter parameters are summarized in Table 6. The torsional flutter parameter versus speed is shown in Figure 9 for the original full-scale blade, the redesigned full-scale blade, and the scaled version. The present nominal blade has a torsional flutter parameter of 1.42, compared with 1.38 for the original full-size blade. Normalized vibratory stress distributions for the first torsional mode are shown in Figure 10. These are presented for a guide to strain gauge locations, since this is the mode of concern, based on the low flutter parameters. They are normalized on the basis of blade tip displacement and are strictly relative.

TABLE 1. DISK AND SPINNER PROPERTIES.

| | Disk | Blades | Bladed Disk | Spinner | Spinner Support | Combined Spinner | Total |
|---|---|---|---|---|---|---|---|
| Weight (lbs) | 18.6 | 8.0 | 26.6 | 3.3 | 6.3 | 9.6 | 36.2 |
| Diametral moment of inertia (lb-in.-sec$^2$) | 0.58 | 0.68 | 1.26 | 0.10 | 0.14 | 0.24 | 1.50 |
| Polar moment of inertia (lb-in.-sec$^2$) | 0.30 | 0.34 | 0.64 | 0.03 | 0.07 | 0.10 | 0.74 |
| Centroid radius (in.) | 3.0 | 5.4 | 3.8 | 3.2 | 2.7 | 2.9 | 3.6 |
| Kinetic energy (in.-lb) | $1.3X10^6$ | $1.5X10^6$ | $2.8X10^6$ | $2.2X10^5$ | $3.2X10^5$ | $5.4X10^5$ | $3.34X10^6$ |

TABLE 2. DISK DESIGN CRITERIA.

| Parameter | Allowable Stress (Percent) |
|---|---|
| Average tangential stress | 55 Ultimate |
| Maximum effective bore stress | 100 Yield |
| Maximum effective web stress | 80 Yield |
| Average effective bore stress | 85 Yield |
| Average radial web stress | 64 Ultimate |

TABLE 3. DISK STRESS SUMMARY, CENTRIFUGAL LOAD ONLY.

| Stress | Allowable (ksi) | Actual (ksi) | Margin of Safety |
|---|---|---|---|
| Average tangential | 80.0 | 42.8 | 0.87 |
| Maximum bore effective | 137.0 | 73.4 | 0.87 |
| Maximum web effective | 110.0 | 45.3 | 1.43 |
| Average neck radial | 92.0 | 36.2 | 1.54 |
| Maximum radial at drive hole with stress concentration of 2.5 | 137.0 | 154.0 | -0.11* |

Burst ratio = 1.7

Burst speed = 34,400 rpm

Notes: Stresses are calculated at 110-percent speed (20,240 rpm).

Allowable stresses are based on 3σ minimum material properties and +50°F above operating temperature.

Burst ratio = $\sqrt{\frac{0.85 \times \text{Ult. Stress}}{\text{Average Tangential}}}$

Material, 17-4PH steel

Margin of safety = $(\frac{\text{allowable}}{\text{actual}}) - 1$

*Local yielding at the drive hole is permissible for short-time rig applications.

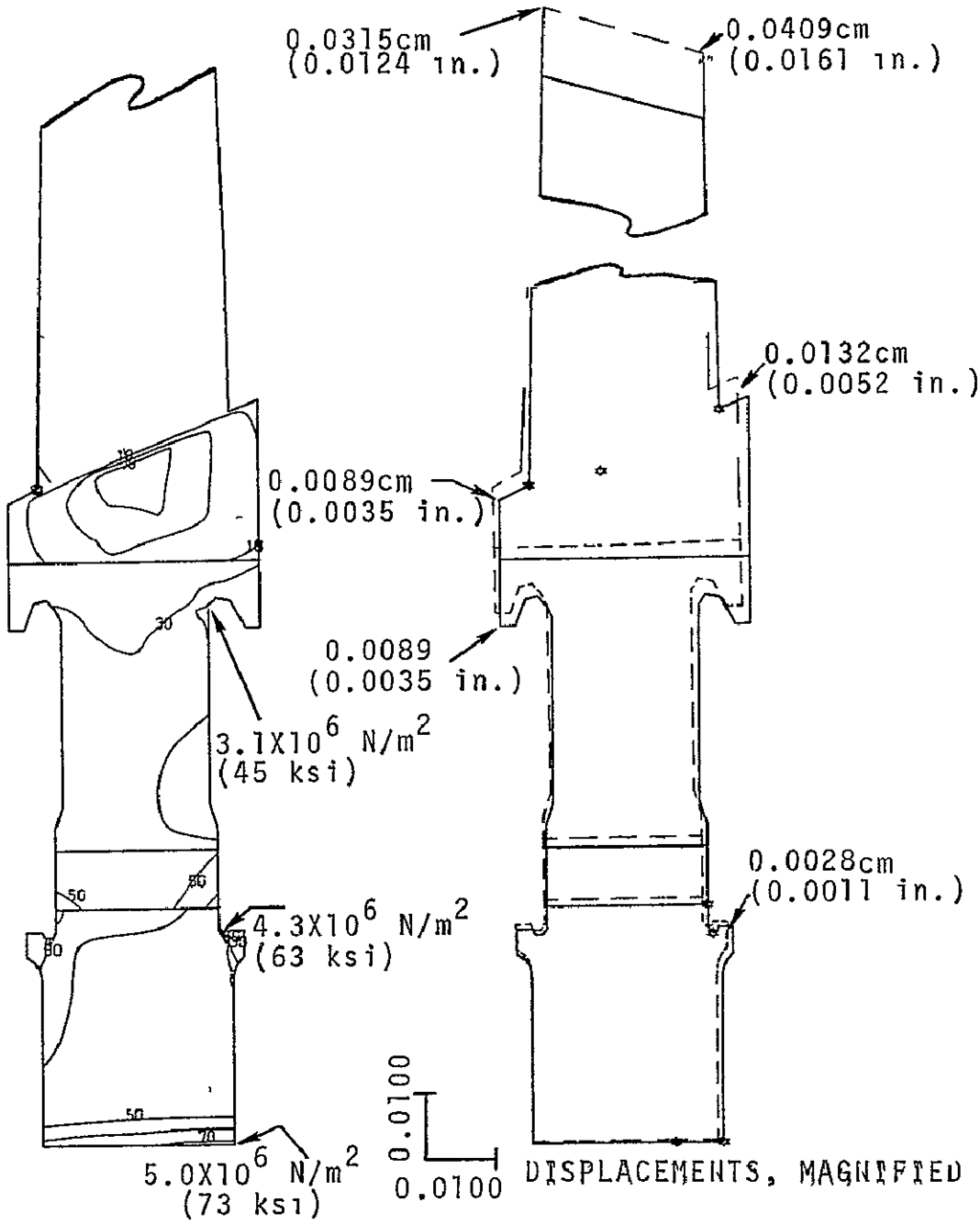


ISOPLETH INTERVAL= 10 KSI

DISK EFFECTIVE STRESS DISK DISPLACEMENT

Figure 2. NASA 20-Inch Scaled Fan, Centrifugal Load Only.

TABLE 4. BLADE-TO-DISK ATTACHMENT STRESSES

| | Blade | | | | Disk | | | |
|---|---|---|---|---|---|---|---|---|
| | Allowable | Nominal | Peak | Margin of Safety | Allowable | Nominal | Peak | Margin of Safety |
| Neck tension or tangen bending | 81.5 | 36.9 | 41 5 | 0 93 | 111 7 | 66 9 | 75 1 | 0 46 |
| Combined fillet | 104 2 | 63 1 | 76.5 | 0.36 | 142 7 | 95 2 | 110 6 | 0 29 |
| Maximum fillet | 61 0 | 0 0 | 126 0 | -0 03 | 83 5 | 0 0 | 145.5 | 0 15 |
| Bearing | 140 0 | 99.3 | 136 2 | 0 03 | 191.8 | 99 3 | 136 2 | 0 41 |
| Shear | 47 3 | 19 8 | 22.3 | 1 09 | 64 8 | 34 9 | 39 3 | 0 62 |

Blade Shank Shedding Speed- - - - - - -32,680 rpm (178 percent)
Disk Shank Shedding Speed - - - - - - -28,470 rpm (155 percent)

Notes
1 All stresses are in ksi
2 All stresses are calculated at 110 percent design speed (20240 rpm)
3. Margin of safety is based on the larger of 1 2 times the nominal stress or the calculated peak stress
4 Margin of safety = (allowable stress/calculated stress) -1
5 Allowable stresses include
5 percent reduction for surface finish and loading rate (except for combined fillet)
4 5 percent reduction for broach angle
6 Allowable maximum fillet stress is 1/2 amplitude equivalent elastic stress

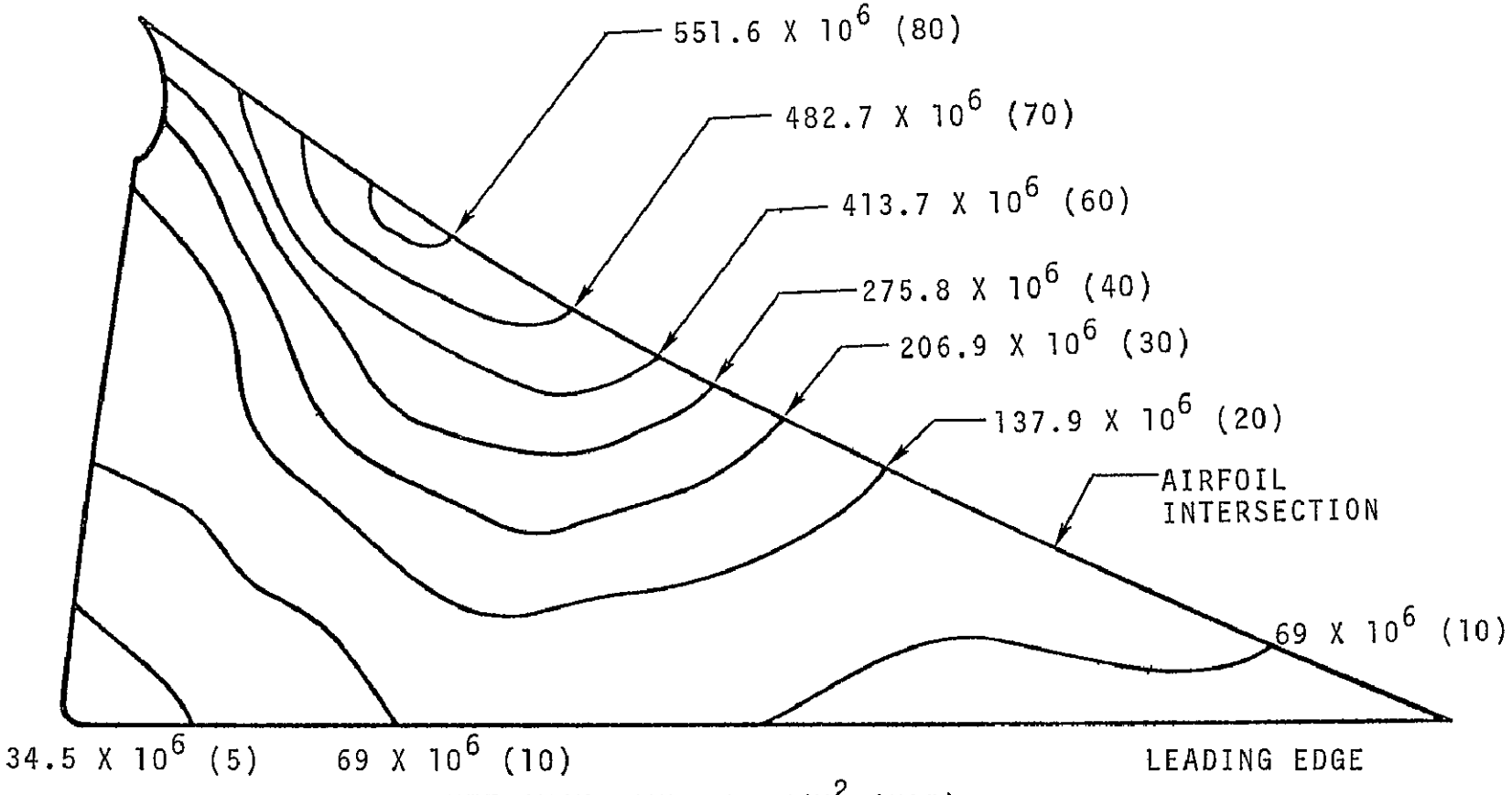


Figure 3. Mid-Span Damper Stress, NASA 20-Inch Scaled Fan.

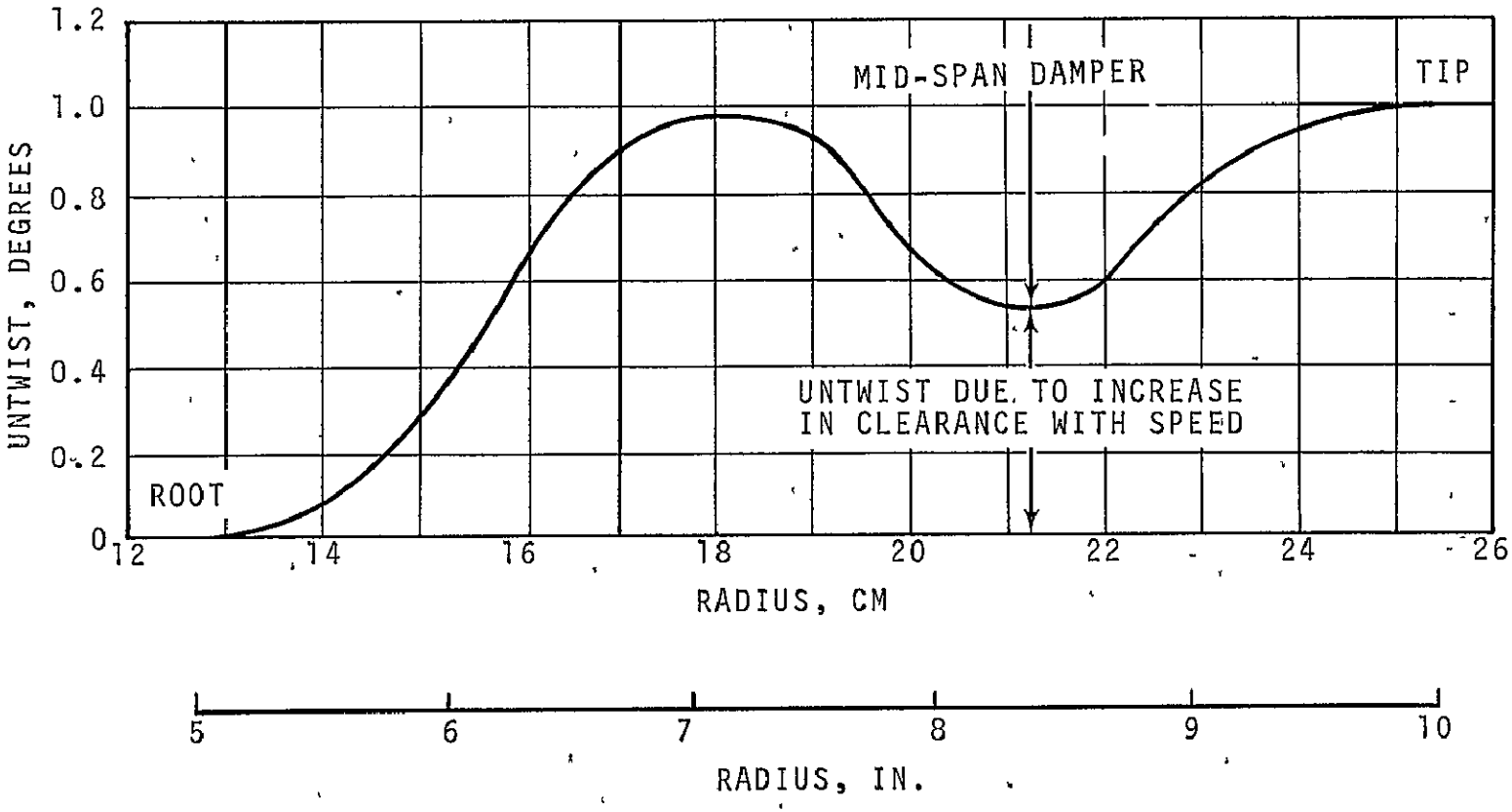


Figure 4. NASA 20-Inch Fan Airfoil Untwist at Design Speed.

TABLE 5. RESULTS OF SALT-PATTERN TESTS ON THE FULL-SCALE BLADE.

FREQUENCY (HZ) WITH MID-SPAN DAMPER FIXED

| | 1st Flex | 1st Torsion | 2nd Flex |
|---|---|---|---|
| Measured A[1] | 616 | 1303 | 1752 |
| Measured B[2] | 620 | 1326 | 1783 |
| Calculated[3] | 618 | 1233 | 1592 |
| Difference[4] | -.32% | -7.0% | -12.0% |

FREQUENCY (HZ) WITH MID-SPAN DAMPER FREE

| | 1st Flex | 2nd Flex | 1st Torsion |
|---|---|---|---|
| Measured A[1] | 111 | 450 | 601 |
| Measured B[2] | 114 | 482 | 604 |
| Calculated | 112 | 468 | 590 |
| Difference[4] | -1.8% | -2.9% | -2.3% |

Notes:
1. Case A refers to only the dovetail clamped
2. Case B refers to both dovetail and platform clamped
3. The mid-span damper constraint is based on its effective spring rate at operation and is "softer" than the fixture constraints.
4. Difference = $\frac{\text{Calculated-Measured B}}{\text{Measured B}}$ in percent

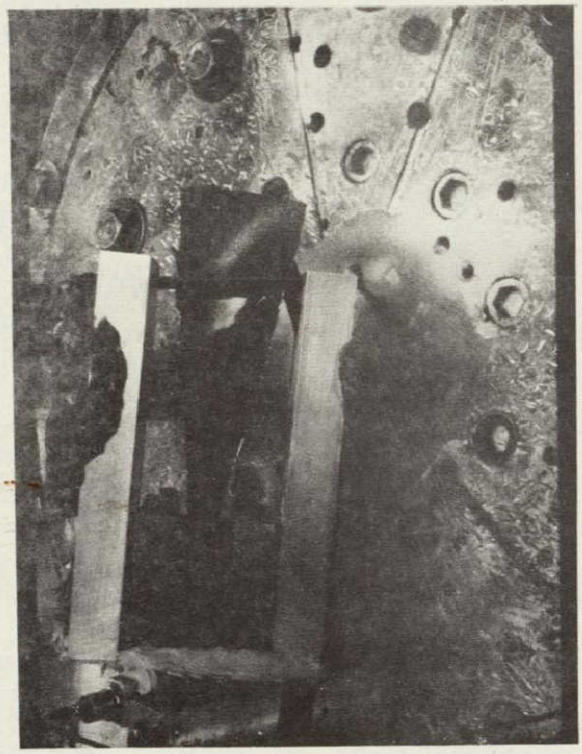

1ST FLEX
CASE B, 620 HZ

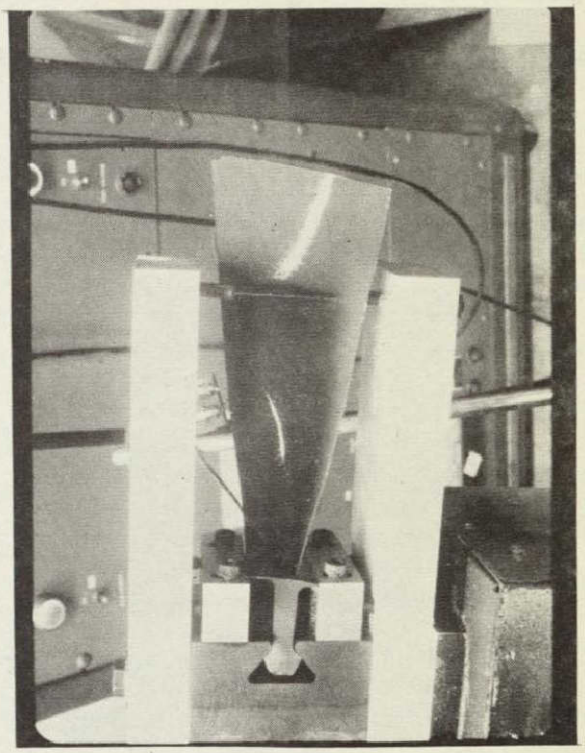

1ST TORSION
CASE B, 1326 HZ

2ND FLEX
CASE B, 1783 HZ

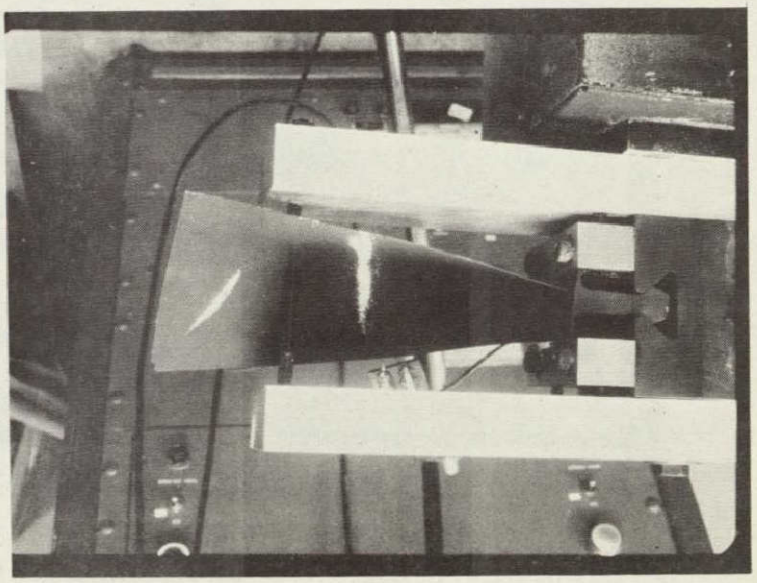

Figure 5. Salt-Pattern Test on 28.74-Inch Blade. Modes and Frequencies for Mid-Span Damper Clamped.

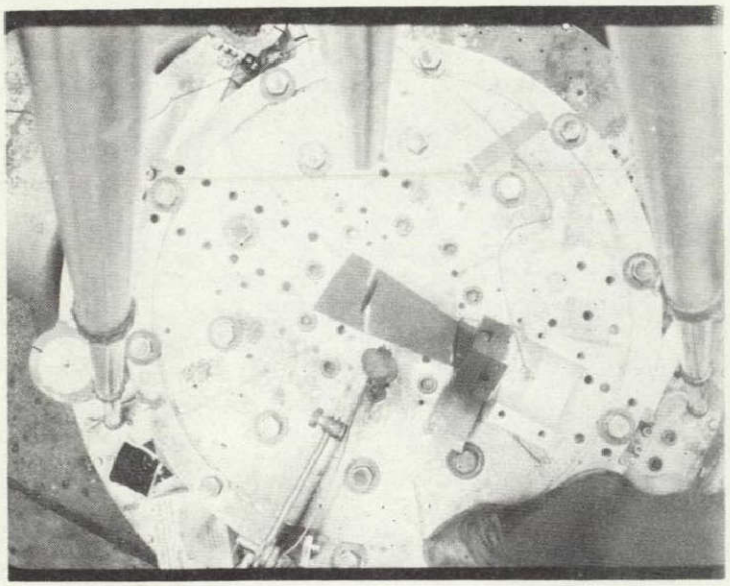

1ST FLEX, CASE A, 450 HZ

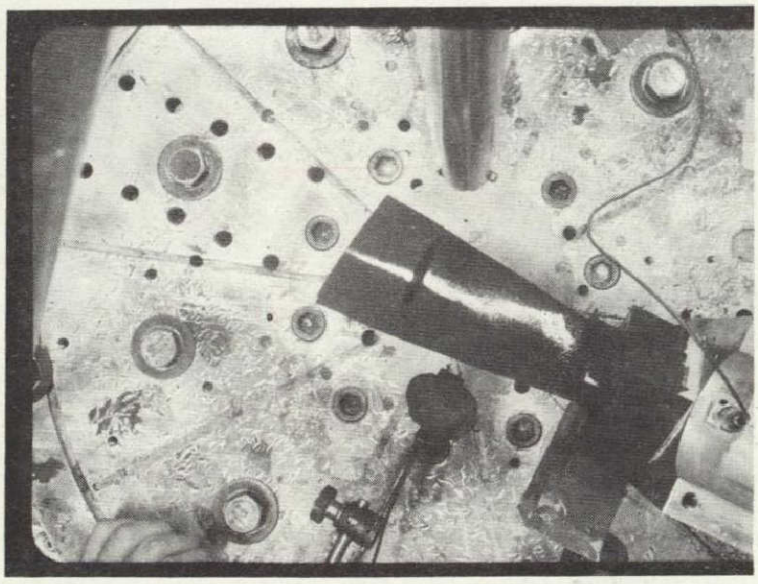

1ST TORSION, CASE A, 601 HZ

Figure 6. Salt-Pattern Test on 28.74-Inch Blade. Modes and Frequencies for Mid-Span Damper Free.

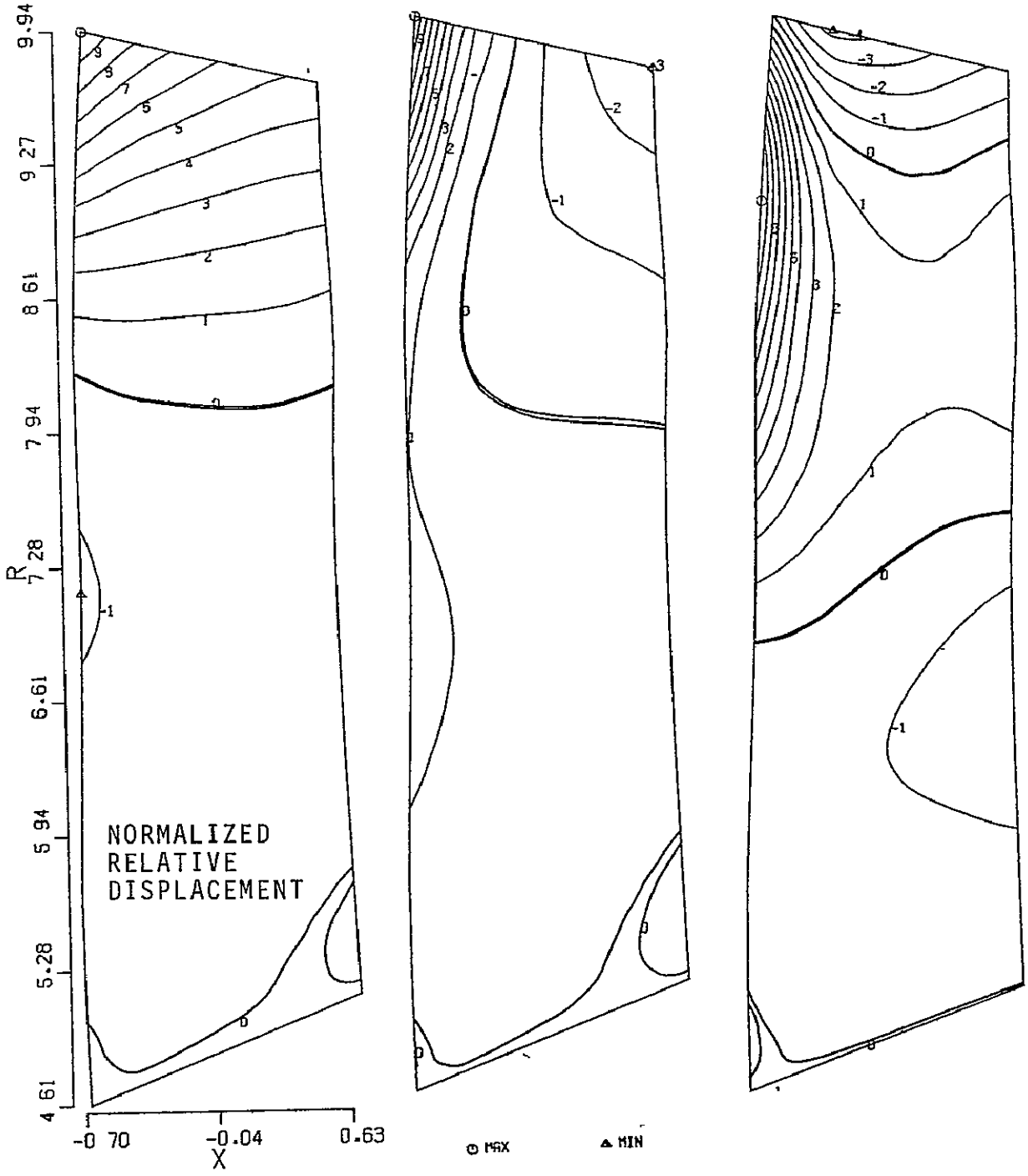


MODE 1
618 HZ

MODE 2
1233 HZ

MODE 3
1592 HZ

Figure 7. NASA 20-Inch Scaled Fan Rotor, Blade Normal Mode Shapes.

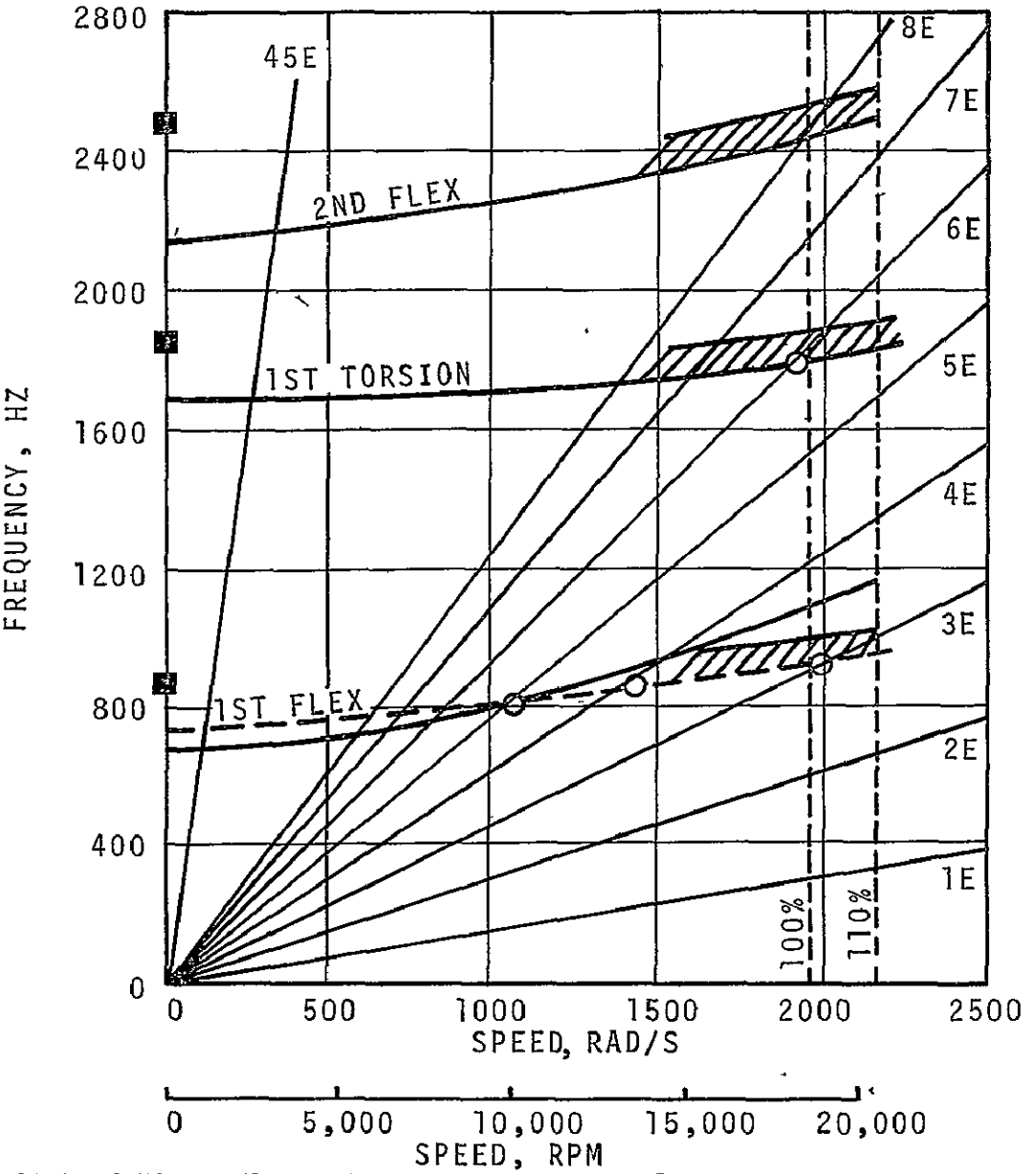


■ SALT PATTERN FROM FULL SCALE BLADE P/N X2401068 SCALED DOWN TO P/N 3550842 SIZE MID-SPAN DAMPERS FULLY CONSTRAINED

○ RIG STRAIN-GAUGE DATA, SCALED FROM FULL SIZE BLADE

——— CALCULATED, MID-SPAN CONSTRAINED WITH SPRINGS, $K_x$ = 4.0 X $10^2$ N/M (3.5 X $10^3$ LB/IN), $K_y$ = 4.0 X $10^4$ N/M (3.5 X $10^5$ LB/INCH)

– – – – ADJUSTED FROM RIG STRAIN-GAUGE TEST

ZZZZZZZ TOLERANCE EFFECT

Figure 8. NASA 20-Inch Fan Blade Interference Diagram.

TABLE 6. BLADE FLUTTER PARAMETER, $\frac{WC'}{V}$, 100% SPEED.

| | 1st Flex | 1st Torsion |
|---|---|---|
| Original Blade, Based on Measured Frequency Response | 0.73 Nominal | 1.38 Nominal |
| Scaled blade, based on the effective mid-span spring rate as determined by measured response of full-scale blade | 0.83 Nominal<br>0.73 Minimum | 1.42 Nominal<br>1.38 Minimum |

Notes: W = frequency, rad/sec

C' = chord length at tip, ft

V = relative fluid velocity at tip, ft/sec

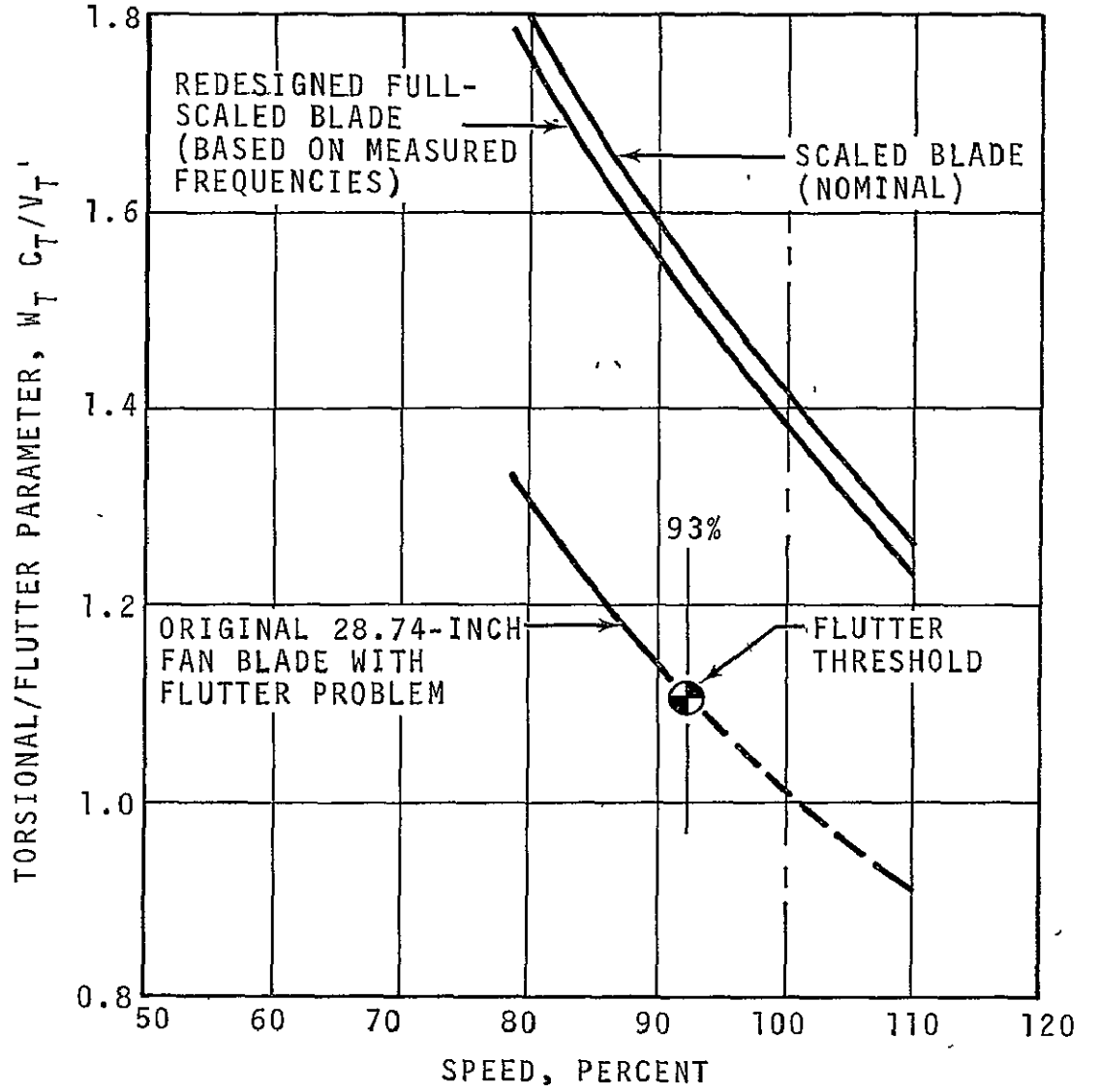


NOTE: 100-PERCENT SPEED = 1926 RAD/S (18,400 RPM) FOR 20-INCH FAN BLADE

Figure 9. NASA 20-Inch Fan Blade Torsional Flutter Parameter.

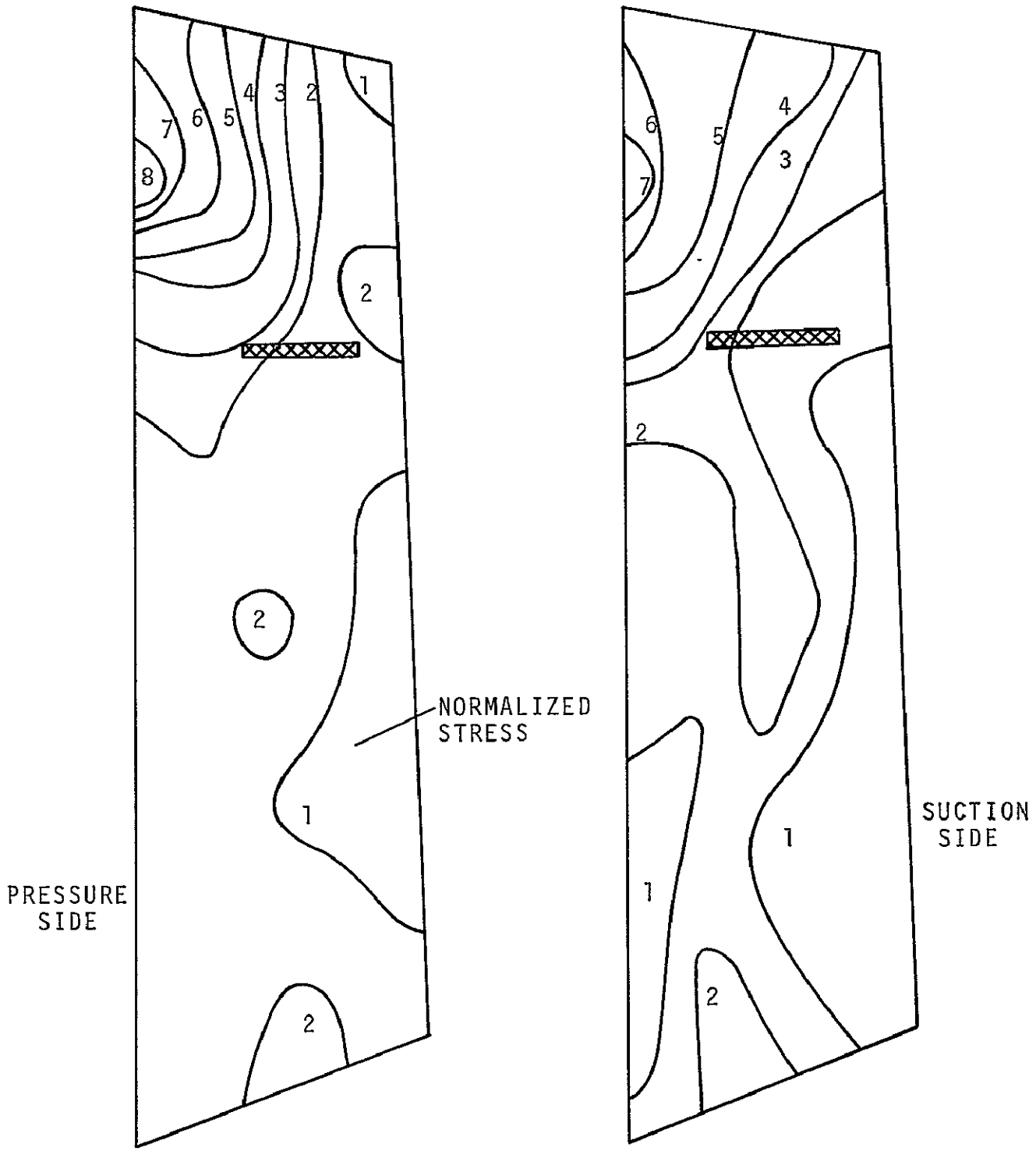


Figure 10. NASA 20-Inch Fan Normalized Vibratory Stress, First Torsional Mode.

Tables 7 and 8 and Figures 11 and 12 summarize the spinner and spinner support centrifugal stresses and deflection. The maximum effective stress occurs in the spinner support with a value of 466 x $10^6$ N/$m^2$ (67.7 ksi) and a margin of safety of 1.01. The spinner burst speed is 44,600 rpm (220 percent speed).

The combined effects of centrifugal loading, thermal, and assembly interaction have been determined for the spinner, spinner support, and rotor disk assembly. Table 9 and Figure 13 summarize the results of this analysis. The maximum effective stress in the disk with this combined effect is 572 x $10^6$ N/$m^2$ (83 ksi) at the base with a margin of safety of 0.65. In the spinner assembly, the maximum effective stress is 517 x $10^6$ N/$m^2$ (75 ksi) with a margin of safety of 0.82.

Disk, spinner, and blade attachment stresses are adequate for the 110-percent-speed mechanical-design point. However, strain-gauge tests are required on the fan blades to check the mechanical integrity of the rotor.

TABLE 7. SPINNER STRESS SUMMARY, CENTRIFUGAL LOAD ONLY.

| Stress | Allowable (ksi) | Actual (ksi) | Margin of Safety |
|---|---|---|---|
| Average Tangential | 80 | 25.2 | 2.18 |
| Maximum effective | 137 | 62.9 | 1.18 |

Burst ratio = 2.2
Burst speed = 44,600 rpm

TABLE 8. SPINNER SUPPORT STRESS SUMMARY, CENTRIFUGAL LOAD ONLY.

| Stress | Allowable (ksi) | Actual (ksi) | Margin of Safety |
|---|---|---|---|
| Average Tangential | 80.0 | 20.3 | 2.95 |
| Maximum effective | 137.0 | 67.7 | 1.01 |
| Maximum radial at drive hole (stress concentration of 2.5) | 137.0 | 80.0 | 0.71 |

Burst ratio = 2.5
Burst speed = 50,600 rpm

*Notes: Stresses are calculated at 110-percent speed (20,240 rpm).

Allowable stresses are based on 3σ minimum properties and +50°F above operating temperature.

$$\text{Burst ratio} = \sqrt{\frac{0.85 \times \text{Ult. Stress}}{\text{Avg. Tangential}}}$$

Material, 17-4PH steel

$$\text{Margin of safety} = \left(\frac{\text{allowable}}{\text{actual}}\right) - 1$$

*Notes are applicable to Tables 7 and 8.

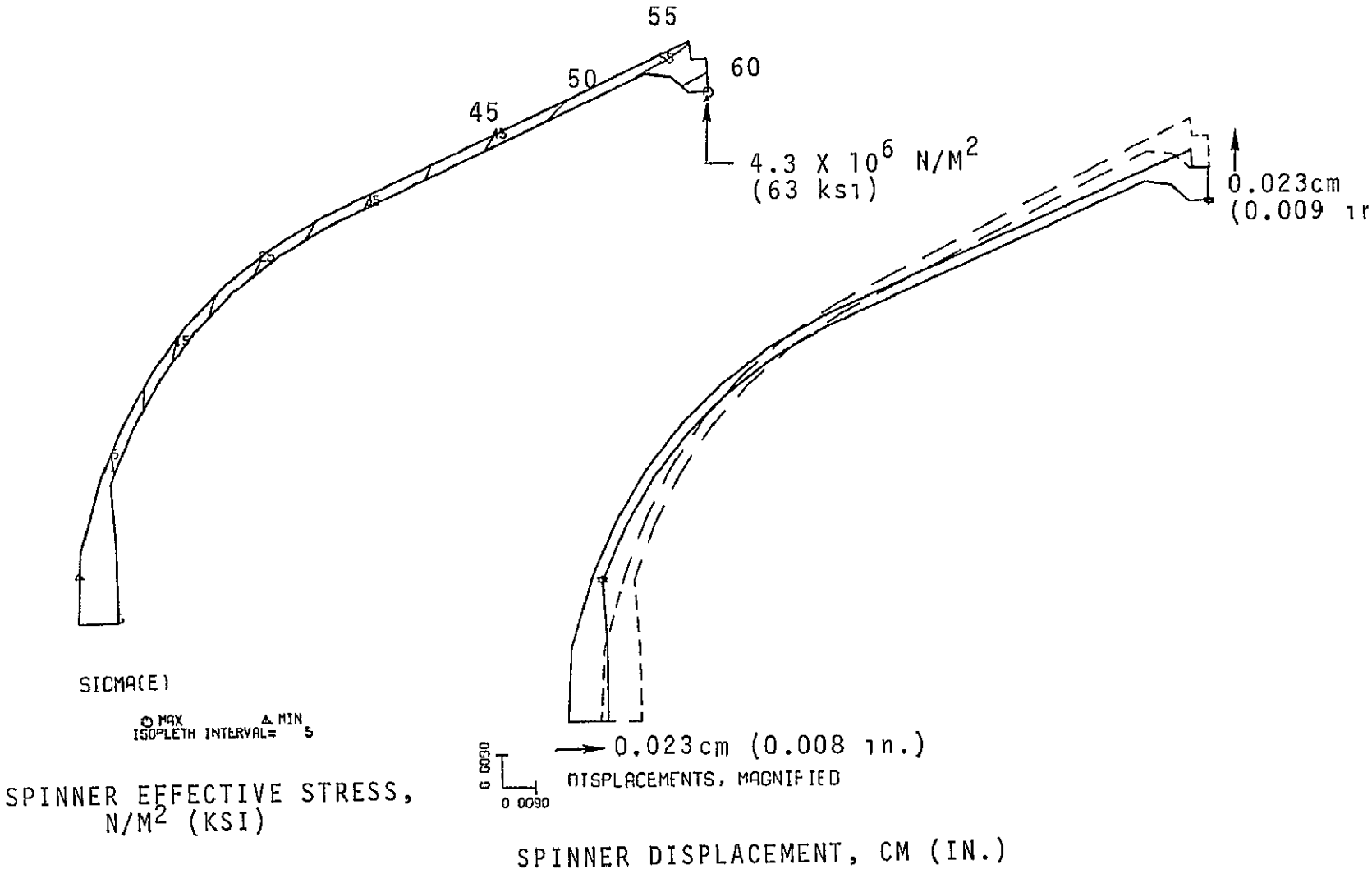


Figure 11. NASA 20-Inch Scaled Fan, Centrifugal Load Only.

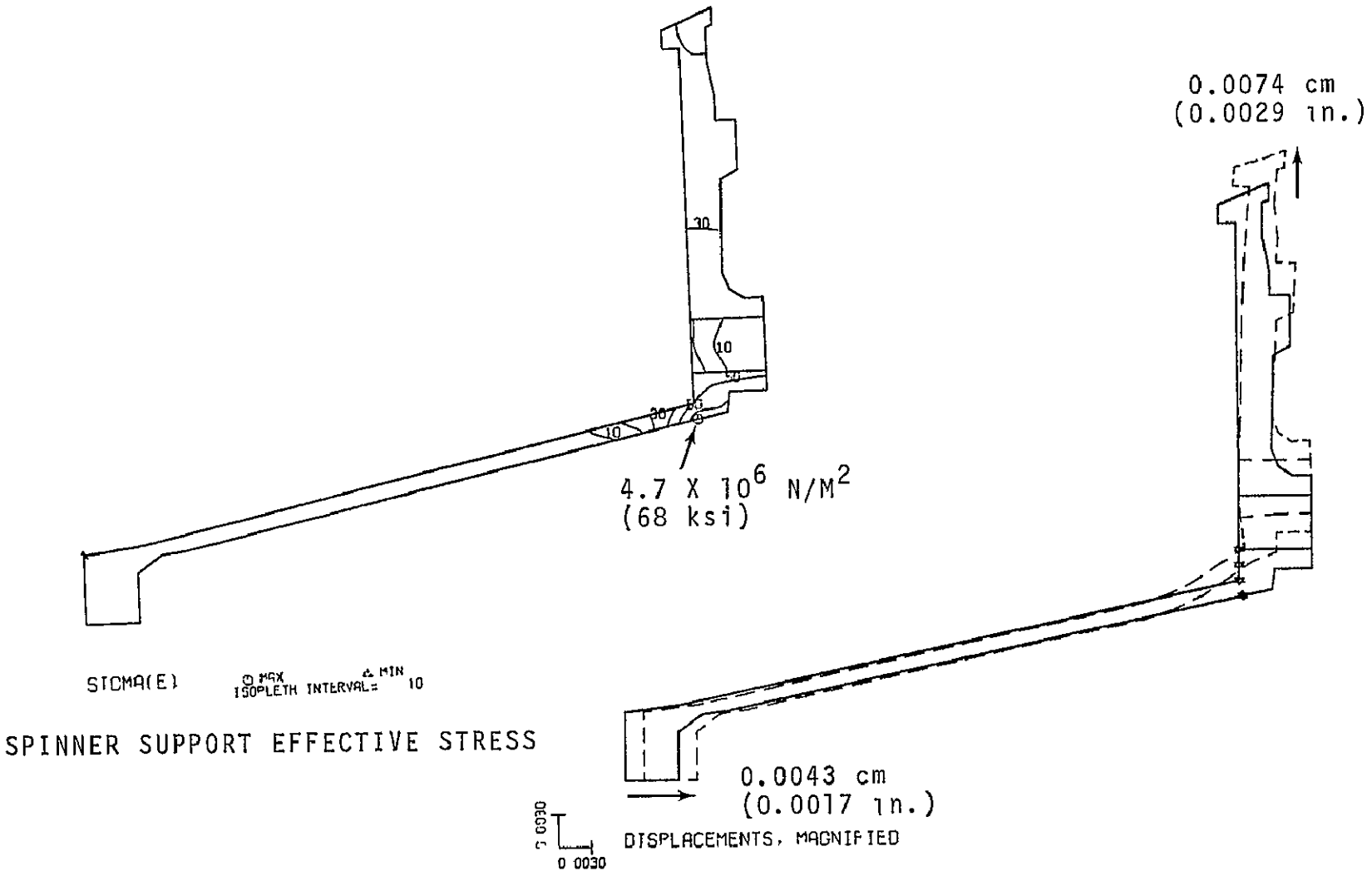


Figure 12. NASA 20-Inch Scaled Fan, Centrifugal Load Only.

TABLE 9. DISK-SPINNER ASSEMBLY STRESS.

Centrifugal, Thermal, and Assembly Interaction Effects Included

| Stress | Allowable (ksi) | Actual (ksi) | Margin of Safety |
|---|---|---|---|
| Disk | | | |
| Maximum bore effective | 137 | 83.1 | 0.65 |
| Maximum web effective | 110 | 58.2 | 0.89 |
| Average neck radial | 92 | 36.2 | 1.55 |
| Maximum radial at drive hole (stress concentration of 2.5) | 137 | 113.0 | 0.21 |
| Spinner Assembly | | | |
| Maximum effective | 137 | 75.3 | 0.82 |
| Maximum radial at drive hole (stress concentration of 2.5) | 137 | 103.0 | 0.32 |

Notes: Stresses are calculated at 110-percent speed (20,240 rpm).

Allowable stresses are based on 3σ minimum properties and +50°F above operating temperature.

$$\text{Burst ratio} = \frac{\sqrt{0.85 \times \text{Ult. Stress}}}{\text{Avg. Tangential}}$$

Material, 17-4PH steel

$$\text{Margin of safety} = \left(\frac{\text{allowable}}{\text{actual}}\right) - 1$$

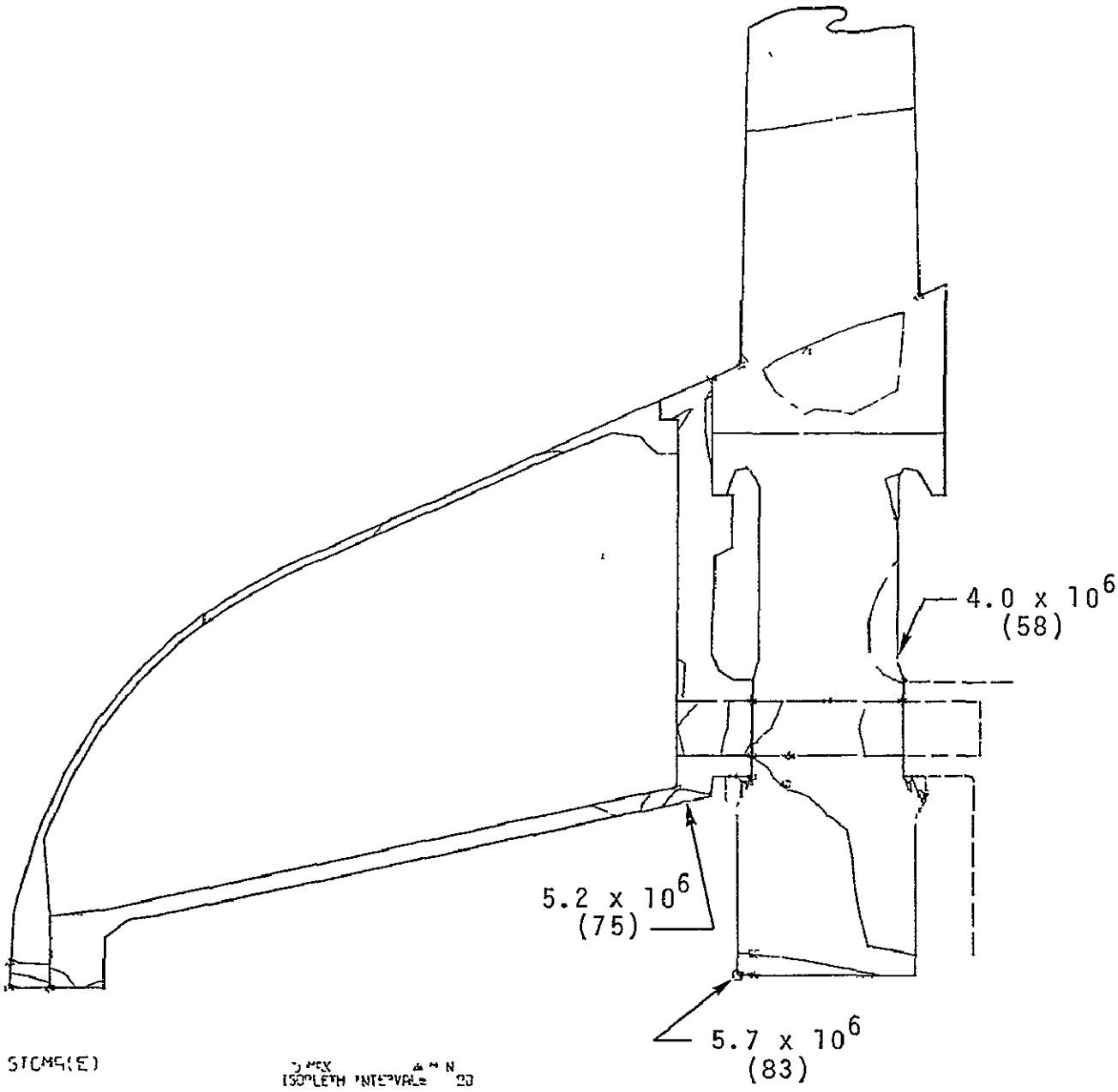


DISK-SPINNER ASSEMBLY EFFECTIVE STRESS, $N/M^2$ (KSI)

Figure 13. NASA 20-Inch Scaled Fan, Centrifugal, Thermal, and Assembly Interaction Effects.

## STATOR DESIGN

### Stator Aerodynamic Design

The stator blades for the 20-inch transonic fan were designed to accommodate the flow measured at the discharge of the similar but larger transonic fan investigated under a previous NASA contract. The flow angle distribution observed during reading No. 117 at 95-percent speed, design airflow, and pressure ratio; and during reading No. 126 at 100-percent speed (airflow 3 percent above design value and a pressure ratio of 1.67) is presented in Figure 14. Variations in inlet flow angle observed between 25- and 35-percent span from the rotor tip are believed to have been strongly influenced by the mid-span damper on the rotor blades. It is believed wise to ignore the angle swing in this zone because angle-measuring instruments are subject to error in the presence of total-pressure gradients. Total-pressure gradients are present in this flow field downstream of the mid-span damper and in the regions adjacent to the hub and tip casings of the compressor. The dotted line shown in Figure 14 represents the variation of inlet air angle versus spanwise position chosen for the stator redesign. An essentially linear variation from about 32 degrees at the tip to around 41 degrees at the hub is assumed to be the inlet air angle distribution that will occur downstream of the 20-inch transonic fan rotor. This compares with a variation from about 21 degrees at the tip to about 39 degrees at the hub as originally anticipated to occur downstream of the 28.74-inch fan rotor.

The variation of inlet Mach number versus percent span is shown in Figure 15. Again, the variation between 25- and 35-percent span is believed to be erroneous due to the effect of nonuniform flow upon instrumentation in this zone. The assumed Mach number variation for use in the stator redesign is represented by a dotted line. The maximum Mach number expected is about 0.71 at the outside diameter, with a linear decrease to about 0.66 at the inside diameter or hub section. The Mach number in the inner region is significantly less than that calculated for the original compressor design. This is largely due to smaller work input by the rotor in the inboard region than was anticipated.

The blade solidity, that is, the ratio of blade chord divided by spacing, has been increased in this stator design because of the observed performance of the previous stator. At the outside diameter or tip section, blade solidity has been increased from about 1.0 to 1.2 (Figure 16). The solidity at the inside diameter has been increased from 1.8 to approximately 2.2. The increase in stator solidity is intended to reduce the diffusion factor in order to reduce the loss through the stator. In addition to this solidity increase, a decrease in the stator exit area has been effected in this stator design. This reduction in exit area and the consequent increase in exit Mach number tend to reduce the D-factor,

| SYM | READING | $\frac{N/\sqrt{\theta}}{(N/\sqrt{\theta})_{DES}}$ | $\frac{W\sqrt{\theta}/\delta}{(W\sqrt{\theta}/\delta)_{DES}}$ | $P_{T12}/P_{T5}$ | $\eta_{ab}$ |
|---|---|---|---|---|---|
| ○ | 117 | 95% | 1.008 | 1.540 | 0.861 |
| □ | 126 | 100% | 1.031 | 1.669 | 0.837 |

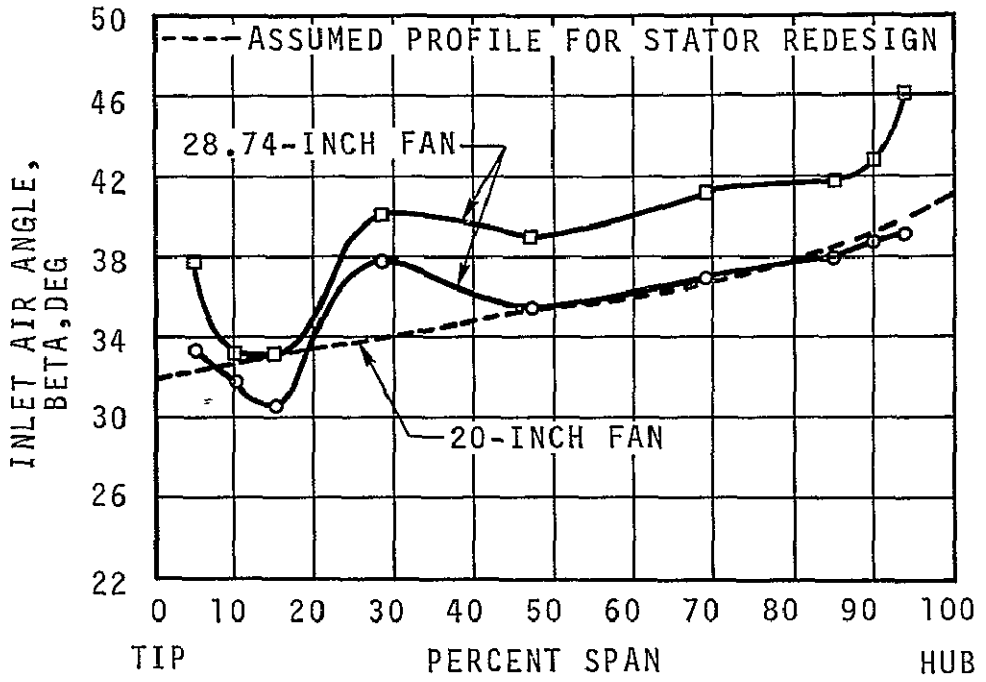


Figure 14. Stator Inlet Angle, $\beta_1$, Versus Span.

| SYM | READING | $\frac{N/\sqrt{\theta}}{(N/\sqrt{\theta})_{DES}}$ | $\frac{W\sqrt{\theta}/\delta}{(W\sqrt{\theta}/\delta)_{DES}}$ | $P_{T12}/P_{T5}$ | $\eta_{ad}$ |
|---|---|---|---|---|---|
| ○ | 117 | 95% | 1.008 | 1.540 | 0.861 |
| □ | 126 | 100% | 1.031 | 1.669 | 0.837 |

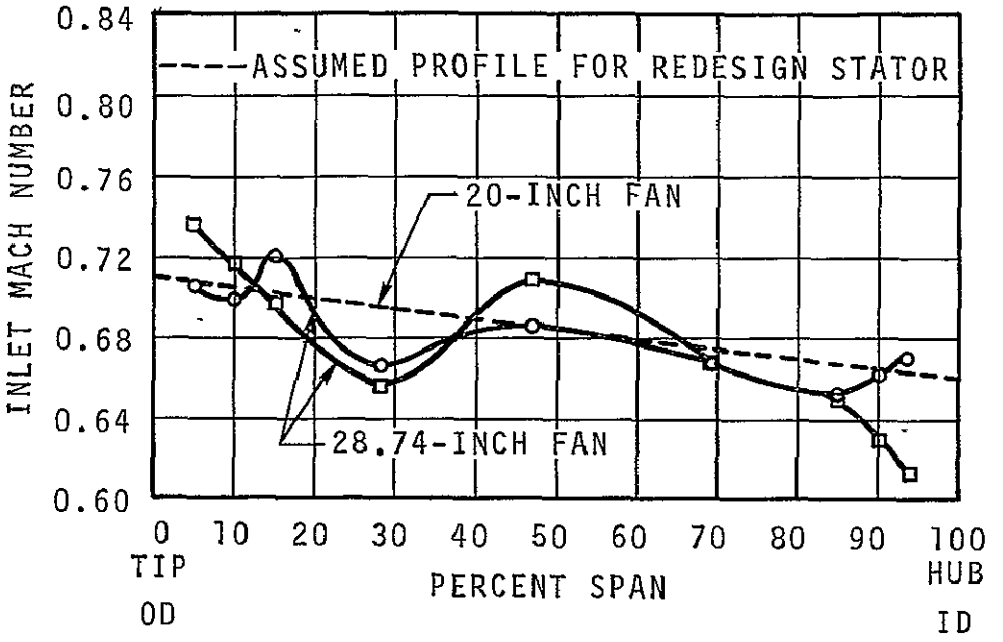


Figure 15. Stator Inlet Mach Number Versus Span.

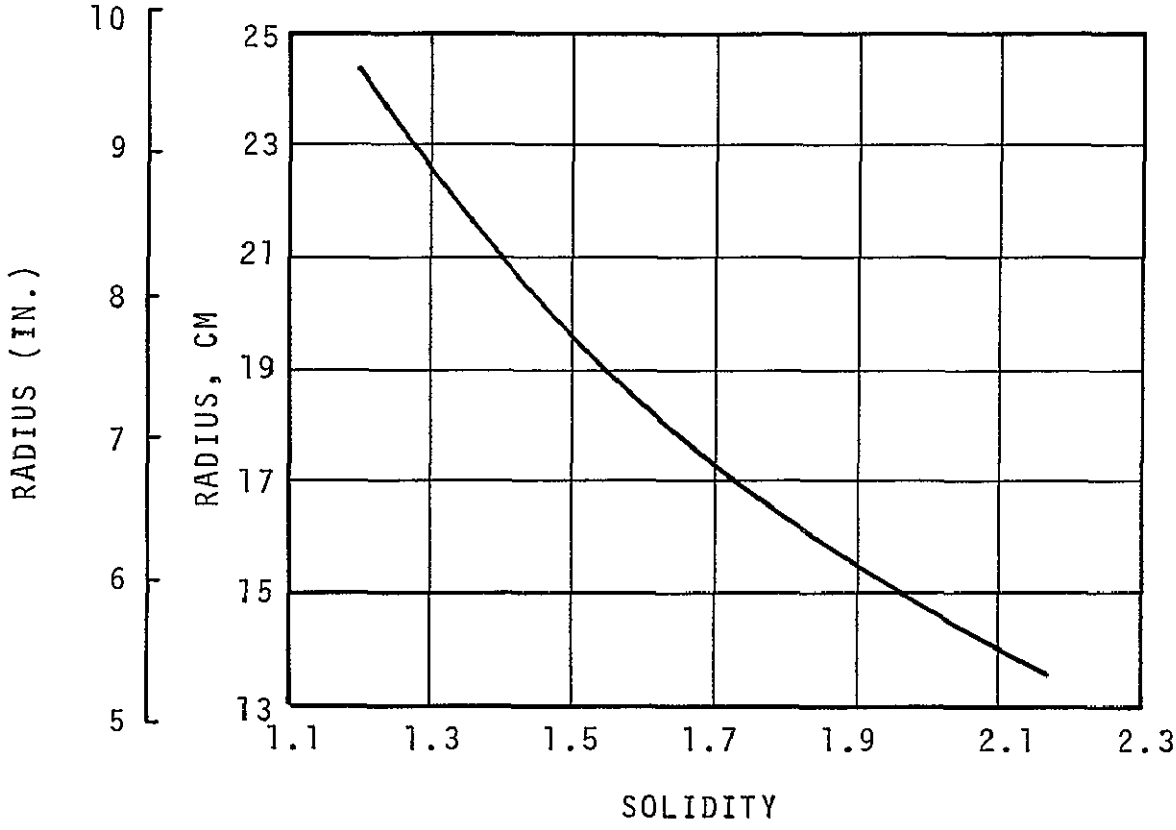


Figure 16. NASA 20-Inch Fan Stator Blade Solidity Versus Radius.

thereby reducing stator losses. The blade solidity shown in Figure 16 results in the blade meanline* chord length variation with radius shown in Figure 17. The chord length varies only slightly, from a value of 1.61 inches at the outside diameter to about 1.63 inches at the inside diameter. If it were to simplify stator construction significantly, a constant stator chord length could be employed without a significant change in aerodynamic properties. The stator chord lengths shown result in a constant axial projection of 1.565 inches.

The appropriate meanline incidence angles for the stator sections have been selected from extensive low-speed cascade data. A correction to increase the angle of incidence by two degrees at all stations from hub to tip has been incorporated to account for high-speed flow effects. The meanline incidence varies from about minus 5 degrees at the outside diameter to about 0 degrees at the stator hub, as shown in Figure 18.

The leading-edge direction of the stator blade changes only about 4 degrees from tip to hub in a continuous manner, as shown in Figure 19. This gradual variation indicates that the stator blade should have a smooth leading edge without significant irregularities and should, therefore, be relatively easy to manufacture. The leading-edge blade angle will be 37 degrees from the axis of rotation at the outside diameter and about 41.3 degrees at the inside diameter.

The flow deviation angle, that is, the angle between the flow leaving direction and the trailing-edge direction of the blade section is shown in Figure 20. This variation of angle with radius follows approximately the variation observed during the earlier tests of the 28.74-inch transonic fan, although increased values of deviation are included in the redesign since study of the original test data suggested that this increase would be advisable to achieve axial exit flow. The deviation angle was estimated primarily from low-speed cascade data. A correction was made for the thickness/chord ratio difference from the 10-percent value of the cascade tests to the 6-percent value to be used with these stators. Furthermore, a correction for the effects of Mach number based on high-speed cascade data has also been made. The deviation angle is seen in Figure 20 to be essentially constant, varying only from about 10 degrees at the outside diameter to a minimum of about 8.7 degrees at a radius of 6.7 inches and increasing again to about 9.6 degrees at the inner diameter.

---

*Also called camber line.

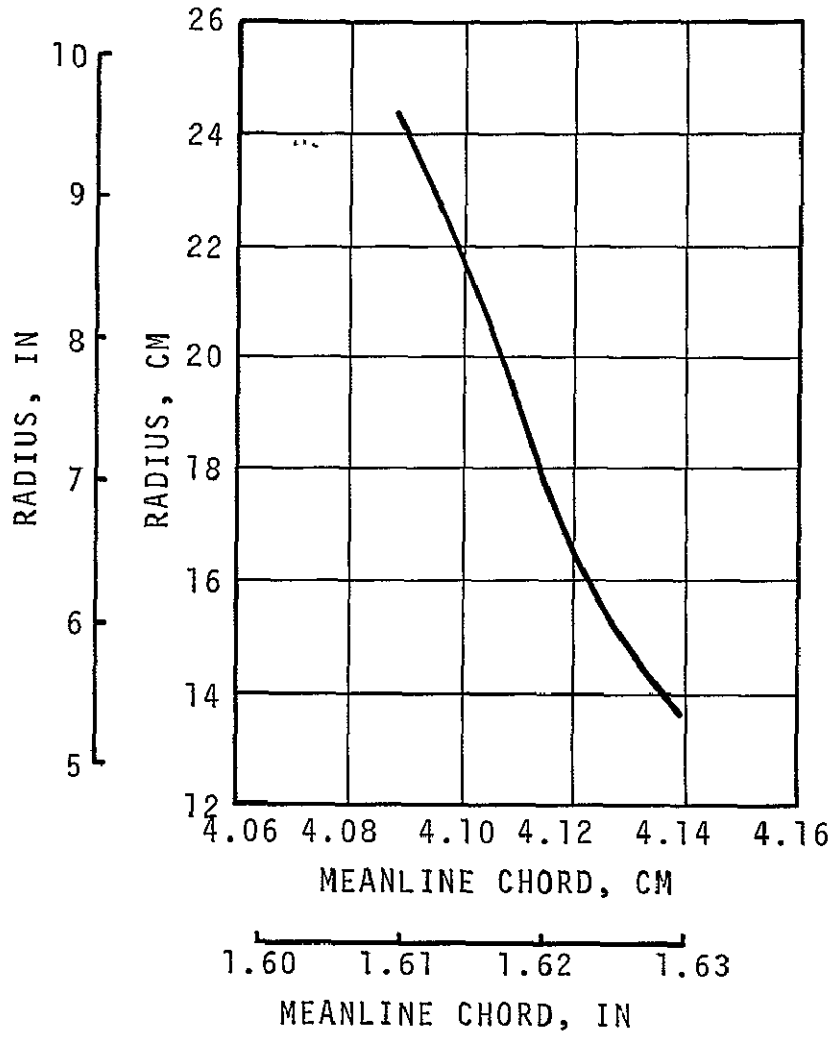


Figure 17. NASA 20-Inch Fan Stator Chord Versus Radius.

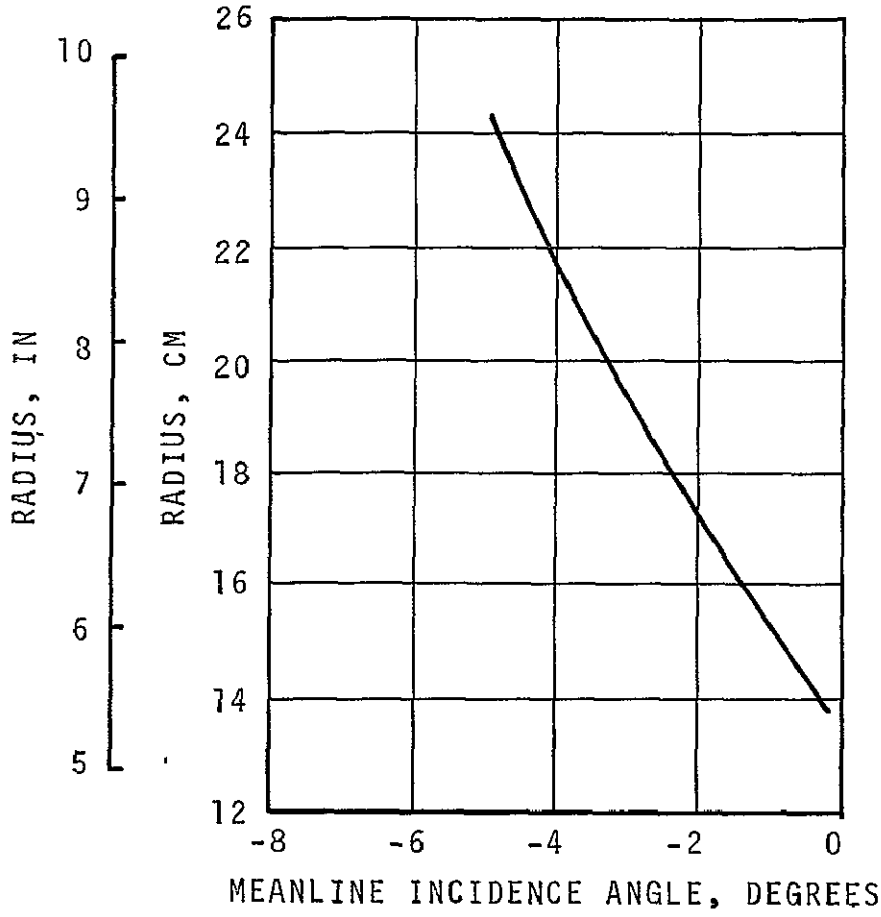


Figure 18. NASA 20-Inch Fan Stator Meanline Incidence Versus Radius.

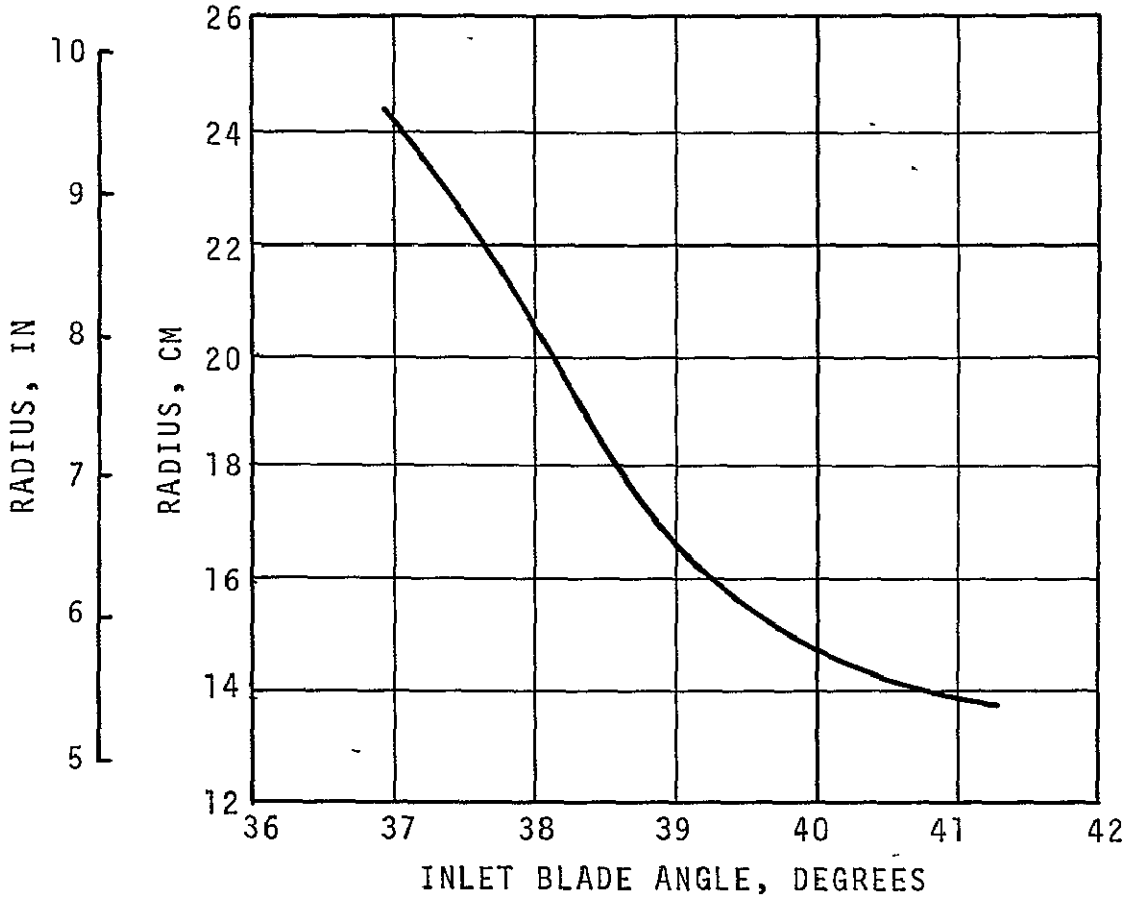


Figure 19. NASA 20-Inch Fan Stator Inlet Blade Angle Versus Radius.

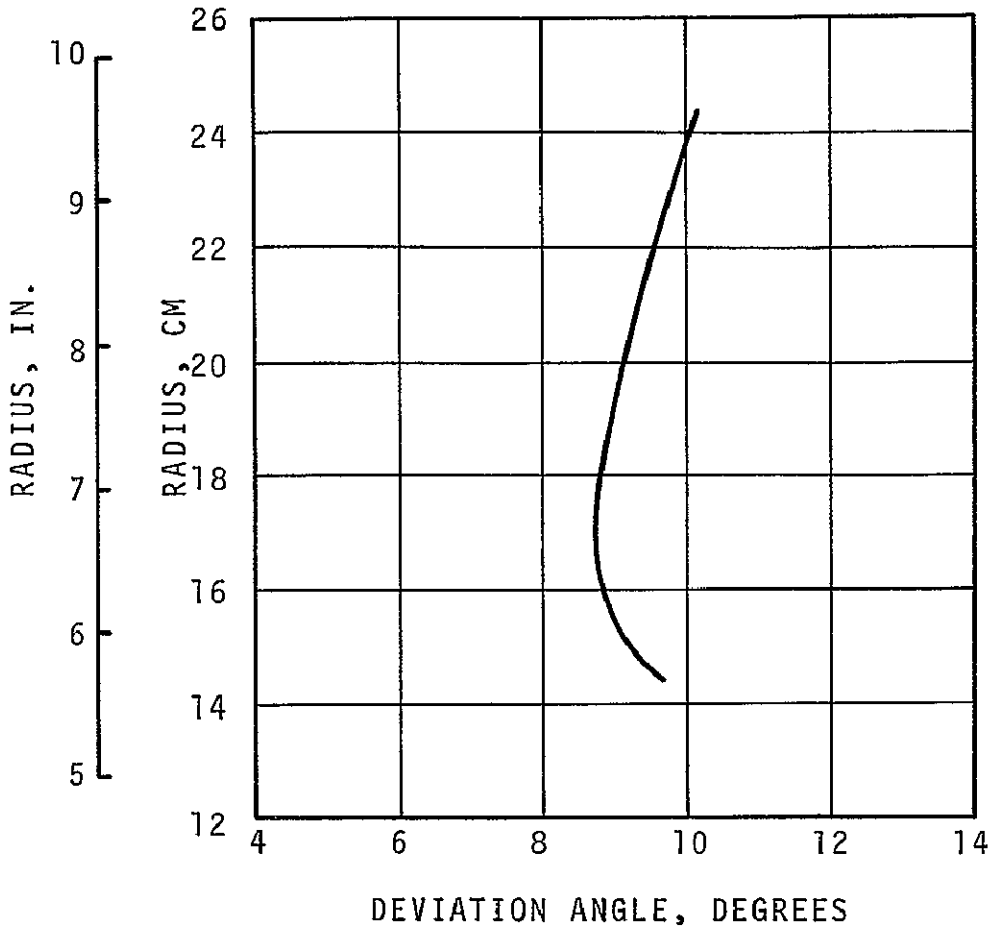


Figure 20. NASA 20-Inch Fan Stator Deviation Angle Versus Radius.

The blade camber plotted in Figure 21 resulted from the incidence and deviation angle selections, as well as the turning required for each radius. The variation of camber is relatively small for this stator, varying from about 47 degrees in the outboard region to a maximum of 51.5 degrees at the inner radius. Camber in this stator blade is greater than the original design because more turning of the flow leaving the rotor will be required. This increase in turning would be expected to increase the diffusion factor, but increases in blade solidity and decreases in stator exit area have been incorporated, and the total result is a decrease in the stator diffusion factor. It is hoped, therefore, that a significant decrease in the stator losses will be experienced due both to decreased diffusion factor and to better matching of the stator to the actual flow entering the stator.

The variation of the blade stagger angle--that is, the angle between the blade chord line and the axis of rotation--is shown in Figure 22. An essentially linear variation is seen from about 13.4 degrees at the outside diameter increasing to about 16.2 degrees at the inner diameter. Because of the small variation in stagger angle (a small amount of blade twist), no particular difficulty is anticipated in the manufacturing of these stator blades.

Because the Mach numbers entering the stator are in the range of 0.66 to 0.71 from hub to tip, NASA 65-series blade sections have been selected for this application. Circular arcs will be used for the camber lines of the sections. The effect of this blade selection is to change the leading-edge shape from that of a double-circular-arc section to a 65-series leading edge. Experience has shown that the NASA 65-series leading edges have a broader range of efficient operation, provided that the Mach number entering the blades is below the critical value. Some improvement in blade operating range should result from the use of these blade sections.

Because of the reduction of stator diffusion factor, an increase in stage efficiency of one to two points may result, so that at 95-percent speed and design flow and pressure ratio, a stage efficiency of about 88 percent may be achieved.

## Stator Mechanical Design

Stator vane analysis was accomplished with the use of finite-element programs ISOBOSS and ISOVIBE for stress and vibration. The design point was 110-percent speed (20,240 rpm). No problems are predicted for the stator, either from a stress or vibration criterion. However, strain-gauge tests are required on the stator vanes to check the mechanical integrity of the system.

The stator vane maximum effective stress due to aerodynamic loading is at the trailing-edge outer ring with a value of

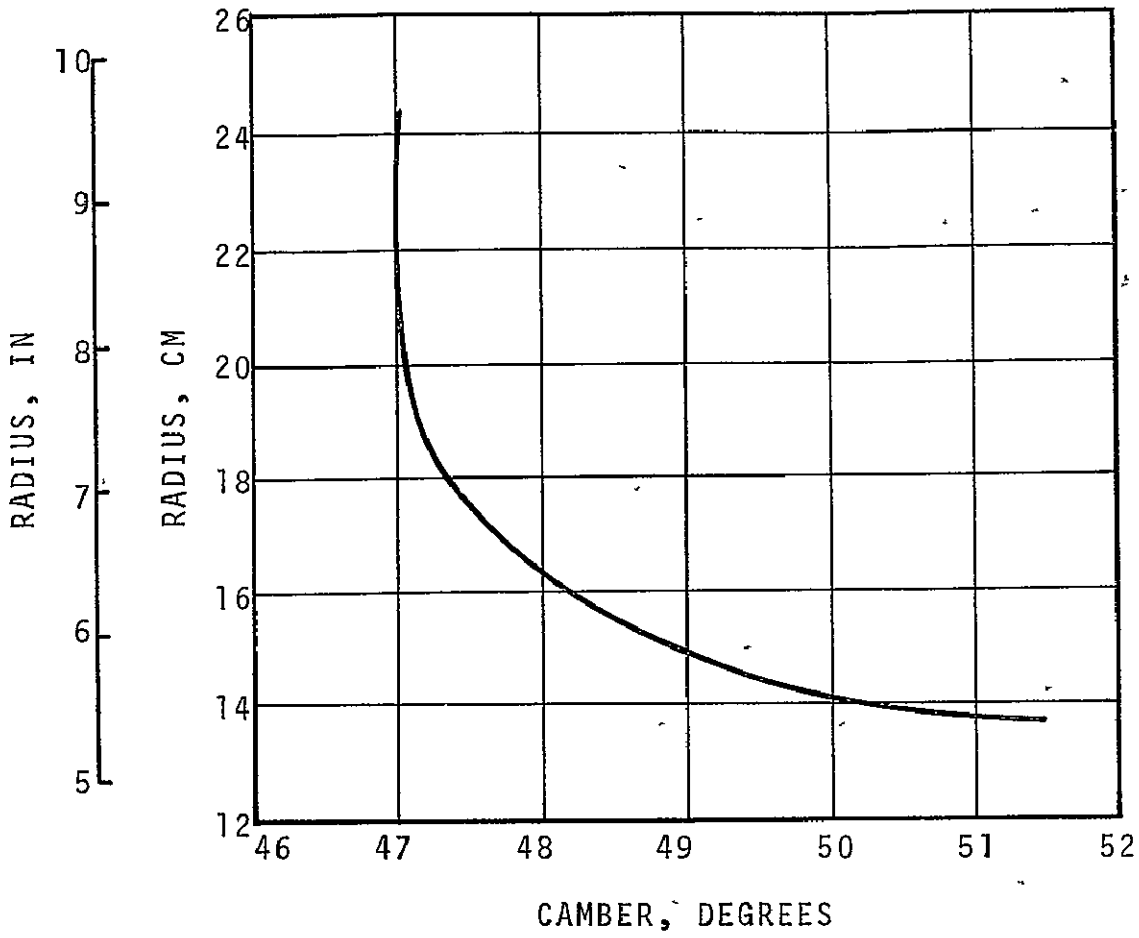


Figure 21. NASA 20-Inch Fan Stator Blade Camber Versus Radius.

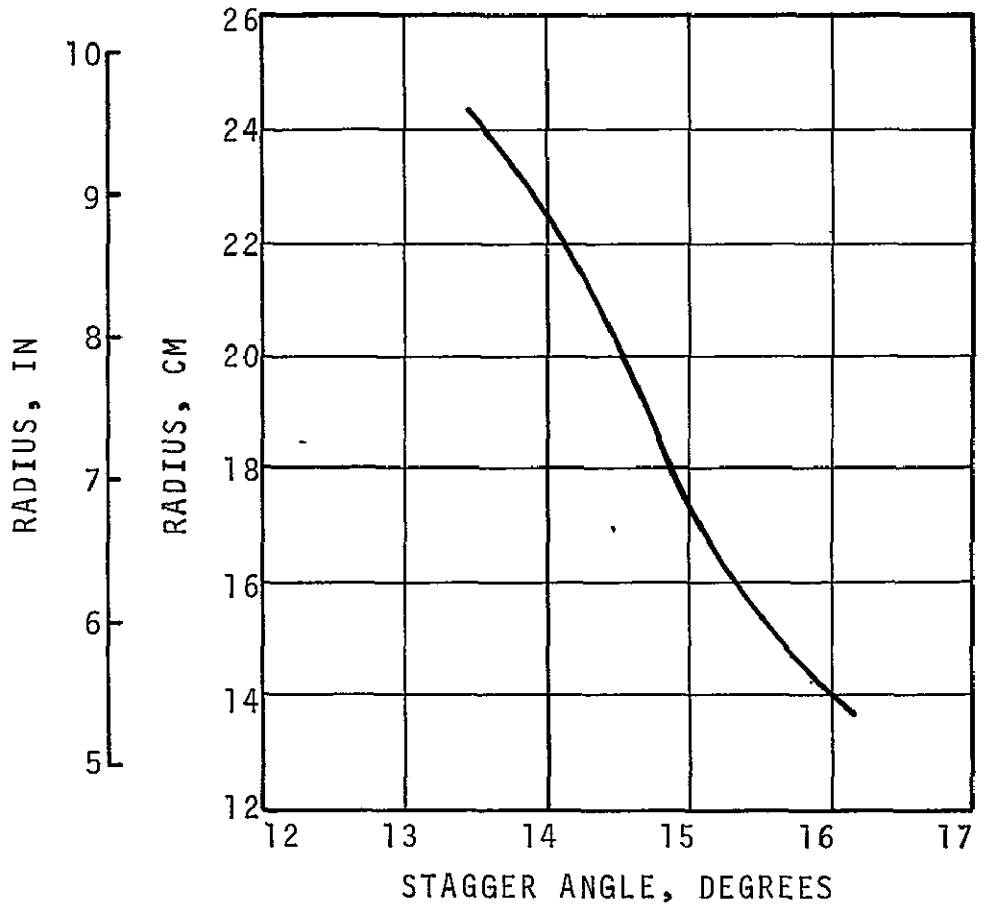


Figure 22. NASA 20-Inch Fan Stator Blade Stagger Angle Versus Radius.

455 x $10^6$ N/$m^2$ (66 ksi) and a margin of safety of 1.07 (see Figure 23). The actual maximum calculated stress in the stator is 66 ksi. Figure 23 was numbered by hand, not by the computer, and all numbers were rounded off in the critical element areas.

The flutter parameters and vane natural frequencies for the stator assemblies were calculated for two conditions. One condition occurs when the vanes vibrate independently, and the inner ring produces a near fixed condition on the vane boundaries. The other condition occurs when the vanes vibrate together as an assembly, which reduces the effective constraint to rotational fixity and allows the vanes to translate axially and tangentially at their inner boundary. The vane response is "bracketed" by these two boundary-condition assumptions, and the results are shown in Table 10 and Figures 24, 25, and 26. Flutter or interference of the vane higher modes with the fan blade count at high speeds is not indicated in these figures.

TABLE 10. STATOR VANE FLUTTER PARAMETER $\lambda = \frac{WC'}{V}$

| Inner Ring Rotational Constraint | First Flex | First Torsion |
|---|---|---|
| Outer ring fixed | 0.68 | 2.18 |
| Inner and outer ring fixed | 2.4 | 2.2 |
| Minimum allowable parameter | 0.33 | 1.6 |

Notes: W = frequency, rad/sec.

C' = chord length, ft

V = fluid velocity, ft/sec.

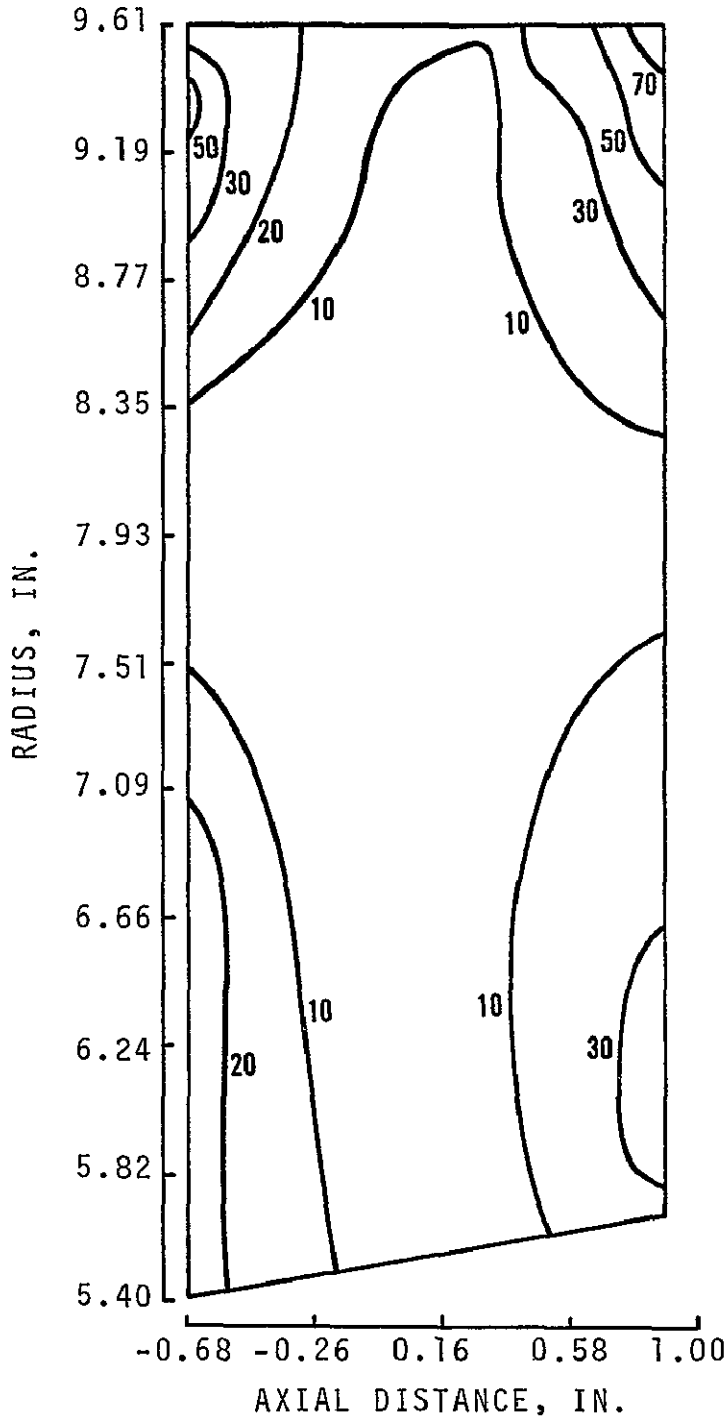


Figure 23. NASA 20-Inch Scaled Fan Stator, Effective Stress (ksi) Due to Aerodynamic Loads (Inner Ring Rotational Constraint on Vanes).

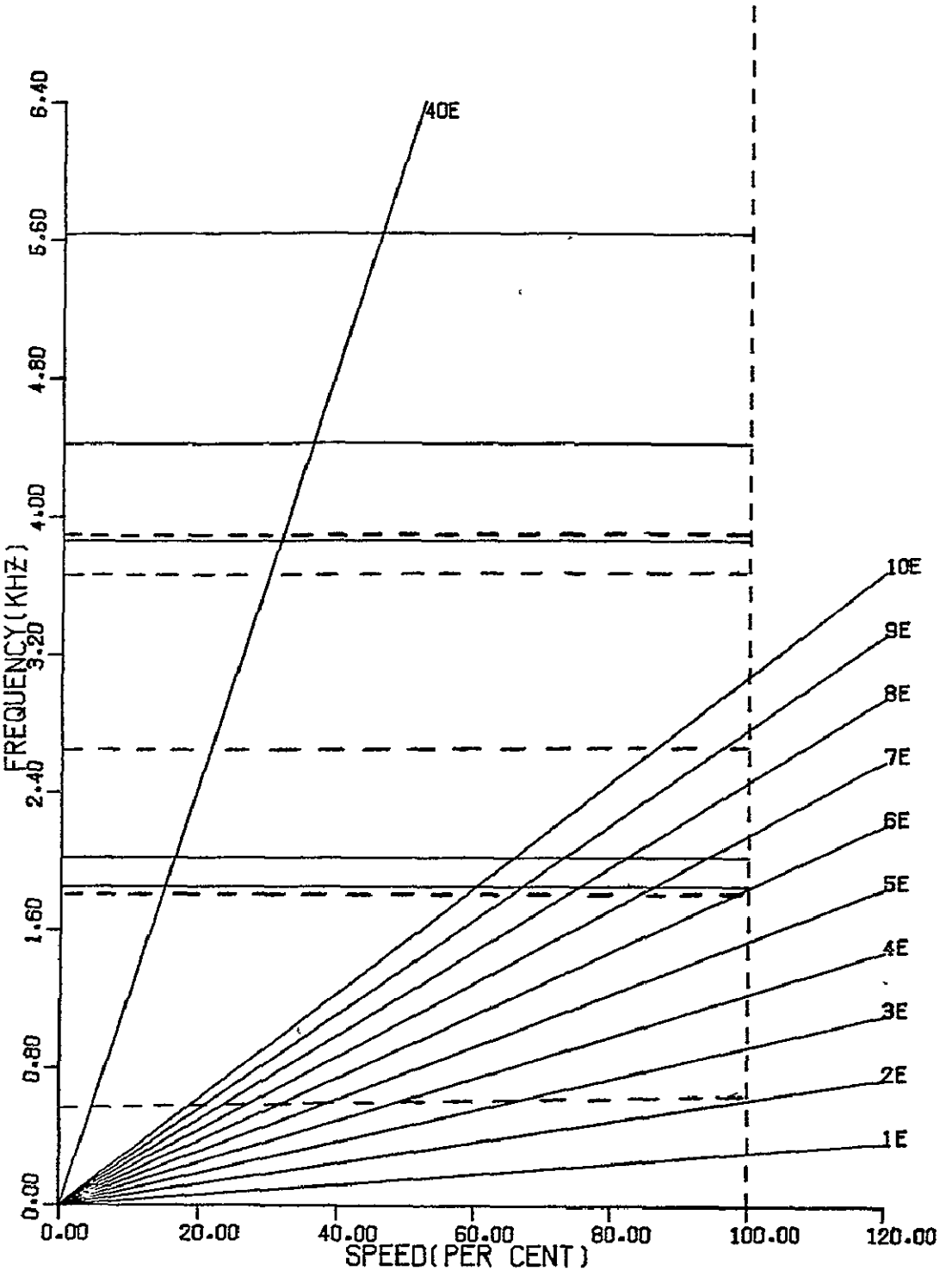


———INNER RING FIXED  100% RPM = 18,400
– – – –INNER RING ROTATIONAL CONSTRAINT ON VANES

Figure 24. NASA 20-Inch Scaled Fan Stator Vane Vibration Frequencies Interference Diagram.

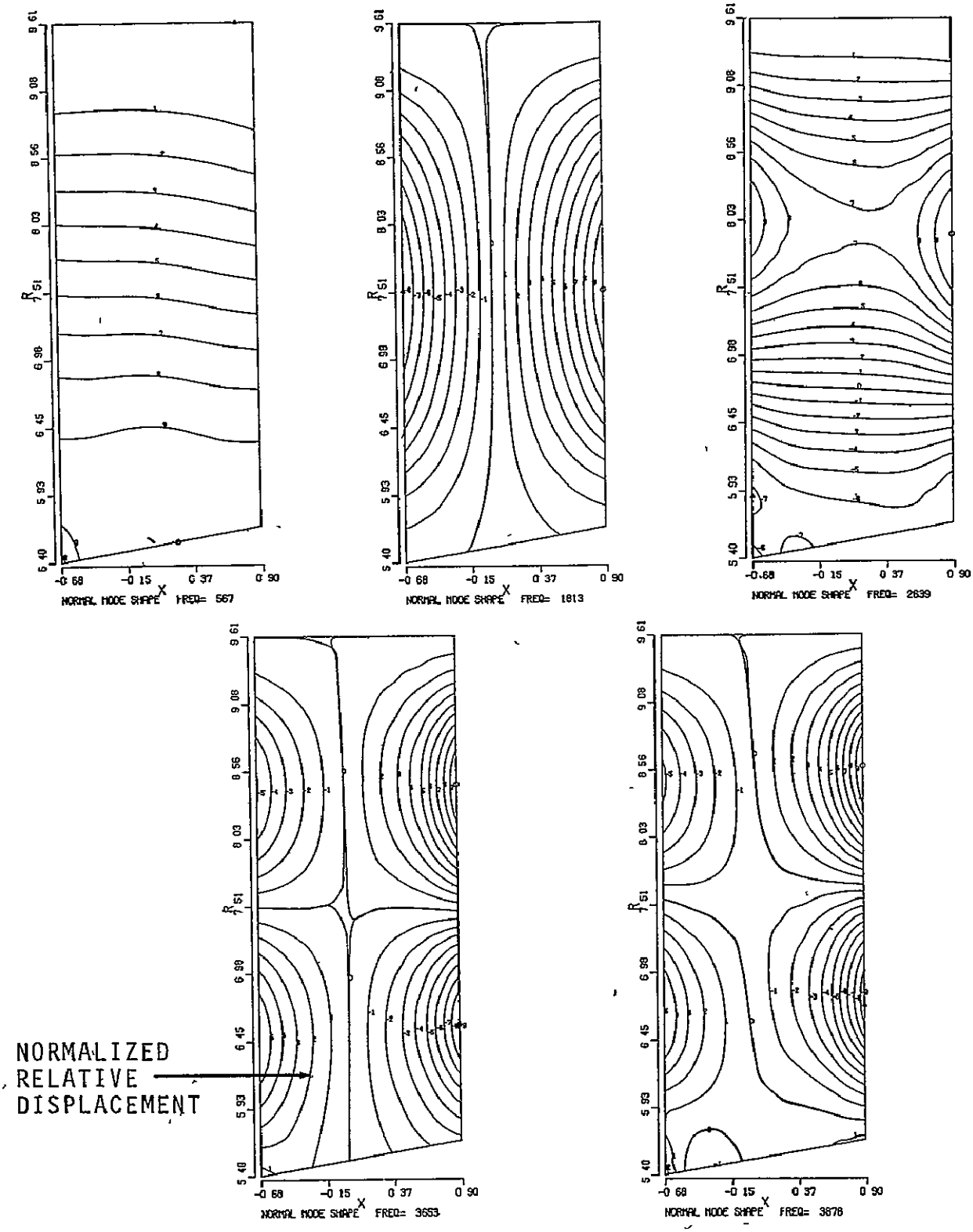


Figure 25. NASA 20-Inch Scaled Fan Normal Mode Shapes, Stator Vane Inner Ring Rotational Constraint on Vanes.

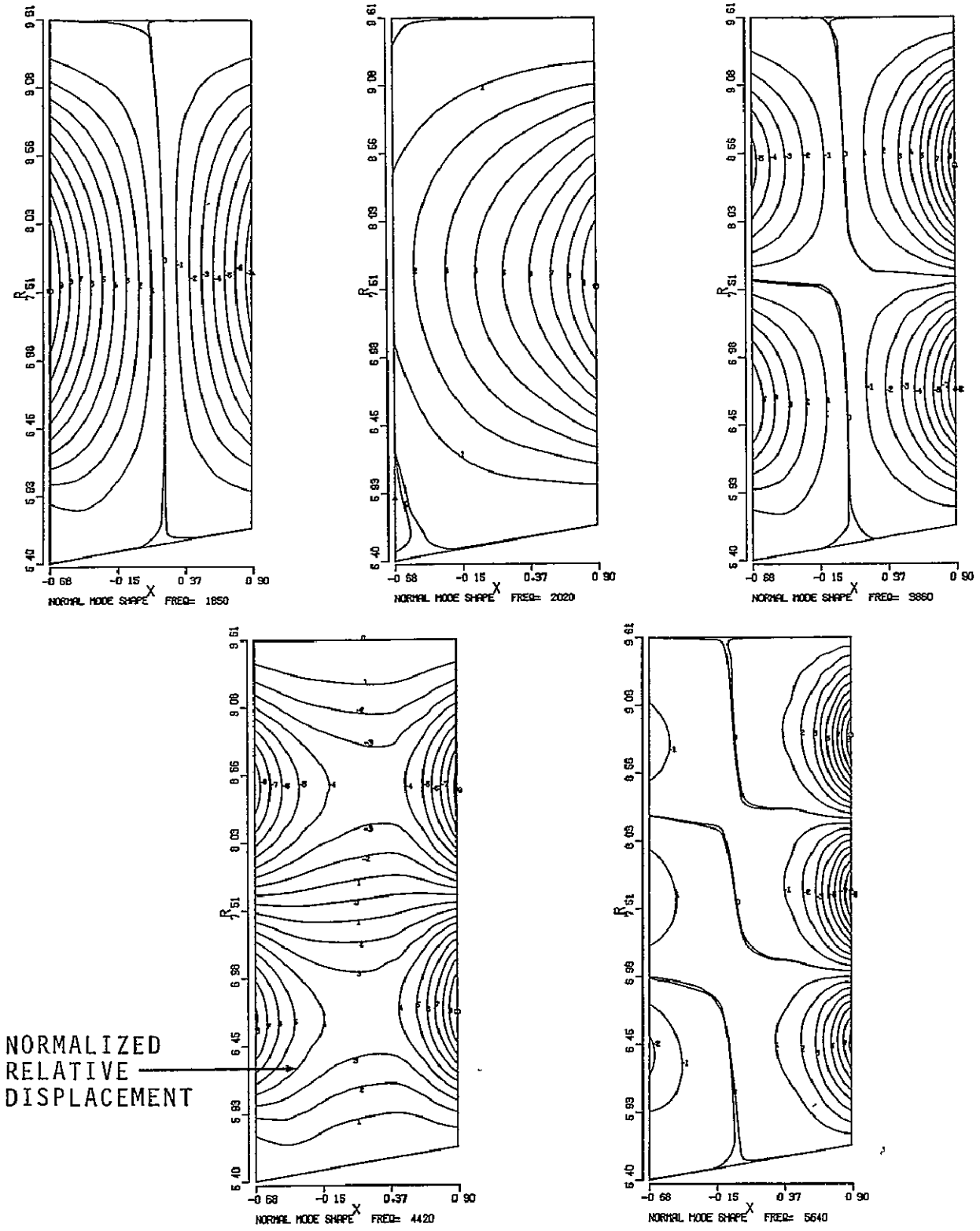


Figure 26. NASA 20-Inch Scaled Fan Normal Mode Shapes, Stator Vane Inner Ring Fixed.

## FAN RIG HARDWARE

The 20-inch fan rig hardware is shown in Figures 27 through 33. The hardware is comprised of two main groups -- the rotor group and the casing group. The rotor group, shown in Figures 27 through 29, consists of the disk, blades, spinner support (which also retains the blades in the disk when the rotor is mounted on the downstream face), spinner, and the separate blade retainer which is used when the rotor is mounted on the upstream face. The casing group, shown in Figures 30 through 33, consists of the main split casing, stator assembly, inner flow path barrel parts, stator spacers (used to position the stator assembly at various axial locations), inlet bellmouth, adapter housing, hub fairing, and various shims (used for setting axial and radial clearances when the rig is installed in the NASA test facilities).

The fan rig assembly is designed to be tested for acoustic evaluation in the NASA-LeRC Engine Fan and Jet Noise facility. The rotor group mounts on the electric motor drive shaft, and the casing mounts on the air collector duct system. The entire assembly (both rotor and casing groups) is reversible to allow either the inlet or exhaust ends of the assembly to face into the anechoic test chamber. In this way, both upstream and downstream propogated noise can be measured.

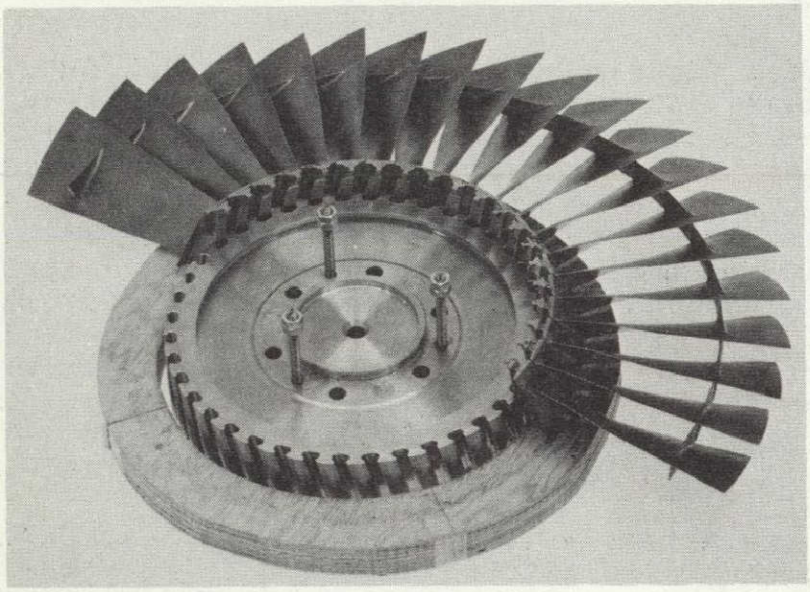

PARTIALLY ASSEMBLED

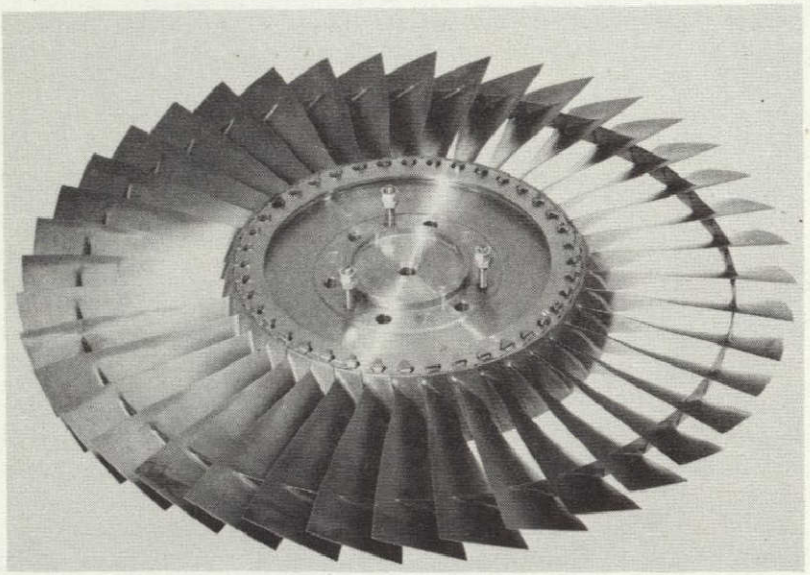

FULLY ASSEMBLED

Figure 27. Fan Rotor Disk and Blades.

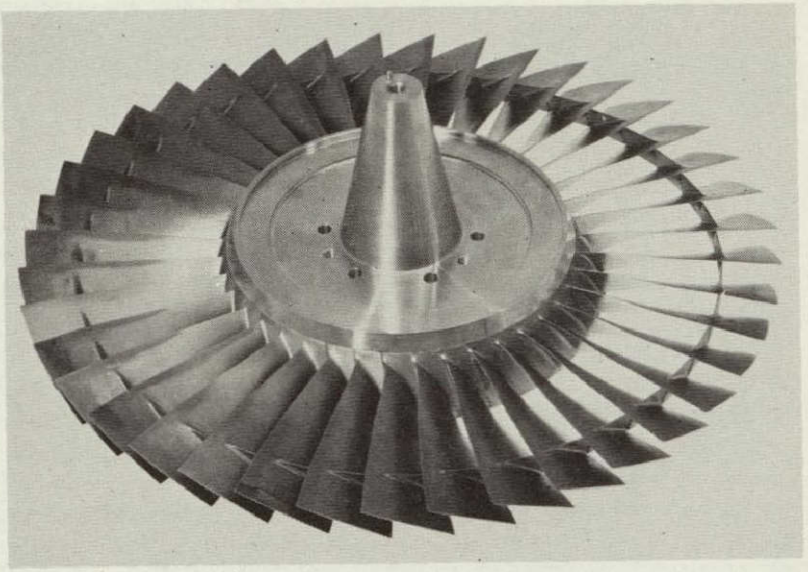

WITH SPINNER SUPPORT

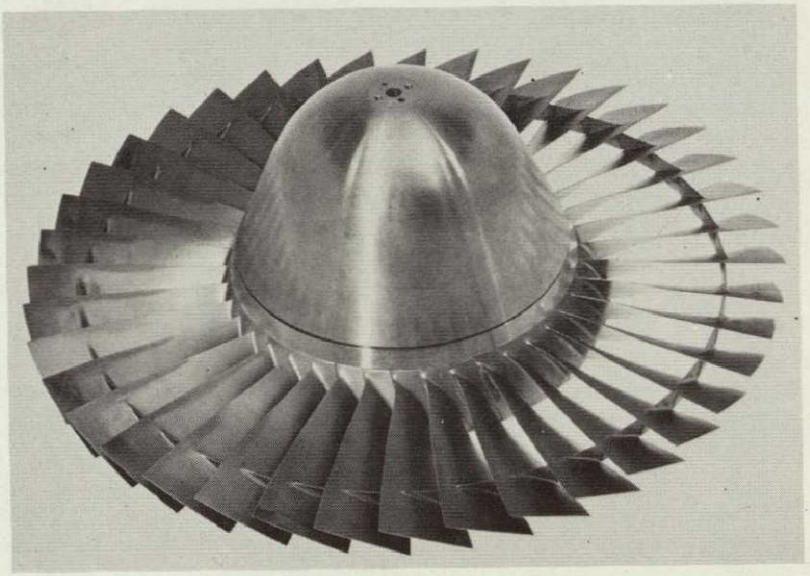

WITH SPINNER

Figure 28. Fan Rotor Assembly Used for Upstream Noise Investigation.

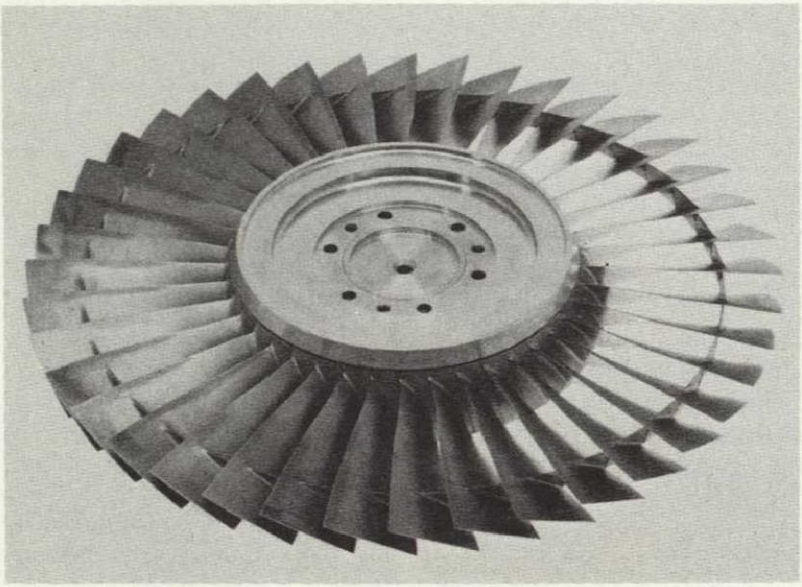

Figure 29. Fan Rotor Assembly with Blade Retainer (Used for Downstream Noise Investigation).

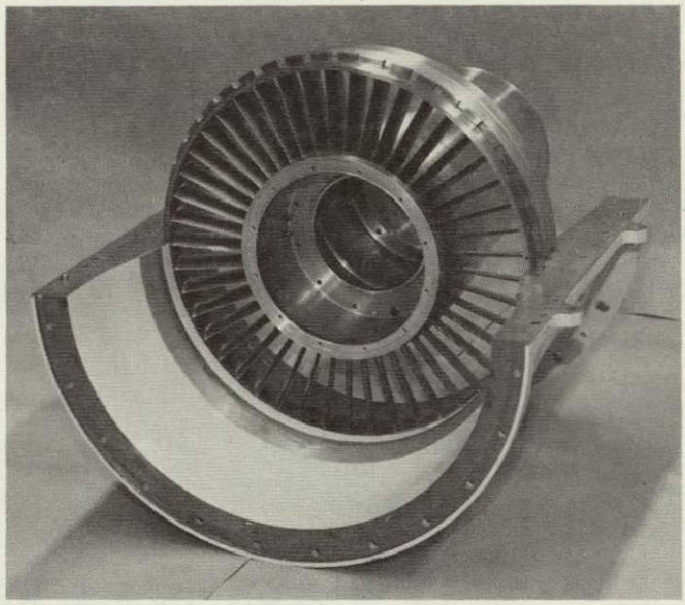

UPSTREAM VIEW

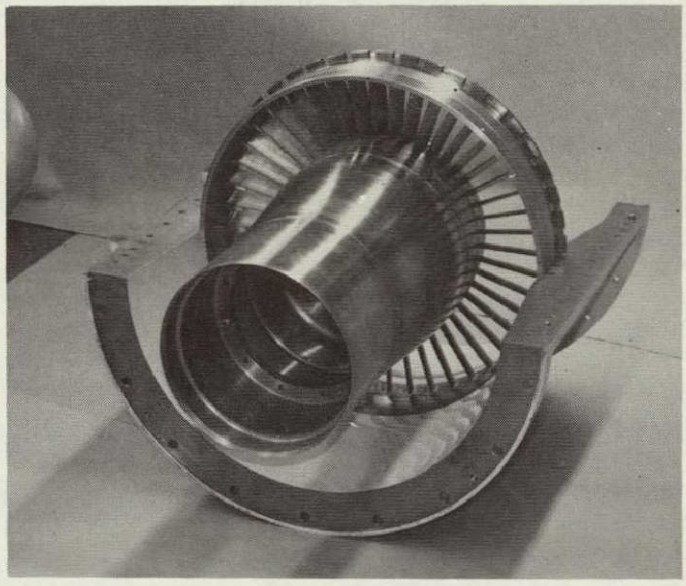

DOWNSTREAM VIEW

Figure 30. Split Casing with Stator Assembly, Stator Spacers, and Inner Flow Path Barrel.

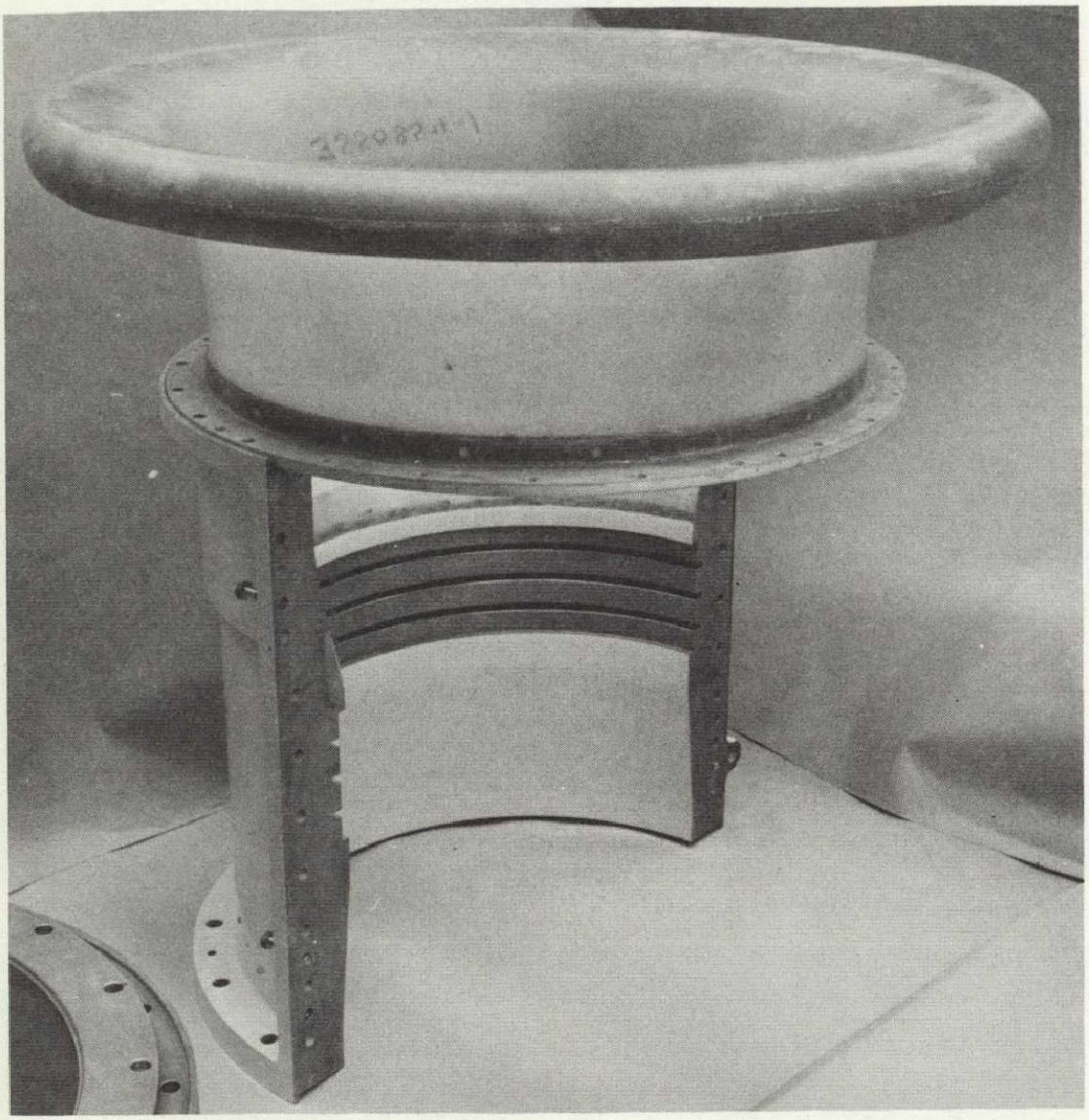

Figure 31. Split Casing with Inlet Bellmouth.

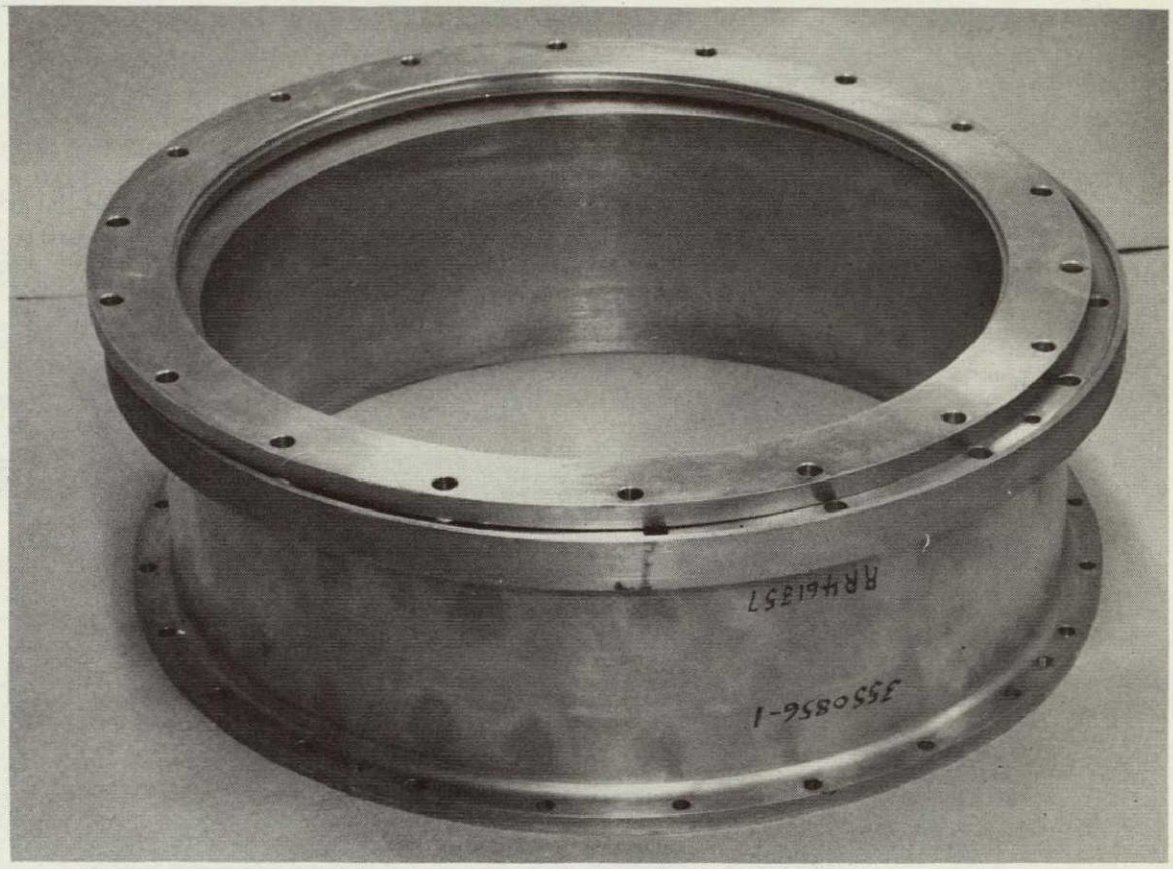


Figure 32. Adapter Housing and Tip Clearance Shim.

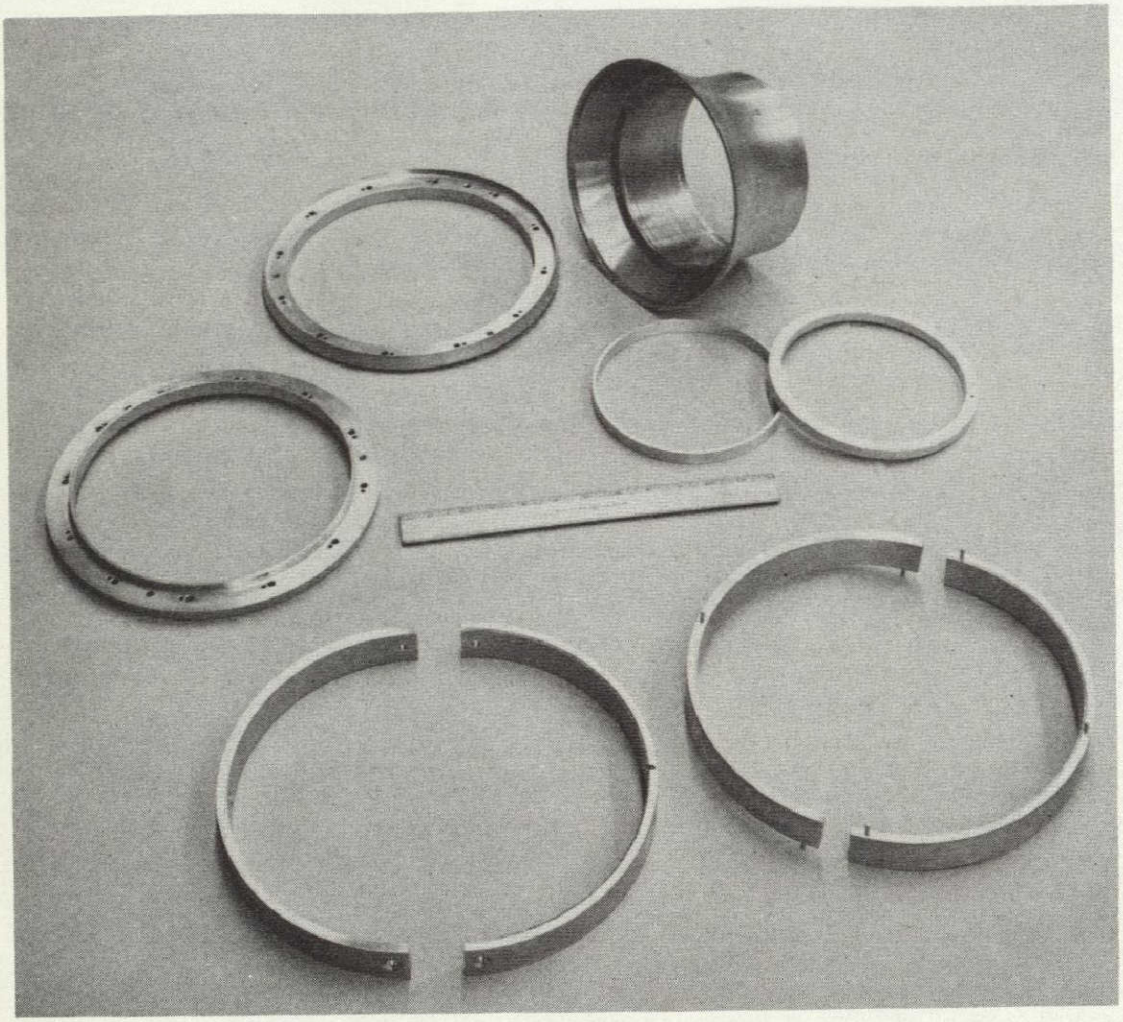

Figure 33. Hub Fairing, Shims and Stator Spacers.

## SCALED FAN BLADE VIBRATION TEST

The NASA scaled transonic fan rotor blade (20-inch tip diameter, Part 3550842) was salt-pattern and holography tested to determine its vibration modes and frequencies, and to compare that data with the calculated frequencies. The fan blade was tested with the mid-span damper free and fixed.

The testing showed that salt-pattern and holography results were not in complete agreement. A comparison of both test techniques with the analysis was required to determine the most probable modes of vibration. The calculated frequencies are considered to have as accurate a resolution as the test data. The predicted analytic interference diagrams of Figure 7 are still valid.

Table 11 presents a comparison between the test data and the analytic results. The salt-pattern tests were run on the small shake table, which is limited to a minimum exciting frequency of 238 Hz. This low frequency range prevented a check on the first flex for the free blade case. The second flex natural frequency was within 10 percent of the calculated values, but did not have enough strength to form a clean mode shape. The first torsion came in very clearly and was within 2 percent of the calculated value.

Salt-pattern test results with the mid-span damper fixed showed that the first flex was 2.3 percent below the calculated value and the second flex was 8.7 percent below the calculated results. The first torsion could not be excited. This may have been due to an interference from a higher frequency mode of approximately 5300 Hz. This mode was responding to a third harmonic excitation of the frequency expected to drive the first torsional mode. Holography testing was able to isolate the first flexural mode with the mid-span damper free, and indicated a 13-percent lower frequency than the calculated results. The first torsional mode, with the mid-span damper free, was within 1 percent of the calculated results. The tests utilizing a fixed mid-span damper were only able to isolate the torsional mode with holography testing. Figures 34 and 35 present the predominant mode shapes isolated by the test program.

TABLE 11.

FREQUENCY (HZ) WITH MID-SPAN DAMPER FIXED

| | 1st Flex | 1st Torsion | 2nd Flex |
|---|---|---|---|
| Calculated[1] | 888 | 1770 | 2290 |
| Salt Pattern | 868 | -- | 2090 |
| Hologram | -- | 1560 | -- |
| Difference[2] | -2.3% | -12% | -8.7% |

FREQUENCY (HZ) WITH MID-SPAN DAMPER FREE

| | 1st Flex | 1st Torsion | | 2nd Flex |
|---|---|---|---|---|
| Calculated[1] | 161 | 848 | | 673 |
| Salt Pattern | -- | 834 | | 607 |
| Hologram | 140 | | 854 | -- |
| Difference[2] | -13% | -1.7% | 0.7% | -10% |

NOTES: 1. Calculated with 3 nodes at mid-span damper location fixed in the plane normal to the blade.

2. Difference = $\frac{\text{Measured - Calculated}}{\text{Calculated}}$ in percent

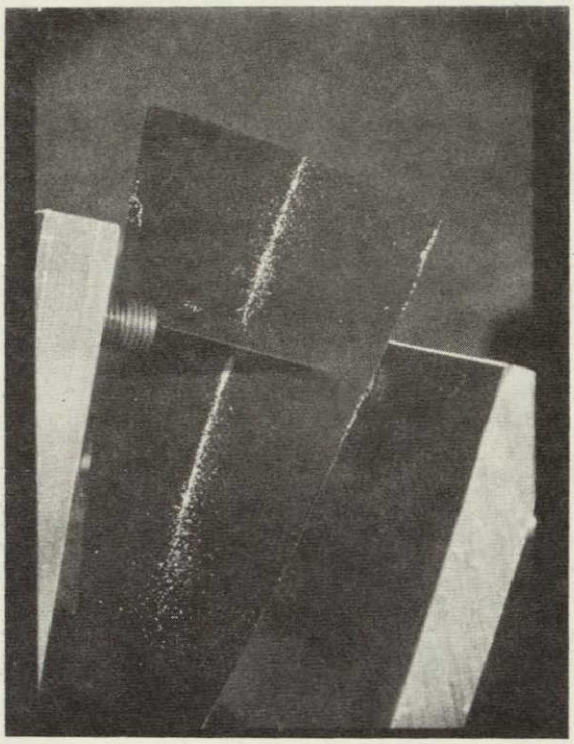

1ST TORSION 834 HZ
MID-SPAN DAMPER FREE

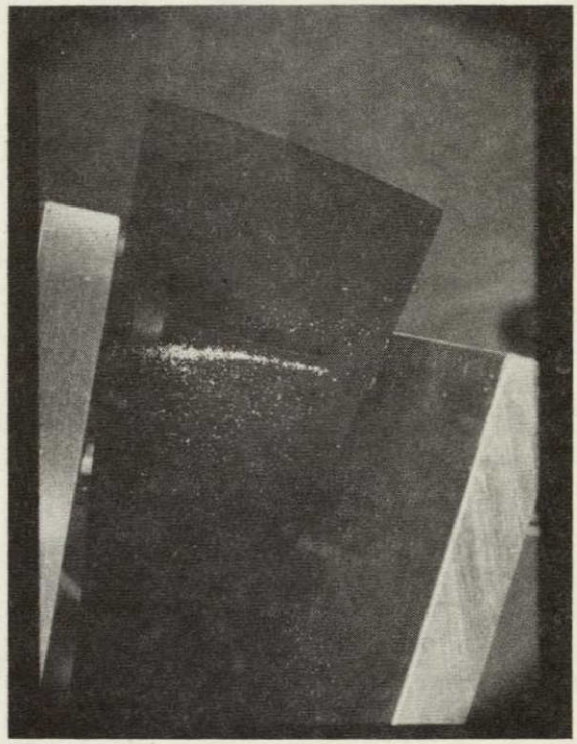

1ST FLEX 868 HZ
MID-SPAN DAMPER FIXED

2ND FLEX 2090 HZ
MID-SPAN DAMPER FIXED

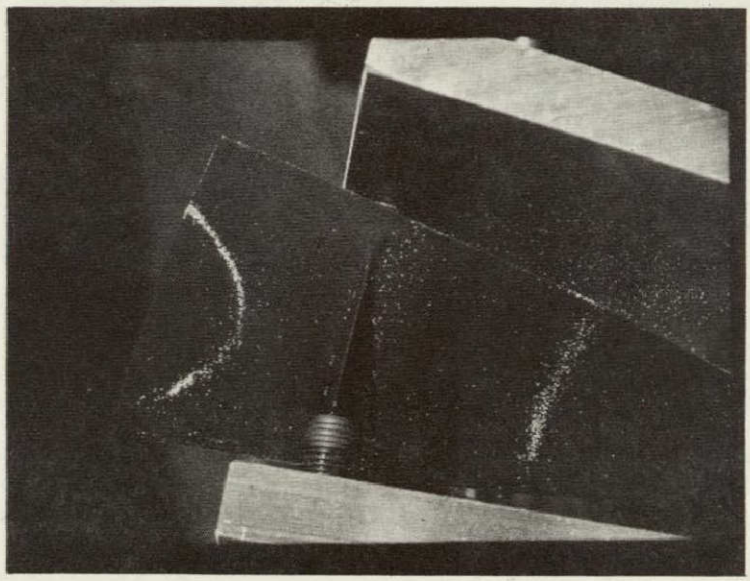

Figure 34. Salt-Pattern Test on Scaled NASA 20-Inch Fan.

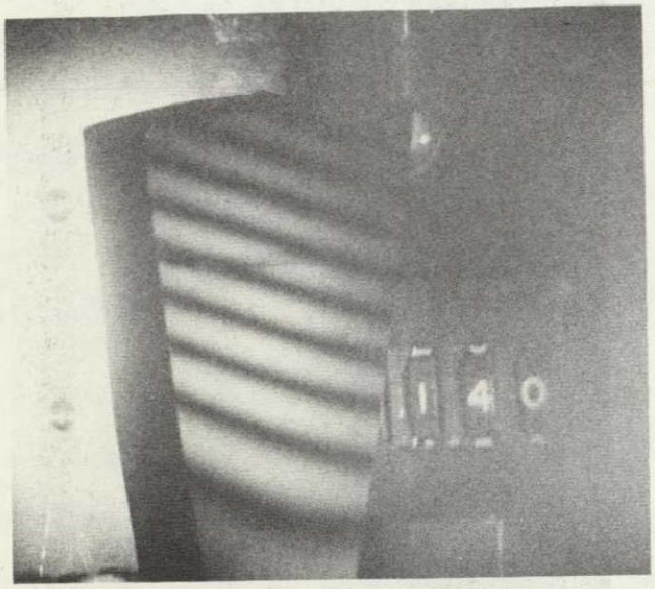


1st FLEX 140 HZ
MID-SPAN DAMPER FREE

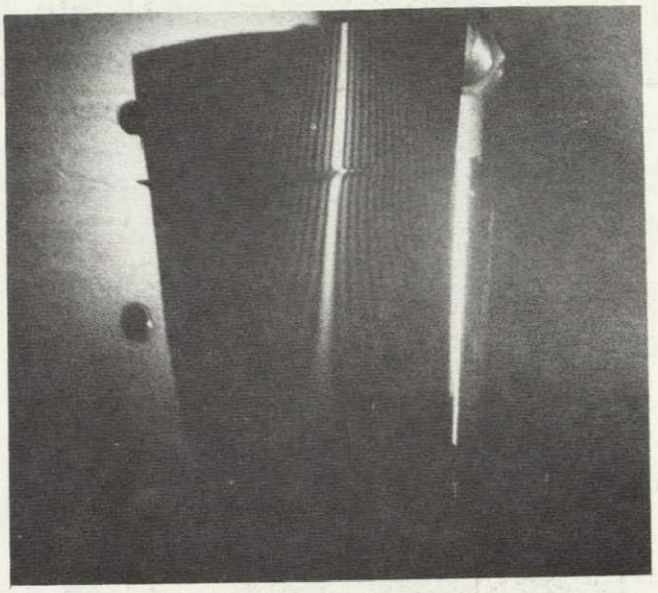

1ST TORSION 854 HZ
MID-SPAN DAMPER FREE

1ST TORSION 1560 HZ
MID-SPAN DAMPER FIXED

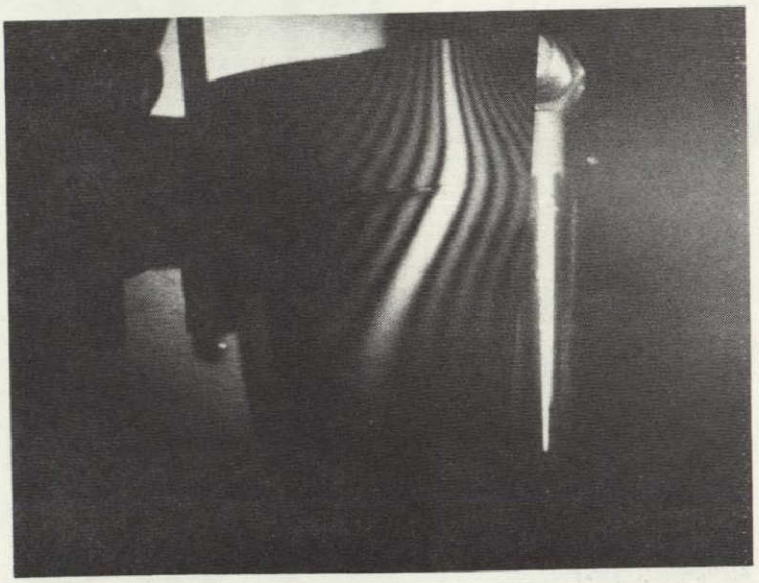

Figure 35. Holography Test on Scaled NASA 20-Inch Fan.

## ROTOR SPIN-PIT TEST

A spin-pit test was conducted with the strain gauge instrumented rotor to verify the design analysis reported in Reference 1. This test was not a requirement of the program, but was conducted as a part of a U.S. Air Force program underway at AiResearch as a convenience to AiResearch, and for the mutual benefit of NASA and the Air Force. Under USAF Aero Propulsion Laboratory (AFAPL) Contract F33615-74-C-2012, AiResearch is developing computer programs for the computation of stresses in turbine engine disks and blades. The AFAPL contract requires that the analytical work be verified by spin tests of fan and/or turbine rotor assemblies. Therefore, since the NASA 20-inch fan represents an advanced design suitable for such verification tests, and was to be instrumented with strain gauges for NASA, permission was requested of NASA and AFAPL to use that fan for the Air Force Program verification tests. Permission was granted by both agencies. Specifically, the spin-pit test sought to determine whether yield would occur at the 100- and/or 122-percent speed conditions (predicted yield under pessimistic material and temperature estimates).

Figure 36 shows the aft side of the bladed disk used in the whirlpit testing. The assembly was mounted horizontally in the whirlpit at the AiResearch, Phoenix, Stress Laboratory.

As recommended by the Stress Measurement Plan in Appendix A, eight strain gauges were used to monitor airfoil strain. Figure 37 identifies gauge locations. Gauge placement was selected from calculated stress distributions. Figures 38 through 41 show the actual gauge installations. Strain gauge leads were routed along the base of the airfoil to the aft edge of the platform, through a notch in the platform, and down the blade shank to junctions on the aft face of the attachment (Figure 42 shows this arrangement).

The leads connecting the junctions on the blade with those on the disk are configured to permit relative motion between the disk and an inserted blade. This arrangement, shown in Figure 42, produced satisfactory results in most cases. A slip-ring assembly is used to pass the strain gauge data to the readout equipment.

Digital strain and speed data were recorded on paper tape for later conversion to punched cards. These cards serve as input to automatic data reduction computer programs.

The bladed disk was subjected to four accel/decel cycles, achieving overspeed on the fourth cycle. Table 12 shows the rotor speeds at which data was obtained. At each speed indicated in the table, rotor speed was stabilized, and three readings were taken from each gauge. Care was taken to avoid cycling the rotor speed when stabilizing for a line of data.

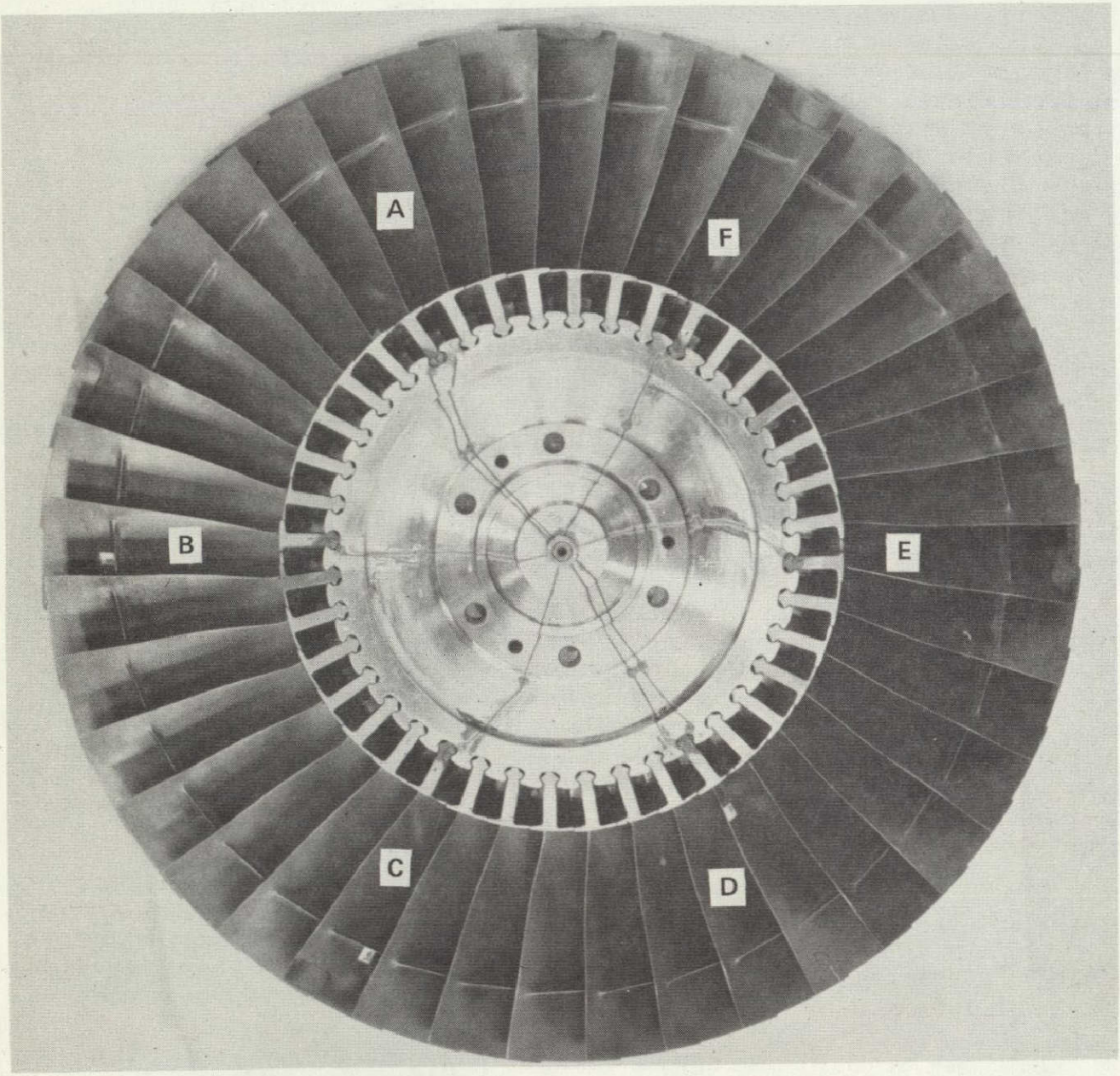


Figure 36. Aft Side of the Fan Rotor Assembly Used During Spin-Pit Testing.

| GAUGE NO. | BLADE* | SIDE |
|---|---|---|
| 1 | A | PRESSURE |
| 2 | A | SUCTION |
| 3 | D | PRESSURE |
| 4 | D | SUCTION |
| 5 | B | PRESSURE |
| 6 | C | PRESSURE |
| 7 | E | PRESSURE |
| 8 | F | PRESSURE |

MATERIAL 90Ti-6Al-4V

*REFER TO FIGURE 36 FOR BLADE LOCATIONS.

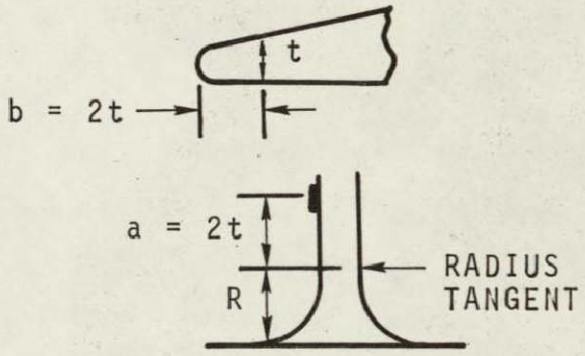


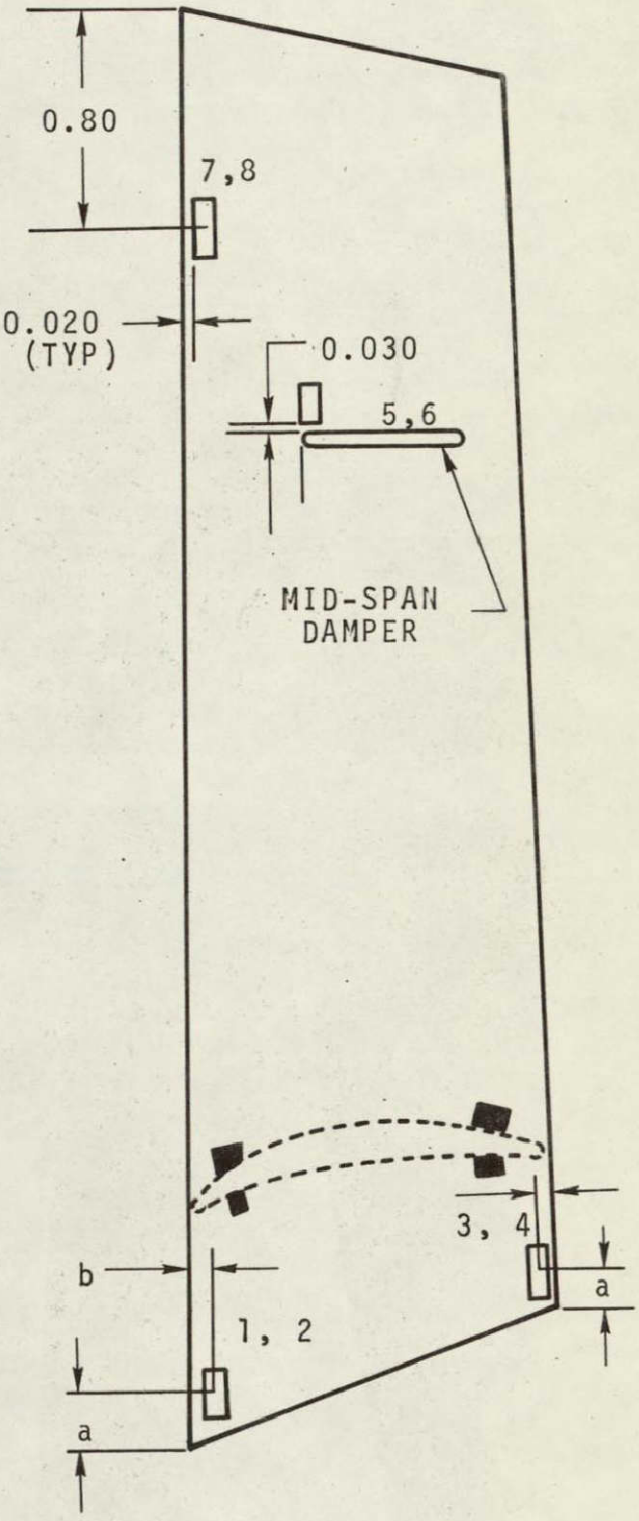


Figure 37. NASA 20-Inch Scaled Fan Blade Strain Gauge Locations.

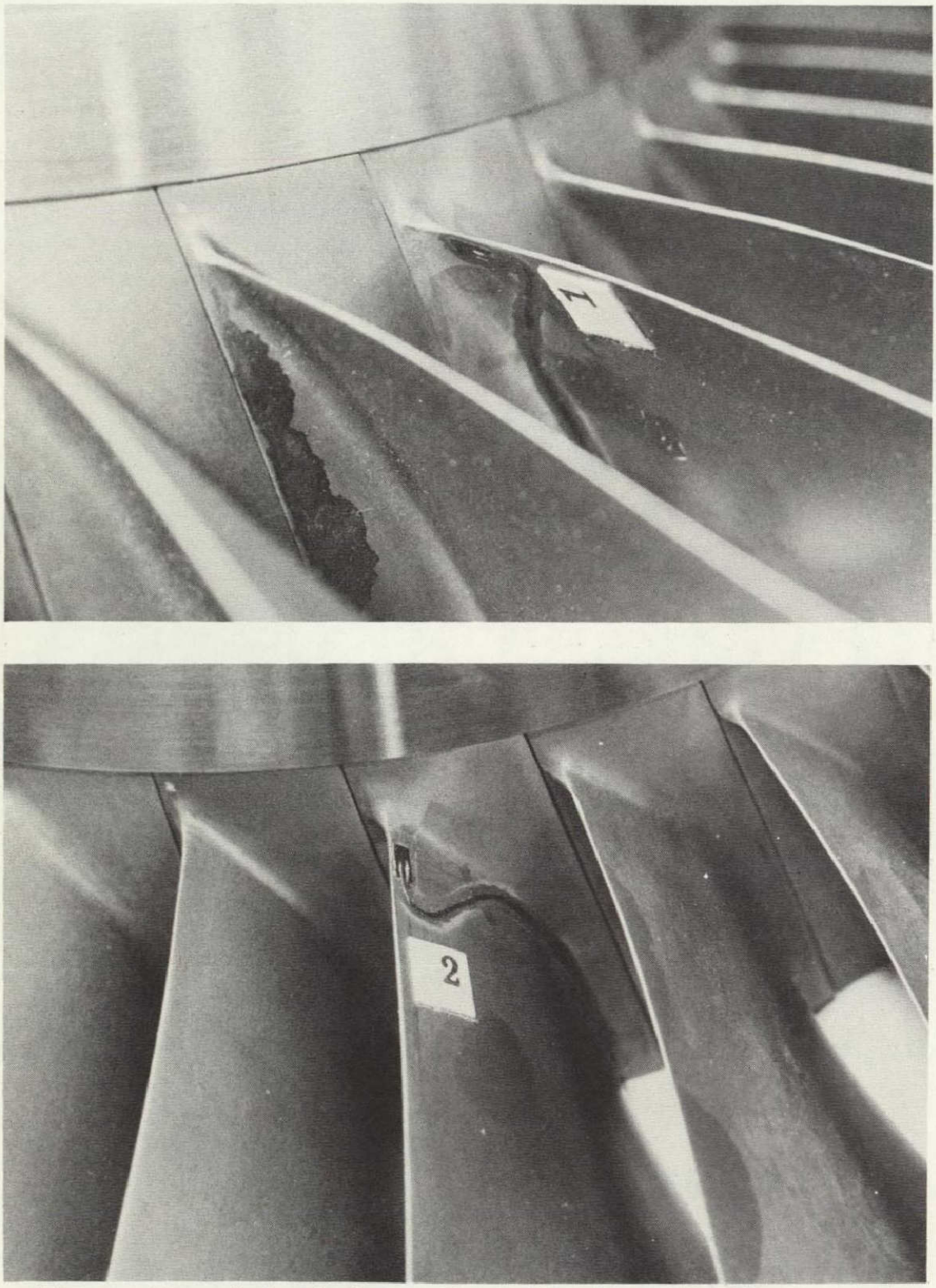


Figure 38. Actual Gauge Installation Locations on the 20-Inch Fan Rotor Disk and Blades.

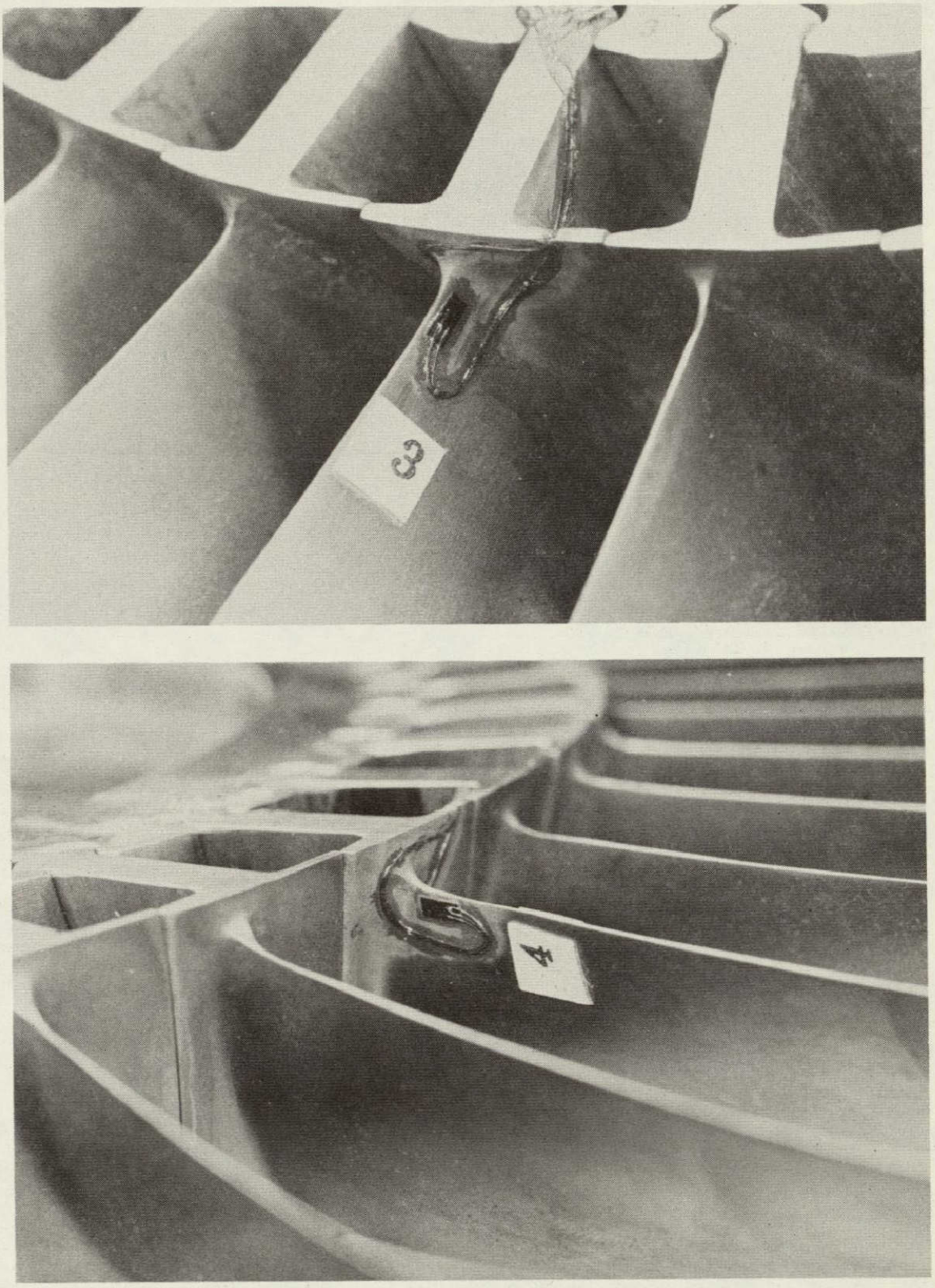


Figure 39. Actual Gauge Installation Locations on the 20-Inch Fan Rotor Disk and Blades.

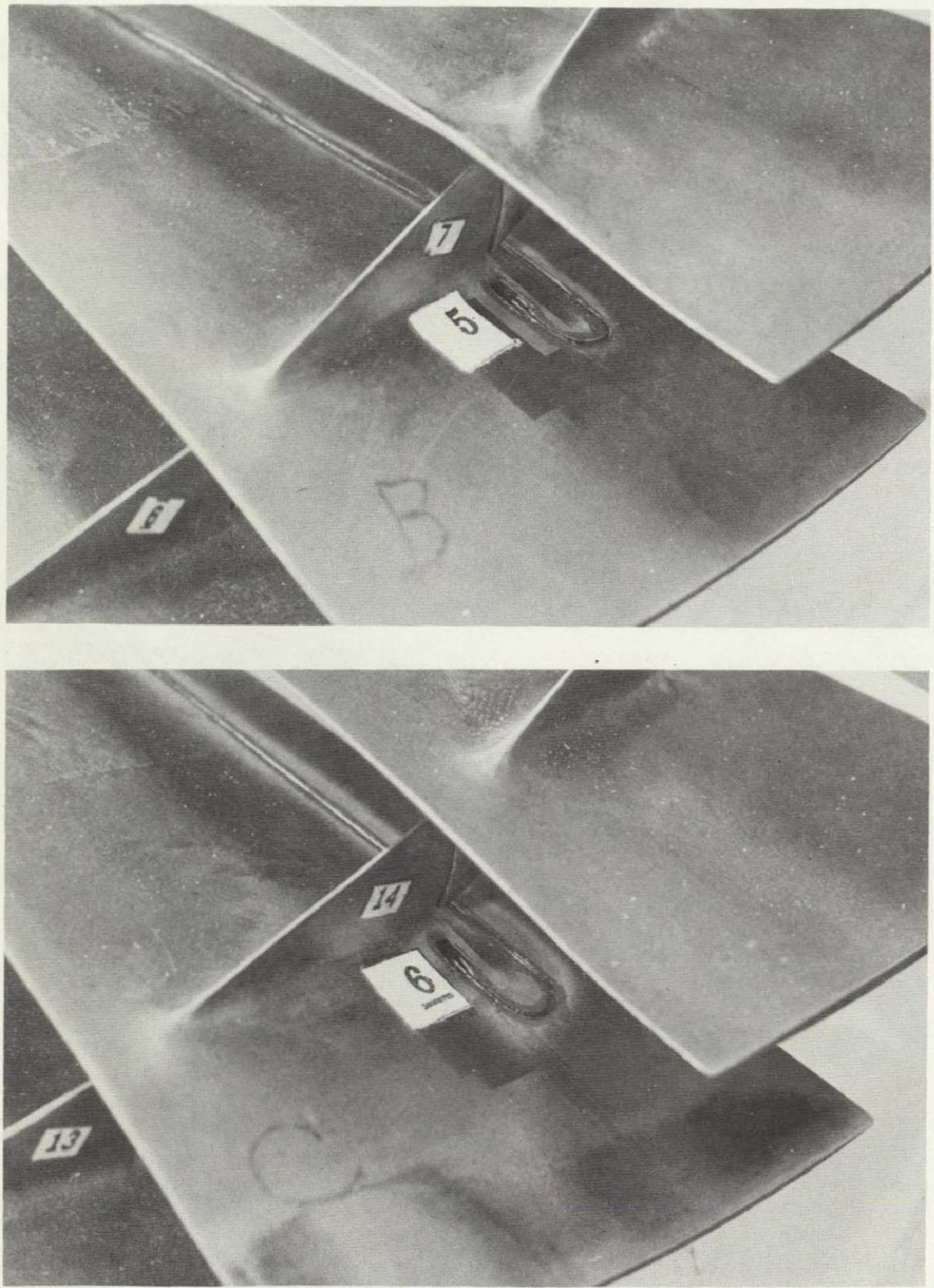


Figure 40. Actual Gauge Installation Locations on the 20-Inch Fan Rotor Disk and Blades.

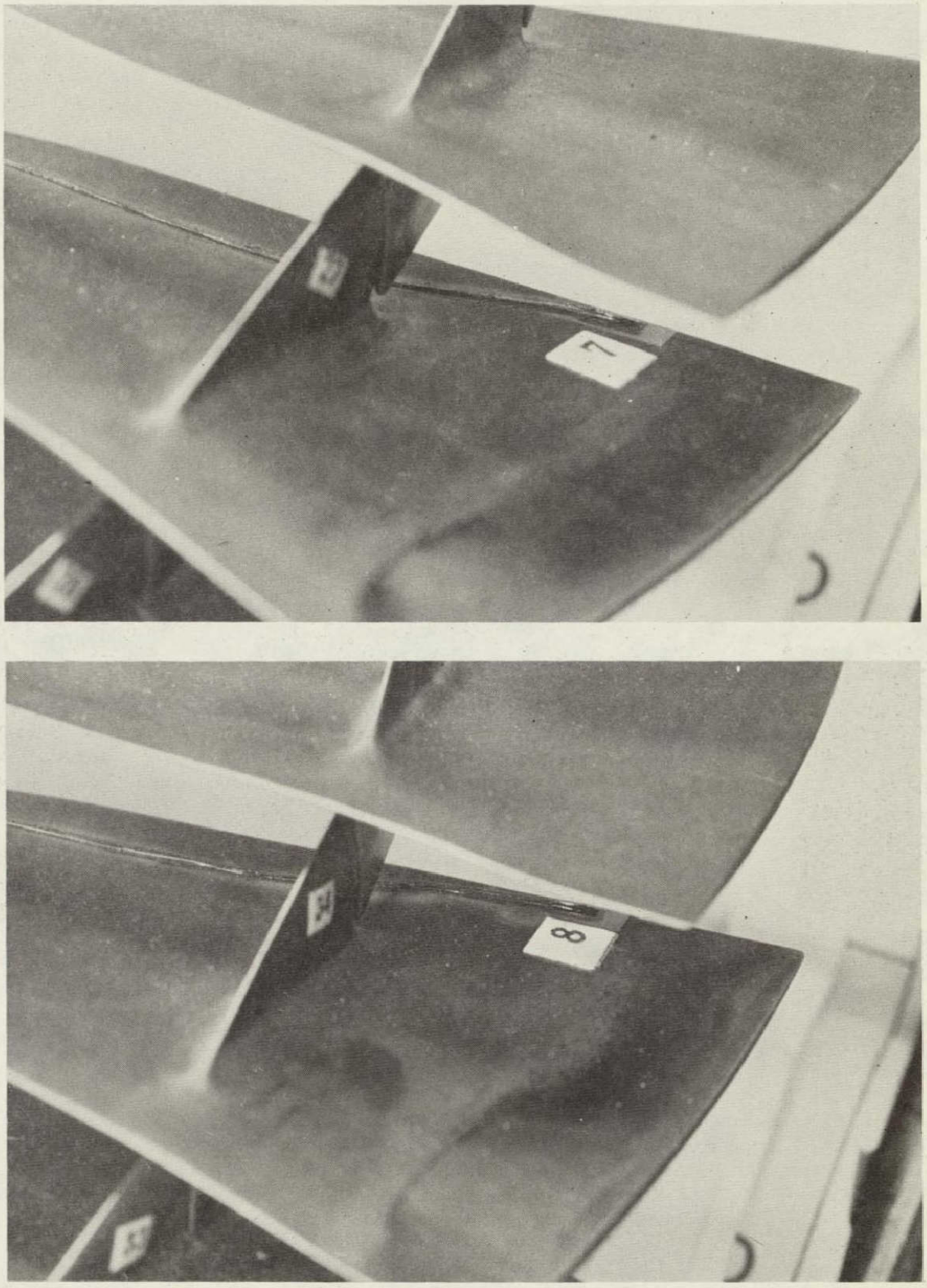


Figure 41. Actual Gauge Installation Locations on the 20-Inch Fan Rotor Disk and Blades.

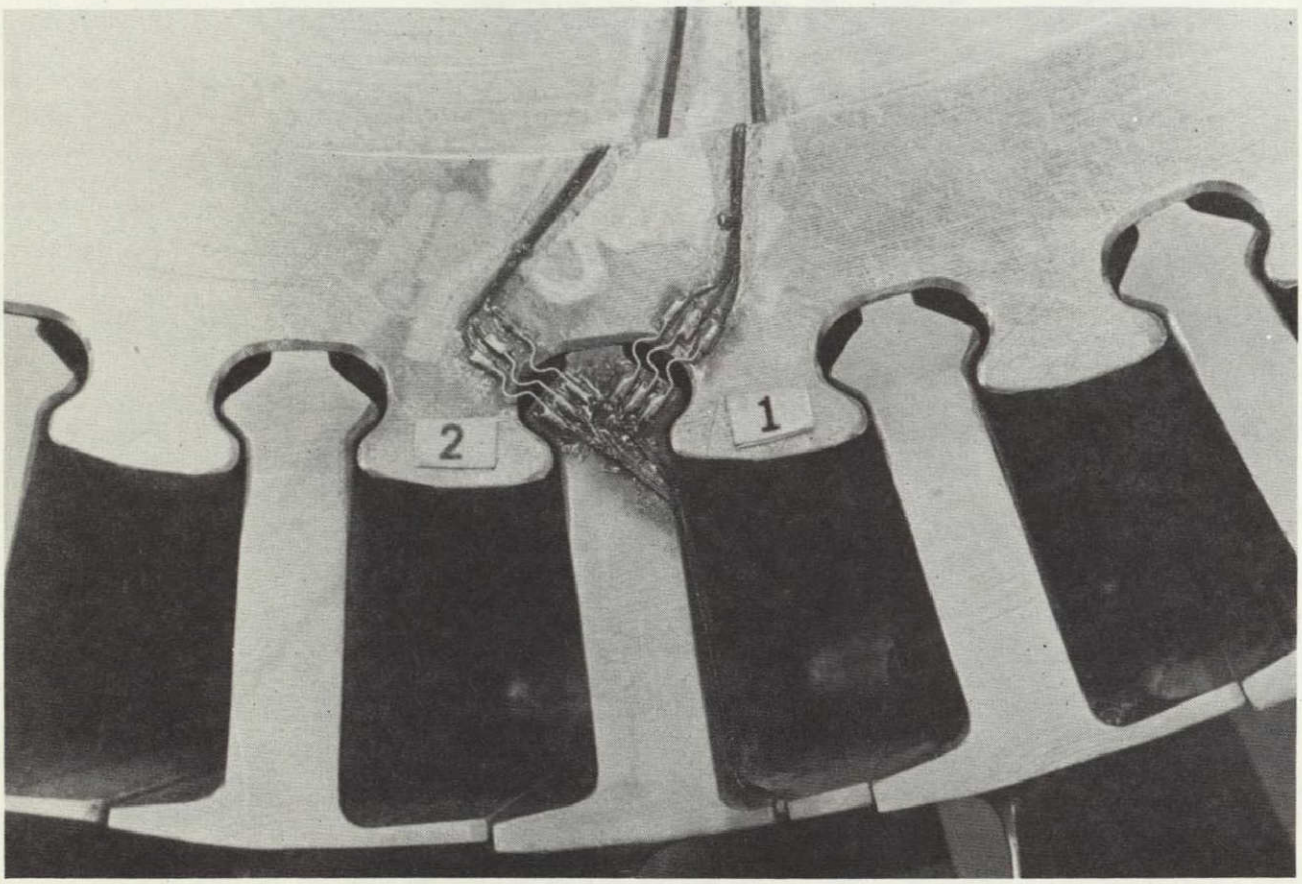


Figure 42. View of the Leads Connecting the Junctions on the Blade with Those on the Disk on the 20-Inch Fan Rotor.

TABLE 12. NASA 20-INCH SCALED FAN BLADE SPIN-PIT STRAIN GAUGE TEST POINTS.

| | Percent Load | ±10 RPM Speed | Run 1 | Run 2 | Run 3 | Run 4 |
|---|---|---|---|---|---|---|
| ACCEL | 0 | 500 | △ | △ | △ | △ |
| | 10 | 5,800 | △ | | | |
| | 20 | 8,200 | △ | △ | | △ |
| | 30 | 10,040 | △ | | | |
| | 40 | 11,600 | △ | △ | △ | △ |
| | 50 | 12,960 | △ | | | |
| | 60 | 14,200 | △ | △ | △ | △ |
| | 70 | 15,340 | | △ | | |
| | 80 | 16,400 | | △ | △ | △ |
| | 90 | 17,400 | | | △ | △ |
| | 100 | 18,330 | | | △ | △ |
| | 148 | 22,300 | | | | △ |
| DECEL | 100 | 18,330 | | | | △ |
| | 90 | 17,400 | | | △ | △ |
| | 80 | 16,400 | | | △ | △ |
| | 70 | 15,340 | | △ | | |
| | 60 | 14,200 | | △ | △ | △ |
| | 50 | 12,960 | △ | | | |
| | 40 | 11,600 | △ | △ | △ | △ |
| | 30 | 10,040 | | | | |
| | 20 | 8,200 | △ | △ | | △ |
| | 10 | 5,800 | | | | |
| | 0 | 500 | △ | △ | △ | △ |

Table 13-A through 13-H present the strain data obtained during the test. Each entry in the tables is the average of three readings taken from each gauge at each speed point. Examination of the raw data showed little variation among the three data samples. Gauges 1 and 2 (leading-edge root) show the only clear evidence of permanent set. Gauge 1 (pressure side) sustained a permanent set of 580 micro-inches/inch following the overspeed test. For Gauge 2 (suction side), the permanent set was 930 micro-inches/inch. Gauge 5 provided a final reading of 120 micro-inches/inch, but this is due to improper zeroing of the bridge circuit following Run 3.

In general, the gauges showed a residual strain following each run. Except for the permanent set on Gauges 1 and 2 discussed above, these residuals are not indicative of a true strain. Strain gauges often experience a "break-in" phenomenon during the first cycle or two, in which the adhesive rearranges itself slightly. This can produce a false compressive residual strain of small (but measurable) magnitude. Instrument drift can also cause small residuals. To minimize the influence of these phenomena, the bridge circuit should be zeroed prior to every run.

Figures 43 through 45 are plots of strain versus speed squared (proportional to load) for Gauges 1 through 3. The data used for these plots was the second of three data samples obtained for each speed point. This data was obtained from Run 4, which featured overspeed running. These plots show that the relationship was linear prior to overspeed. At some speed, between 100 and 122 percent, the material in the leading-edge root area experienced plastic deformation. This is clearly indicated by the permanent set displayed by the strain data.

Tables 13-A through 13-H show good reproducibility of strain data between the accel and decel phases of the tests, with three exceptions. Two of these exceptions involve permanent set at the leading edge root, as discussed above. The third exception, shown in Figure 45, is not well understood. Gauge 3 did not show close agreement in accel and decel phases of Run 4, although no evidence of permanent deformation was noted from the residual strain.

The results of the fan blade design analysis were based on 3σ minimum properties at 250°F. The assumed yield strength was 689 x $10^6$ N/$m^2$ (100 ksi). This corresponds to 122-percent speed. The test hardware, operating at a lower temperature (100° to 150°F) should have been free of yield to even higher speeds, but this is not the case. Substantial yielding occurred between 100- and 122-percent speed.

TABLE 13-A. NASA 20-INCH SCALED FAN BLADE SPIN-PIT STRAIN GAUGE TEST DATA.

| Gauge No. 1 | | | Strain (Micro-Inches/Inch) | | | |
|---|---|---|---|---|---|---|
| | Percent Load | Speed RPM | Run 1 | Run 2 | Run 3 | Run 4 |
| ACCEL | 0 | 500 | 0 | 0 | 0 | 0 |
| | 10 | 5,800 | 430 | | | |
| | 20 | 8,200 | 930 | 1,000 | | 1,040 |
| | 30 | 10,040 | 1,440' | | | |
| | 40 | 11,600 | 1,940 | 1,970 | 2,010 | 2,040 |
| | 50 | 12,960 | 2,430 | | | |
| | 60 | 14,200 | 2,930 | 2,960 | 3,000 | 3,030 |
| | 70 | 15,340 | | 3,450 | | |
| | 80 | 16,400 | | 3,940 | 3,980 | 4,000 |
| | 90 | 17,400 | | | 4,490 | 4,490 |
| | 100 | 18,330 | | | 4,970 | 4,980 |
| | 148 | 22,300 | | | | 8,020 |
| DECEL | 100 | 18,330 | | | | 5,700 |
| | 90 | 17,400 | | | 4,500 | 5,160 |
| | 80 | 16,400 | | | 4,050 | 4,580 |
| | 70 | 15,340 | | 3,470 | | |
| | 60 | 14,200 | | 2,960 | 2,920 | 3,450 |
| | 50 | 12,960 | 2,470 | | | |
| | 40 | 11,600 | 1,920 | 1,870 | 1,820 | 2,420 |
| | 30 | 10,040 | | | | |
| | 20 | 8,200 | 810 | 760 | | 1,530 |
| | 10 | 5,800 | | | | |
| | 0 | 500 | -50 | -10 | -20 | 580 |

NOTE: All strains are an average of three readings at each speed point.

TABLE 13-B. NASA 20-INCH SCALED FAN BLADE SPIN-PIT STRAIN GAUGE TEST DATA.

| Gauge No. 2 | | | Strain (Micro-Inches/Inch) | | | |
|---|---|---|---|---|---|---|
| | Percent Load | Speed RPM | Run 1 | Run 2 | Run 3 | Run 4 |
| ACCEL | 0 | 500 | 0 | 0 | 0 | 0 |
| | 10 | 5,800 | 520 | | | |
| | 20 | 8,200 | 1,060 | 1,100 | | 1,160 |
| | 30 | 10,040 | 1,600 | | | |
| | 40 | 11,600 | 2,140 | 2,180 | 2,220 | 2,240 |
| | 50 | 12,960 | 2,670 | | | |
| | 60 | 14,200 | 3,220 | 3,230 | 3,270 | 3,300 |
| | 70 | 15,340 | | 3,750 | | |
| | 80 | 16,400 | | 4,280 | 4,320 | 4,350 |
| | 90 | 17,400 | | | 4,870 | 4,850 |
| | 100 | 18,330 | | | 5,400 | 5,370 |
| | 148 | 22,300 | | | | 8,990 |
| DECEL | 100 | 18,330 | | | | 6,580 |
| | 90 | 17,400 | | | 4,880 | 6,040 |
| | 80 | 16,400 | | | 4,370 | 5,440 |
| | 70 | 15,340 | | 3,760 | | |
| | 60 | 14,200 | | 3,230 | 3,220 | 4,270 |
| | 50 | 12,960 | 2,700 | | | |
| | 40 | 11,600 | 2,100 | 2,070 | 2,140 | 3,140 |
| | 30 | 10,040 | | | | |
| | 20 | 8,200 | 920 | 880 | | 2,080 |
| | 10 | 5,800 | | | | |
| | 0 | 500 | -50 | -20 | -10 | 930 |

NOTE: All strains are an average of three readings at each speed point.

TABLE 13-C. NASA 20-INCH SCALED FAN BLADE SPIN-PIT STRAIN GAUGE TEST DATA.

| Gauge No. 3 | | | Strain (Micro-Inches/Inch) | | | |
|---|---|---|---|---|---|---|
| | Percent Load | Speed RPM | Run 1 | Run 2 | Run 3 | Run 4 |
| ACCEL | 0 | 500 | 0 | 0 | 0 | 0 |
| | 10 | 5,800 | 220 | | | |
| | 20 | 8,200 | 450 | 390 | | 390 |
| | 30 | 10,040 | 680 | | | |
| | 40 | 11,600 | 910 | 850 | 840 | 840 |
| | 50 | 12,960 | 1,140 | | | |
| | 60 | 14,200 | 1,370 | 1,330 | 1,330 | 1,320 |
| | 70 | 15,340 | | 1,570 | | |
| | 80 | 16,400 | | 1,830 | 1,840 | 1,830 |
| | 90 | 17,400 | | | 2,100 | 2,110 |
| | 100 | 18,330 | | | 2,340 | 2,350 |
| | 148 | 22,300 | | | | 3,590 |
| DECEL | 100 | 18,330 | | | | 2,240 |
| | 90 | 17,400 | | | 2,060 | 1,940 |
| | 80 | 16,400 | | | 1,790 | 1,690 |
| | 70 | 15,340 | | 1,550 | | |
| | 60 | 14,200 | | 1,310 | 1,300 | 1,120 |
| | 50 | 12,960 | 1,110 | | | |
| | 40 | 11,600 | 940 | 840 | 790 | 600 |
| | 30 | 10,040 | | | | |
| | 20 | 8,200 | 430 | 320 | | 110 |
| | 10 | 5,800 | | | | |
| | 0 | 500 | -20 | 0 | -20 | -40 |

NOTE: All strains are an average of three readings at each speed point.

TABLE 13-D. NASA 20-INCH SCALED FAN BLADE SPIN-PIT STRAIN GAUGE TEST DATA.

| Gauge No. 4 | | | Strain (Micro-Inches/Inch) | | | |
|---|---|---|---|---|---|---|
| | Percent Load | Speed RPM | Run 1 | Run 2 | Run 3 | Run 4 |
| ACCEL | 0 | 500 | 0 | 0 | GAUGE OUT | GAUGE OUT |
| | 10 | 5,800 | 250 | | | |
| | 20 | 8,200 | 560 | 590 | | |
| | 30 | 10,040 | 860 | | | |
| | 40 | 11,600 | 1,160 | 1,220 | | |
| | 50 | 12,960 | 1,450 | | | |
| | 60 | 14,200 | 1,740 | 1,820 | | |
| | 70 | 15,340 | | 2,130 | | |
| | 80 | 16,400 | | 2,450 | | |
| | 90 | 17,400 | | | | |
| | 100 | 18,330 | | | | |
| | 148 | 22,300 | | | | |
| DECEL | 100 | 18,330 | | | GAUGE OUT | GAUGE OUT |
| | 90 | 17,400 | | | | |
| | 80 | 16,400 | | | | |
| | 70 | 15,340 | | 2,120 | | |
| | 60 | 14,200 | | 1,810 | | |
| | 50 | 12,960 | 1,410 | | | |
| | 40 | 11,600 | 1,160 | 1,240 | | |
| | 30 | 10,040 | | | | |
| | 20 | 8,200 | 560 | 610 | | |
| | 10 | 5,800 | | | | |
| | 0 | 500 | -100 | -40 | | |

NOTE: All strains are an average of three readings at each speed point.

TABLE 13-E. NASA 20-INCH SCALED FAN BLADE SPIN-PIT STRAIN GAUGE TEST DATA.

| | Gauge No. 5 | | Strain (Micro-Inches/Inch) | | | |
|---|---|---|---|---|---|---|
| | Percent Load | Speed RPM | Run 1 | Run 2 | Run 3 | Run 4 |
| ACCEL | 0 | 500 | 0 | 0 | 0 | 90 |
| | 10 | 5,800 | 110 | | | |
| | 20 | 8,200 | 210 | 200 | | 320 |
| | 30 | 10,040 | 320 | | | |
| | 40 | 11,600 | 420 | 400 | 390 | 460 |
| | 50 | 12,960 | 510 | | | |
| | 60 | 14,200 | 610 | 600 | 600 | 680 |
| | 70 | 15,340 | | 690 | | |
| | 80 | 16,400 | | 790 | 790 | 900 |
| | 90 | 17,400 | | | 900 | 1,000 |
| | 100 | 18,330 | | | 1,000 | 1,070 |
| | 148 | 22,300 | | | | 1,480 |
| DECEL | 100 | 18,330 | | | | 1,050 |
| | 90 | 17,400 | | | 880 | 920 |
| | 80 | 16,400 | | | 780 | 890 |
| | 70 | 15,340 | | 690 | | |
| | 60 | 14,200 | | 580 | 620 | 660 |
| | 50 | 12,960 | 500 | | | |
| | 40 | 11,600 | 400 | 390 | 410 | 500 |
| | 30 | 10,040 | | | | |
| | 20 | 8,200 | 210 | 190 | | 350 |
| | 10 | 5,800 | | | | |
| | 0 | 500 | 0 | 0 | 10 | 120 |

NOTE: All strains are an average of three readings at each speed point.

TABLE 13-F. NASA 20-INCH SCALED FAN BLADE SPIN-PIT STRAIN GAUGE TEST DATA.

| Gauge No. 6 | | | Strain (Micro-Inches/Inch) | | | |
|---|---|---|---|---|---|---|
| | Percent Load | Speed RPM | Run 1 | Run 2 | Run 3 | Run 4 |
| ACCEL | 0 | 500 | 0 | 0 | 0 | 30 |
| | 10 | 5,800 | 100 | | | |
| | 20 | 8,200 | 220 | 200 | | 250 |
| | 30 | 10,040 | 320 | | | |
| | 40 | 11,600 | 430 | 410 | 410 | 450 |
| | 50 | 12,960 | 530 | | | |
| | 60 | 14,200 | 630 | 600 | 620 | 640 |
| | 70 | 15,340 | | 700 | | |
| | 80 | 16,400 | | 800 | 810 | 840 |
| | 90 | 17,400 | | | 910 | 940 |
| | 100 | 18,330 | | | 1,010 | 1,030 |
| | 148 | 22,300 | | | | 1,450 |
| DECEL | 100 | 18,330 | | | | 1,030 |
| | 90 | 17,400 | | | 910 | 940 |
| | 80 | 16,400 | | | 810 | 850 |
| | 70 | 15,340 | | 680 | | |
| | 60 | 14,200 | | 590 | 650 | 660 |
| | 50 | 12,960 | 520 | | | |
| | 40 | 11,600 | 440 | 430 | 460 | 470 |
| | 30 | 10,040 | | | | |
| | 20 | 8,200 | 250 | 240 | | 290 |
| | 10 | 5,800 | | | | |
| | 0 | 500 | 10 | 0 | 20 | 40 |

NOTE: All strains are an average of three readings at each speed point.

TABLE 13-G. NASA 20-INCH SCALED FAN BLADE SPIN-PIT STRAIN GAUGE TEST DATA.

| Gauge No. 7 | | | Strain (Micro-Inches/Inch) | | | |
|---|---|---|---|---|---|---|
| | Percent Load | Speed RPM | Run 1 | Run 2 | Run 3 | Run 4 |
| ACCEL | 0 | 500 | 0 | 0 | 0 | 10 |
| | 10 | 5,800 | 10 | | | |
| | 20 | 8,200 | 40 | 30 | | 50 |
| | 30 | 10,040 | 70 | | | |
| | 40 | 11,600 | 90 | 80 | 80 | 100 |
| | 50 | 12,960 | 120 | | | |
| | 60 | 14,200 | 150 | 120 | 130 | 150 |
| | 70 | 15,340 | | 150 | | |
| | 80 | 16,400 | | 180 | 190 | 200 |
| | 90 | 17,400 | | | 220 | 230 |
| | 100 | 18,330 | | | 250 | 260 |
| | 148 | 22,300 | | | | 400 |
| DECEL | 100 | 18,330 | | | | 260 |
| | 90 | 17,400 | | | 230 | 240 |
| | 80 | 16,400 | | | 200 | 210 |
| | 70 | 15,340 | | 160 | | |
| | 60 | 14,200 | | 130 | 160 | 160 |
| | 50 | 12,960 | 120 | | | |
| | 40 | 11,600 | 100 | 90 | 110 | 130 |
| | 30 | 10,040 | | | | |
| | 20 | 8,200 | 60 | 50 | | 80 |
| | 10 | 5,800 | | | | |
| | 0 | 500 | 0 | 0 | 10 | 20 |

NOTE: All strains are an average of three readings at each speed point.

TABLE 13-H. NASA 20-INCH SCALED FAN BLADE SPIN-PIT STRAIN GAUGE TEST DATA.

| | Gauge No. 8 | | Strain (Micro-Inches/Inch) | | | |
|---|---|---|---|---|---|---|
| | Percent Load | Speed RPM | Run 1 | Run 2 | Run 3 | Run 4 |
| ACCEL | 0 | 500 | 0 | 0 | 0 | 0 |
| | 10 | 5,800 | 10 | | | |
| | 20 | 8,200 | 20 | 10 | | 20 |
| | 30 | 10,040 | 40 | | | |
| | 40 | 11,600 | 60 | 40 | 50 | 80 |
| | 50 | 12,960 | 80 | | | |
| | 60 | 14,200 | 100 | 80 | 90 | 90 |
| | 70 | 15,340 | | 100 | | |
| | 80 | 16,400 | | 120 | 140 | 140 |
| | 90 | 17,400 | | | 170 | 160 |
| | 100 | 18,330 | | | 200 | 190 |
| | 148 | 22,300 | | | | 320 |
| DECEL | 100 | 18,330 | | | | 220 |
| | 90 | 17,400 | | | 180 | 200 |
| | 80 | 16,400 | | | 150 | 170 |
| | 70 | 15,340 | | 120 | | |
| | 60 | 14,200 | | 110 | 140 | 140 |
| | 50 | 12,960 | 90 | | | |
| | 40 | 11,600 | 90 | 80 | 110 | 110 |
| | 30 | 10,040 | | | | |
| | 20 | 8,200 | 60 | 50 | | 80 |
| | 10 | 5,800 | | | | |
| | 0 | 500 | 10 | 0 | 30 | 30 |

NOTE: All strains are an average of three readings at each speed point.

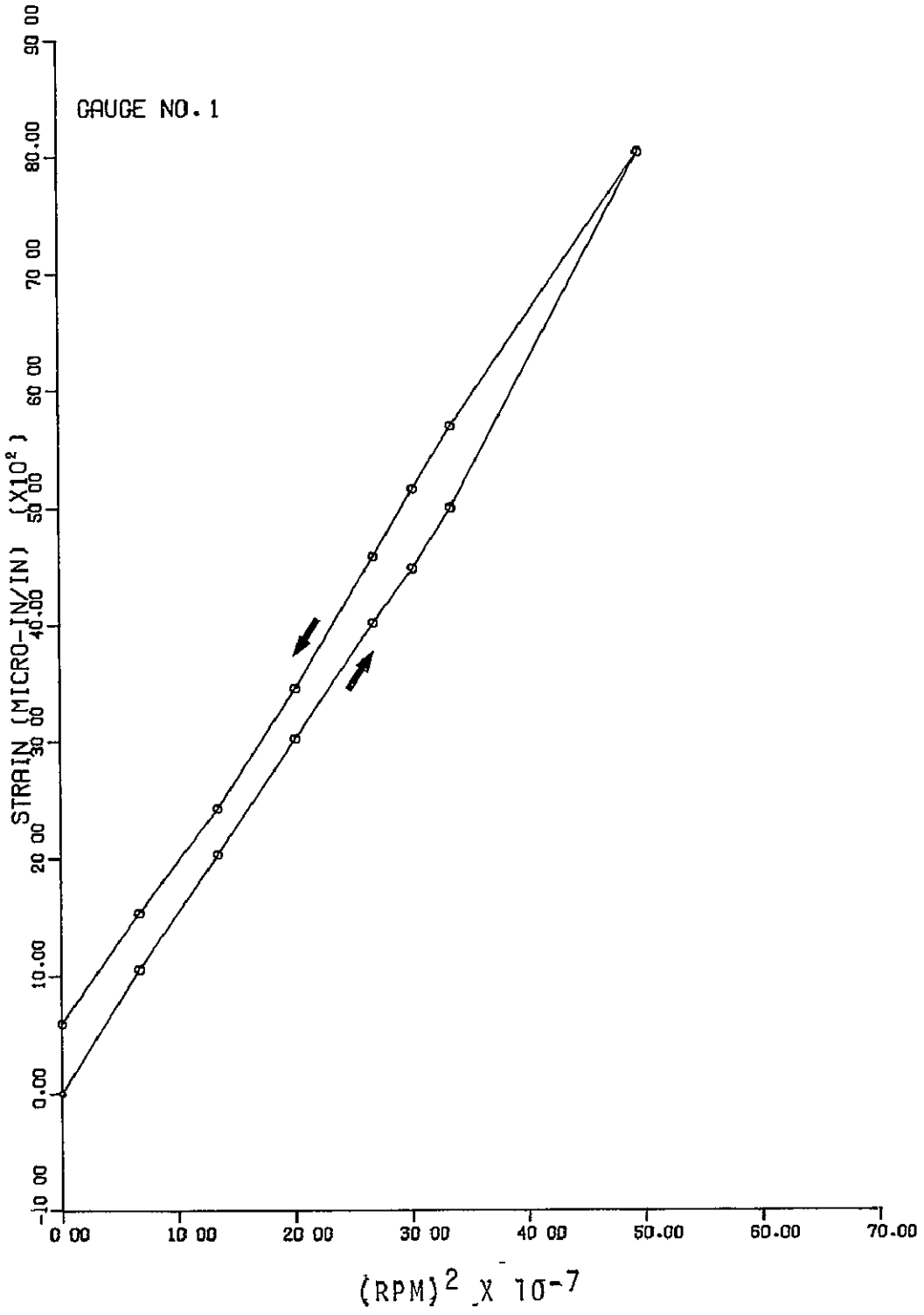


Figure 43. Spin-Pit Strain Gauge Test of NASA 20-Inch Scaled Fan Blade.

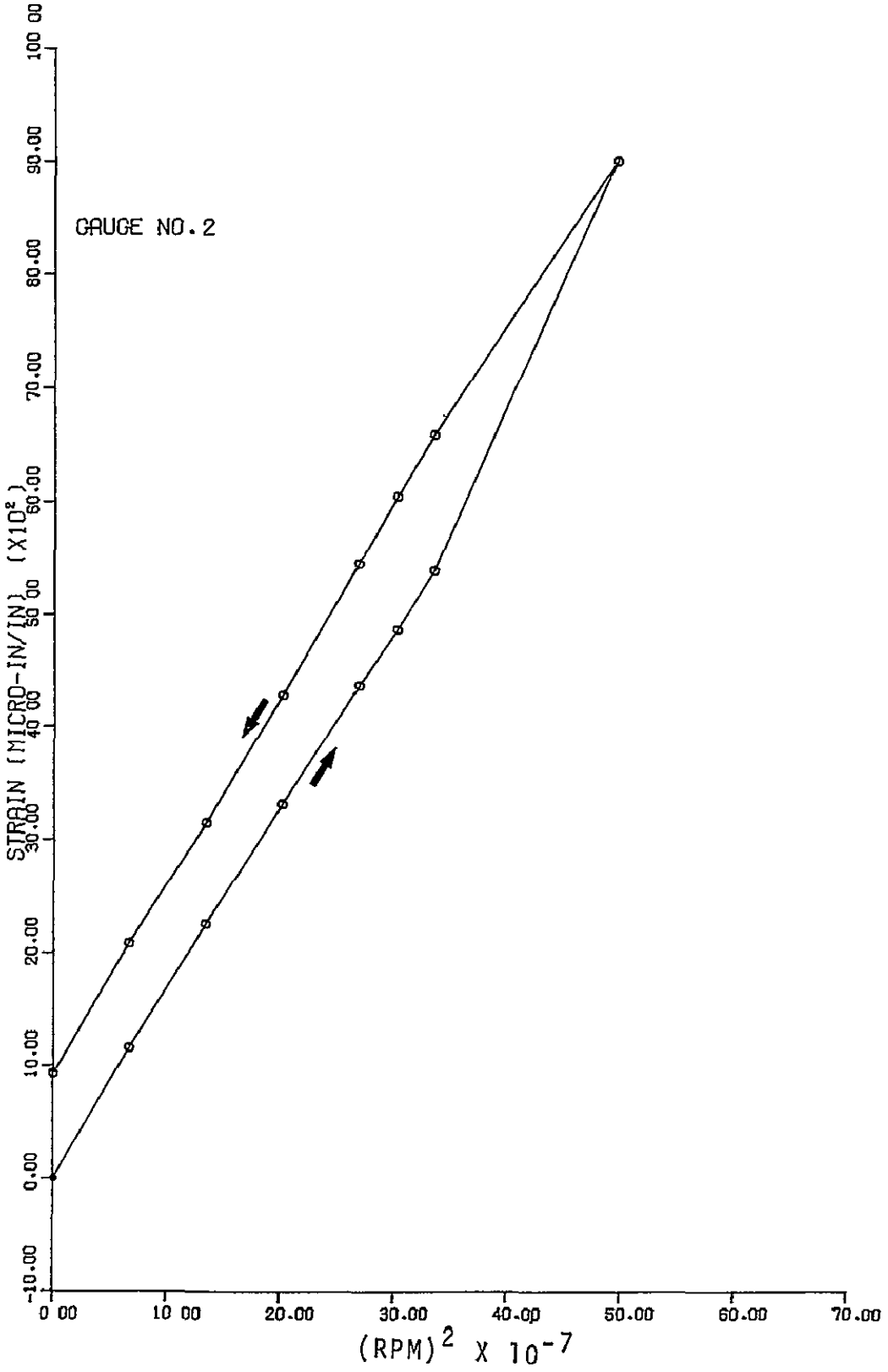


Figure 44. Spin-Pit Strain Gauge Test of NASA 20-Inch Scaled Fan Blade.

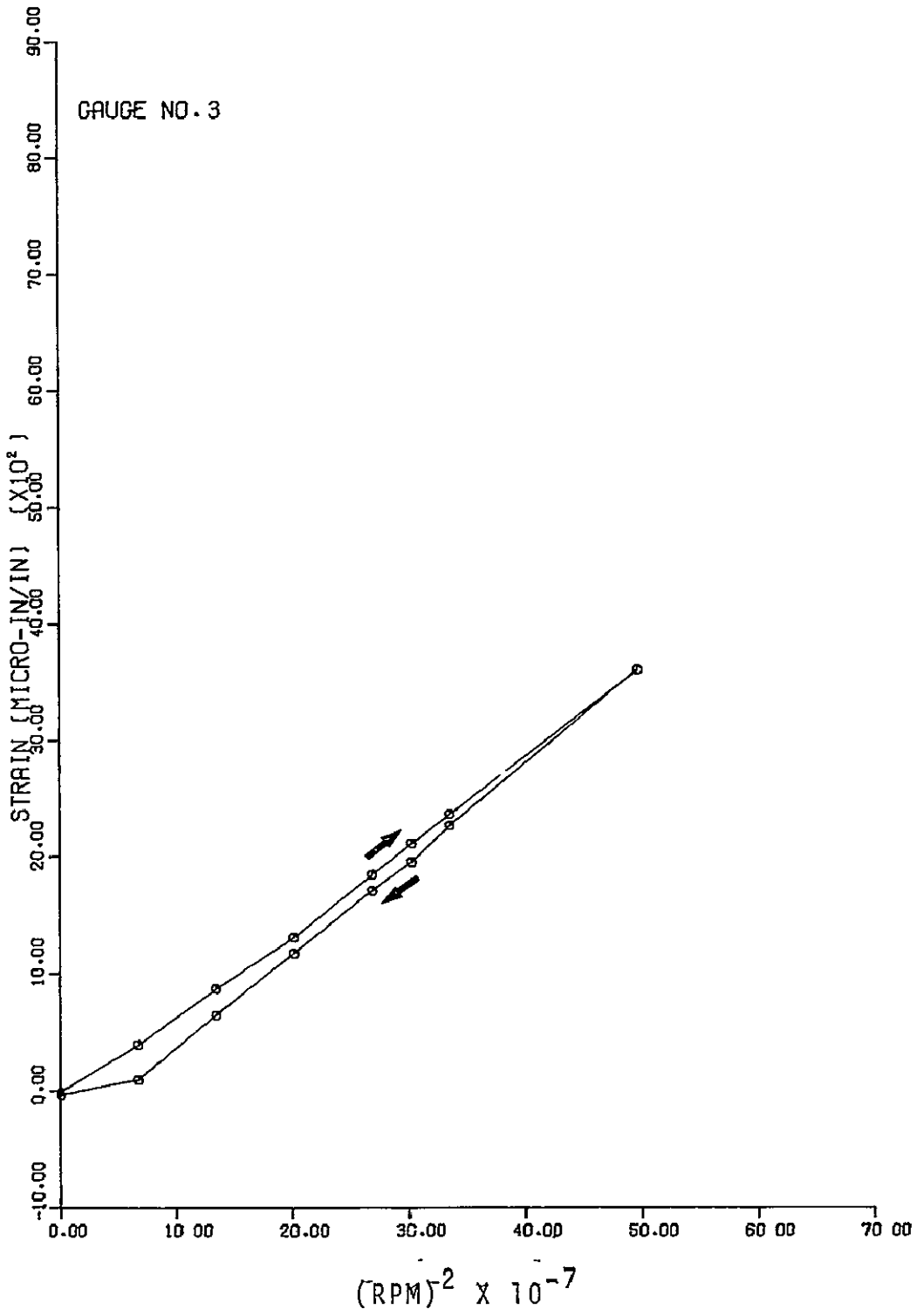


Figure 45. Spin-Pit Strain Gauge Test of NASA 20-Inch Scaled Fan Blade.

The stress distributions shown in Figure 1 were obtained using a finite-element model that relies on constant-thickness, triangular elements. It is likely that an improved stress distribution could be obtained using more powerful finite-element techniques. A variable thickness, three-dimensional finite-element program is now available and presumably would furnish more accurate results.

For the test configuration, assuming nominal properties, the yield strength corresponds to uniaxial strain between 8000 and 8200 micro-inches/inch. The maximum strain recorded in the testing was nearly 9000 micro-inches/inch, which is consistent with the observation of yield.

There is no evidence of yielding at 100-percent speed. Strain gauges at the leading-edge root (pressure and suction sides) showed clear indications of yielding following testing at 122-percent speed. The stress distribution shown in Figure 1 evidently overstates blade resistance to yield. The observation of yielding is consistent with measured strain data, assuming nominal material properties.

For the spin-pit test conducted at AiResearch, it was necessary to array the strain gauge leads at the back face of the disk, and route them through the disk center hole to the front face, as shown in Figure 36. However, for the NASA facility, it was necessary to route the leads to the front face of the disk through three holes that are configured to match a NASA terminal plate located within the disk pilot ring. Figures 46 and 47 show the final disk configuration with the strain gauge leads rerouted as required for the NASA test facility.

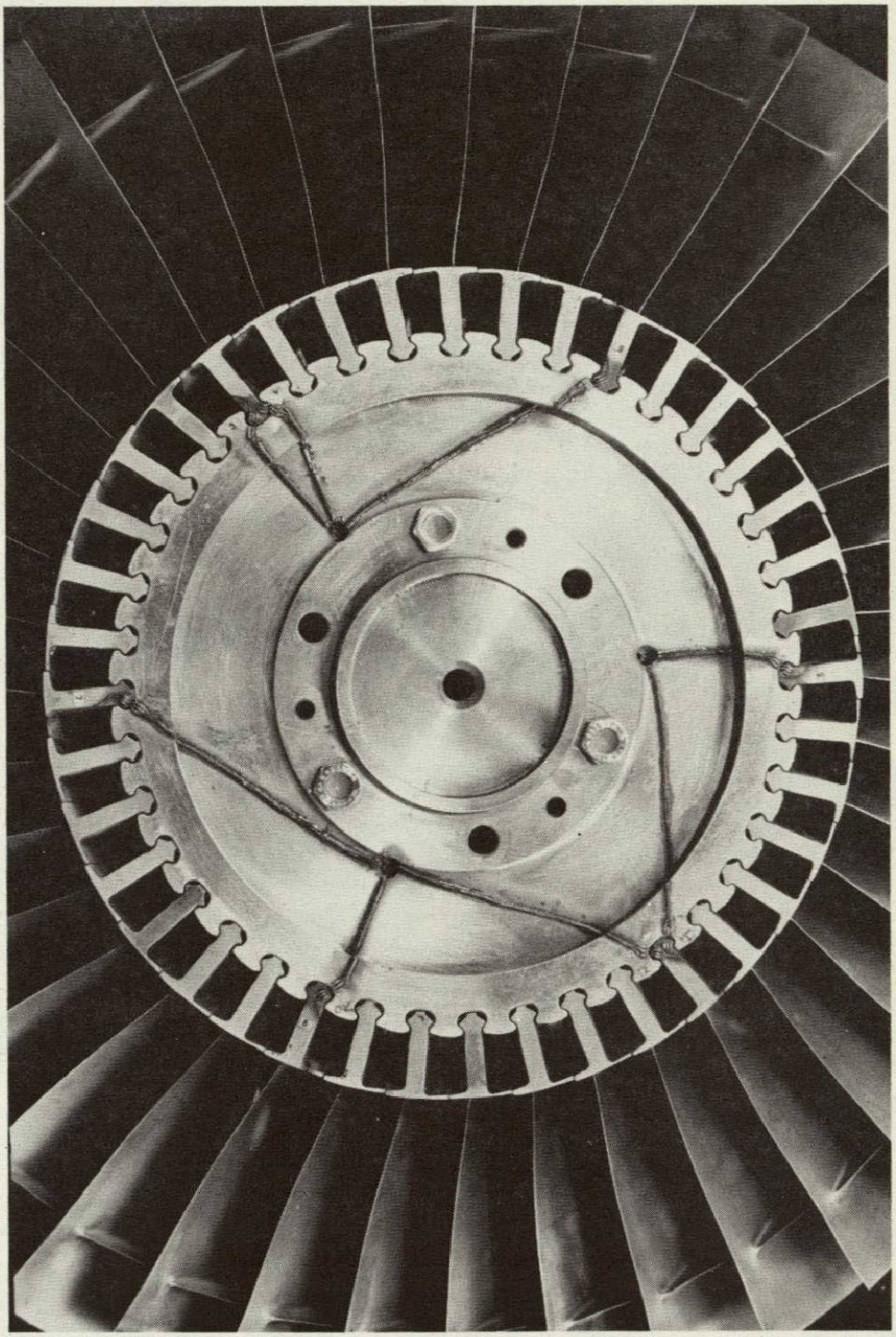

Figure 46. Aft Side of the 20-Inch Fan Assembly With Strain Gauge Leads Routed for NASA Tests.

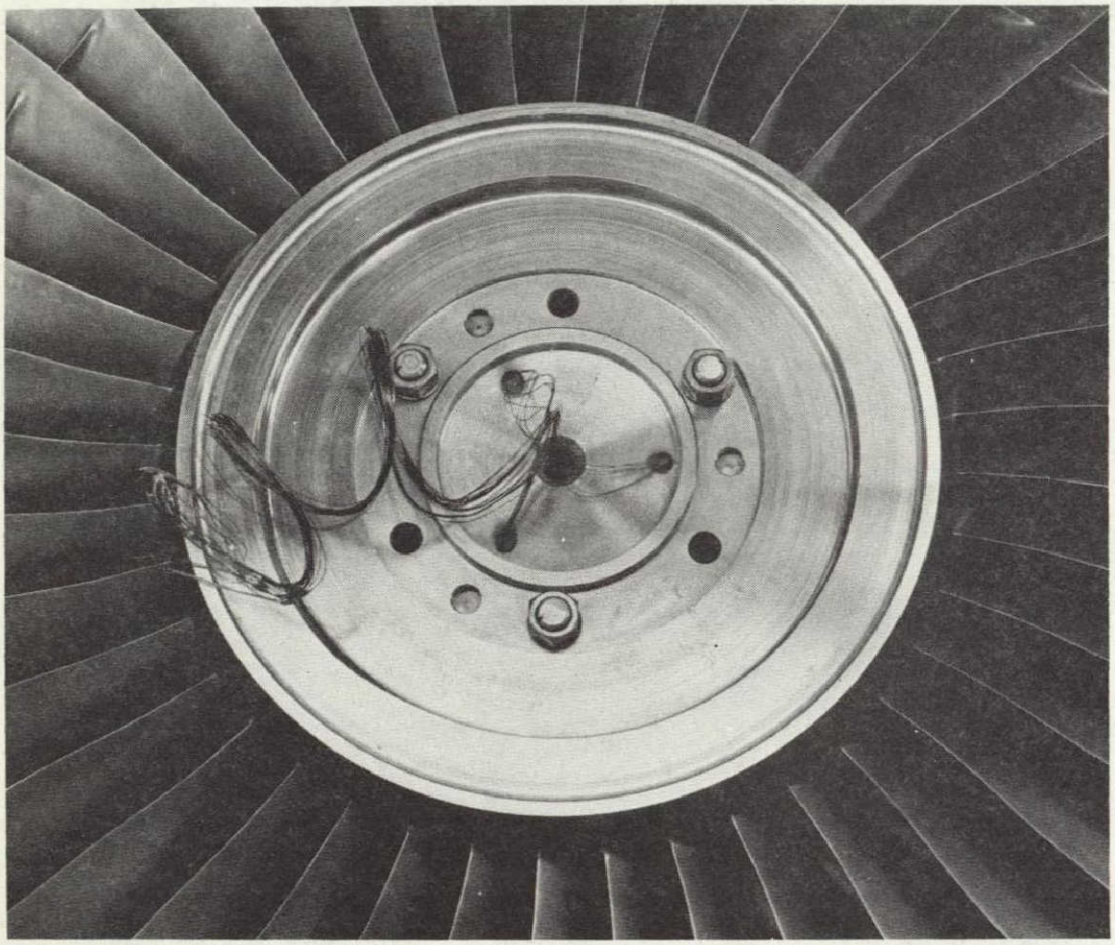

Figure 47. Front Side of 20-Inch Fan Assembly With Strain Gauge Leads Routed for NASA Tests.

## POTENTIAL BENEFITS AND PENALTIES

An assessment was made of the potential benefits and penalties associated with this type of fan in a turbofan engine. The assessment was made in terms of efficiency, weight, and cost, as discussed below.

In order to provide a basis for comparison, three fan types were examined. Engine cycle analyses were performed with each fan type in conjunction with a common-core engine, and low-pressure turbine sections appropriate to each fan type were assessed. Since the principal benefits and penalties were expected to be associated only with the fan and low-pressure turbine components, no attempt was made to evaluate second order effects on other areas of the engine. Therefore, minor changes to shafts, housings, frames and sheet metal due to differences in speed, torque, thrust, pressure, etc. were not considered. The results of the assessment are given in Tables 14, 15, and 16.

Table 14 summarizes the pertinent performance parameters for the three fan and low-pressure turbine components used in the analyses. As shown, it was assumed that all three fans were 0.508 meter (20 inches) in diameter. However, flow rates and efficiencies were consistent with current technology components. Similarly, the performance parameters for the low-pressure turbines were based on current practice. The slight improvement in low-pressure turbine efficiency with increasing numbers of stages is indicative of the effect of interstage reheating. Thus, it appears that the effects of efficiencies are no more significant with the high-tip-speed fan than with a low-tip-speed fan.

Table 15 presents the weights estimated for the fan and low-pressure rotors. Weights of shafts, seals, bearings, and the fan stator are not included. However, the weights of the low-pressure turbine are included since they form a significant portion of the low-pressure turbine section weight. As shown in Table 15, the principal effects of increased fan speed are that, as speed increases, the fan section weight increases due primarily to the disk stresses, while the low-pressure turbine weight decreases due primarily to the number of stages required to drive the fan. The net effect for the cases analyzed is that the high-speed assembly is slightly lighter weight than the lower-speed assemblies; however, it is again noted that a detailed analysis that includes all affected components would be necessary to confirm this finding.

TABLE 14. 20-INCH FAN PERFORMANCE PARAMETERS FOR PENALTIES AND BENEFITS ANALYSIS.

| Parameter | Fan Designation | | |
|---|---|---|---|
| | A | B | C |
| Fan diameter (meter) | 0.508 | 0.508 | 0.508 |
| Fan tip speed (meter/second) | 309.7 | 372.5 | 487.7 |
| Fan speed (rpm) | 11,643 | 14,003 | 18,335 |
| Fan corrected flow (kg/s) | 34.40 | 31.38 | 32.76 |
| Fan pressure ratio | 1.50 | 1.50 | 1.50 |
| Fan efficiency | 0.879 | 0.877 | 0.880 |
| LP turbine stages | 5 | 3 | 2 |
| LP turbine pressure ratio | 3.713 | 3.713 | 3.704 |
| LP turbine efficiency | 0.892 | 0.890 | 0.887 |

TABLE 15. 20-INCH FAN ESTIMATED COMPONENT WEIGHTS FOR PENALTIES AND BENEFITS ANALYSIS.

| Parameter | Fan Designation | | |
|---|---|---|---|
| | A | B | C |
| Fan: | | | |
| Blade weight (kg) | 5.79 | 5.78 | 5.26 |
| Disk weight (kg) | 2.54 | 3.58 | 6.67 |
| Assembly weight (kg) | 8.33 | 9.36 | 11.93 |
| Low Pressure Turbine: | | | |
| Blade weight (kg) | 6.74 | 5.42 | 4.46 |
| Disk weight (kg) | 12.92 | 11.09 | 9.68 |
| Stator weight (kg) | 5.86 | 4.67 | 3.80 |
| Assembly weight (kg) | 25.52 | 21.18 | 17.94 |
| Total | 33.85 | 30.54 | 29.87 |

TABLE 16. 20-INCH FAN PENALTIES AND BENEFITS ANALYSIS COST FACTORS.

| Parameter | Fan Designation | | |
|---|---|---|---|
| | A | B | C |
| Fan: | | | |
| Rotor blades | 30 | 30 | 40 |
| Stator vanes: Bypass | 67 | 71 | 89 |
| Core | 53 | 67 | 71 |
| Assembly weight (kg) | 8.33 | 9.36 | 11.93 |
| Relative cost | Lowest | → | Highest |
| Low Pressure Turbine: | | | |
| Stages | 5 | 3 | 2 |
| Total rotor blades | 408 | 171 | 88 |
| Total stator vanes | 394 | 147 | 72 |
| Assembly weight (kg) | 25.52 | 21.18 | 17.94 |
| Relative cost | Highest | ← | Lowest |

Table 16 summarizes the principal cost factors associated with the three fans examined. As indicated, the relative costs of the fans are primarily related to the fan assembly weight that is mainly influenced by the requirement for a heavier fan disk. The fan disk weight is, in turn,a function of the higher stress level that results from the higher fan tip speed. The relative costs of the low-pressure turbines is primarily a function of the number of pieces involved in the total assembly. The far greater number of rotor blades and nozzle vanes required for the lower-speed, five-stage turbine will obviously result in a markedly higher cost for that component, and it can be expected that the total engine relative cost will also be higher for the low-speed fan configuration as a result of the higher turbine cost.

It may be noted that component diameter did not enter into the weight or cost analyses. Since the fans were all 0.508 meter in diameter, and the turbine inlet and exit areas were approximately equal, the effects of diameter on weight and cost were insignificant.

In summary, for the three configurations analyzed, it is concluded that no major performance or weight penalties (or benefits) to a turbofan engine would result from the selection of any of the fan types. However, it appears that a significant cost benefit would result from the selection of a high-speed fan over a lower-speed fan. It does not appear, however, that, given the selection among various high-speed fan configurations, any appreciable performance, weight,or cost penalties or benefits would result.

# APPENDIX A
# STRESS MEASUREMENT PLAN
# STRAIN GAUGE TEST PROGRAM FOR THE NASA FAN

## INTRODUCTION

The objective of this test is to determine if any detrimental vibration occurs in the fan blades or stator vanes in the operating range of the NASA test rig. Specifically, flutter conditions in the fan blade are of primary concern based on the low margin on torsional flutter that exists.

## TEST INSTRUMENTATION

The fan rotor will be strain gauged as shown on the map in Figure 48. Eight strain gauges are recommended to provide redundancy, and to map strain response at critical areas in the blades. Eight strain gauges will be required on the stator vanes to determine their response characteristics (Figure 49).

The rotor and stator strain gauges must be capable of operating at a temperature of 300°F. Dynamic strain only will be monitored and should be either recorded on tape or analyzed on line, such that the frequency and strain response versus speed can be obtained.

The strain gauges will be installed on the fan rotor following balancing and spin testing. The gauge locations and orientation have been established to minimize the fan unbalance. Strain gauge lead wire will be terminated at the disk bore. The stator vanes will have 4 to 6 feet of loose lead wire remaining in the stator assembly.

The strain gauge type will be FAB12-35 with a gauge factor of approximately 2.0. Specific gauge factors will be noted at time of strain gauging.

| GAUGE NO. | BLADE* | SIDE |
|---|---|---|
| 1 | A | PRESSURE |
| 2 | A | SUCTION |
| 3 | D | PRESSURE |
| 4 | D | SUCTION |
| 5 | B | PRESSURE |
| 6 | C | PRESSURE |
| 7 | E | PRESSURE |
| 8 | F | PRESSURE |

MATERIAL 90T1-6A1-4V

*REFER TO FIGURE 36 FOR BLADE LOCATIONS.

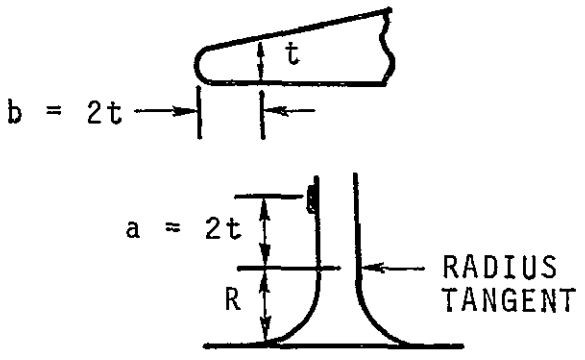


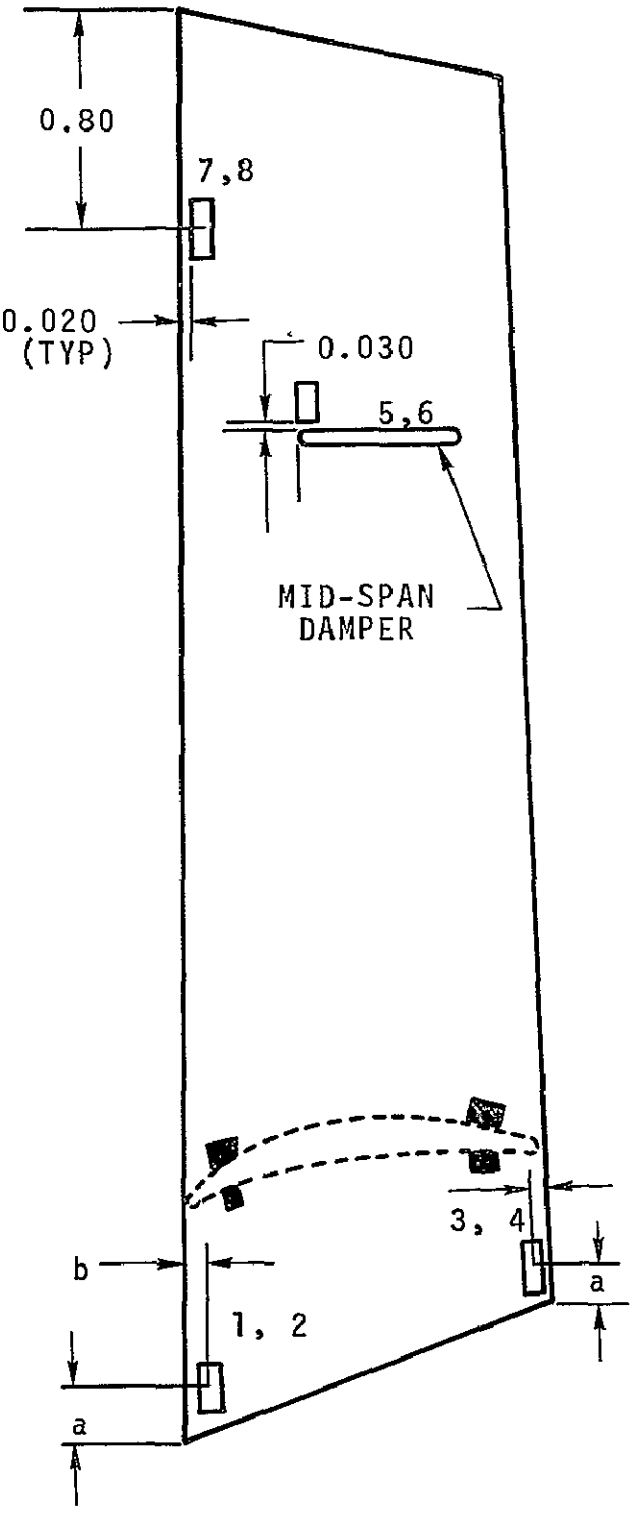


Figure 48. NASA 20-Inch Scaled Fan Blade Strain Gauge Locations.

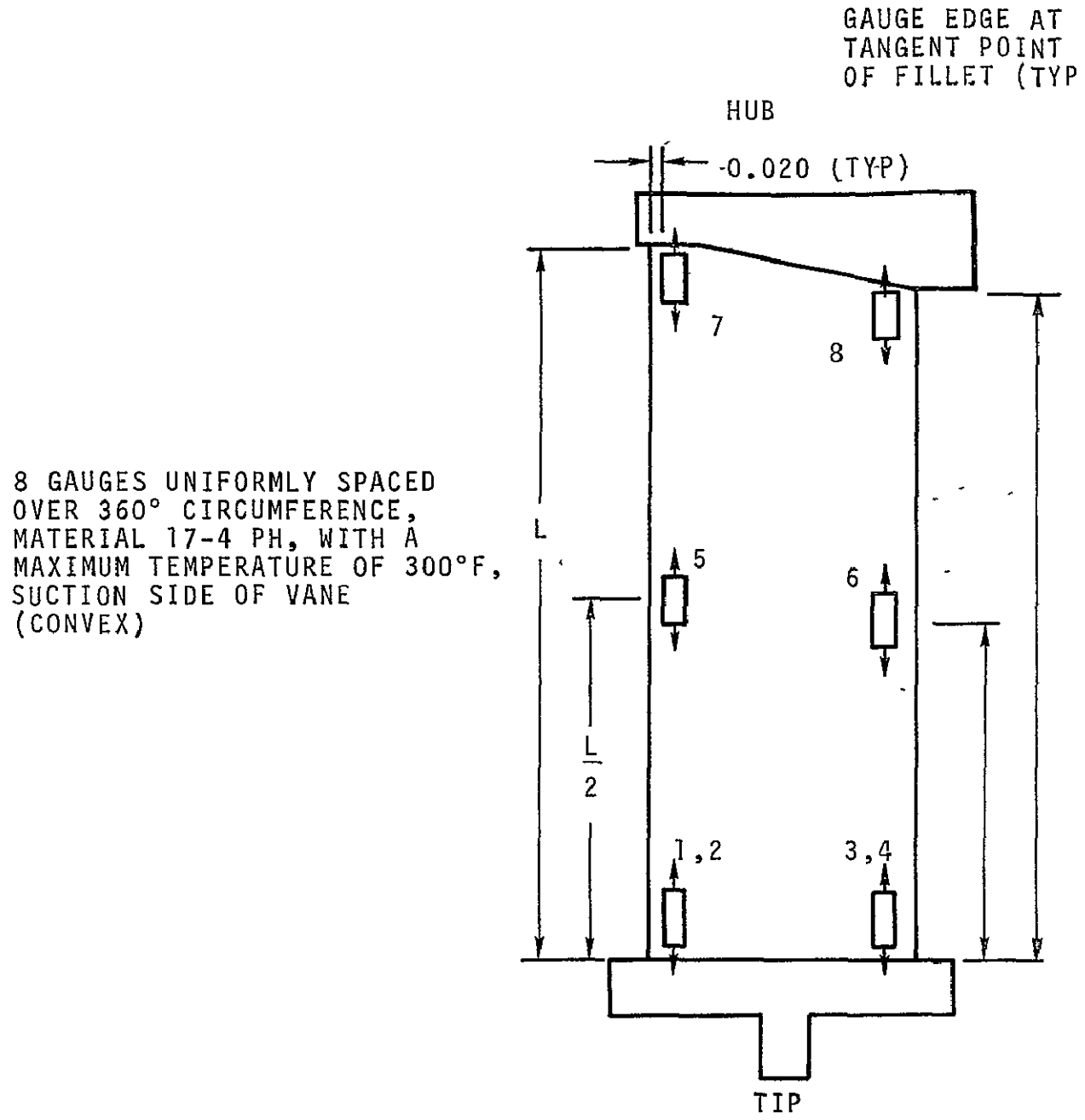


Figure 49. NASA 20-Inch Scaled Fan Stator Vane Strain Gauge Locations.

## RECOMMENDED TEST PROCEDURE

It is recommended that the strain gauges be monitored during the initial running and mechanical checkout of the rig. The fan rotor strain gauge limits should be 2000 microstrain peak-to-peak for mechanical interference (integer order numbers of rotor speed) for transient conditions, and 500 microstrain for forced vibration at steady-state dwell periods. It is recommended that no dwell time be spent while at resonance. Near 100-percent speed, the vibration response should be monitored with particular attention to 18kHz frequencies. If this frequency response occurs and persists independent of speed change (does not follow an integer order of rotor speed), it is indicative of flutter and should be limited to 500 microstrain. The interference diagram in Figure 50 shows the calculated natural frequencies for the fan blade and can be used as a guideline for expected areas of response during testing.

The stator vane vibration should be limited to 1000 microstrain transient response (no dwell) and 500 microstrain forced vibration (not at resonant point). The predominant response in stator vanes is generally due to the rotor wake passing frequency. Higher modes can be excited with significant response at the wake energy levels associated with the higher speed energy levels. It is recommended that no dwell time be spent at any resonant response points.

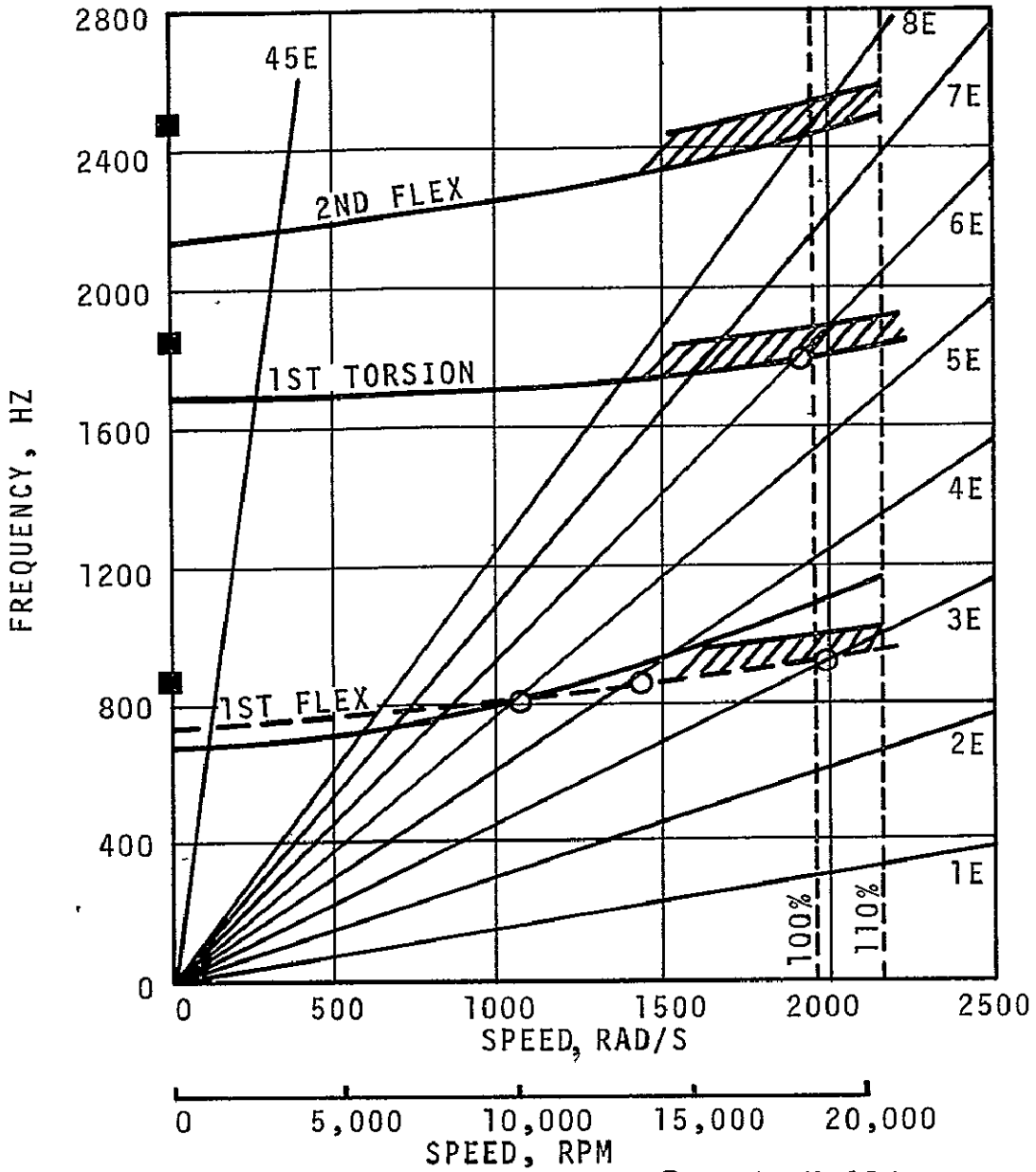


■ SALT PATTERN FROM FULL SCALE BLADE P/N X2401068 SCALED DOWN TO P/N 3550842 SIZE MID-SPAN DAMPERS FULLY CONSTRAINED

○ RIG STRAIN-GAUGE DATA, SCALED FROM FULL SIZE BLADE

——— CALCULATED, MID-SPAN CONSTRAINED WITH SPRINGS, $K_x = 4.0 \times 10^2$ N/M ($3.5 \times 10^3$ LB/IN), $K_y = 4.0 \times 10^4$ N/M ($3.5 \times 10^5$ LB/INCH)

– – – – ADJUSTED FROM RIG STRAIN-GAUGE TEST

▨ TOLERANCE EFFECT

Figure 50. NASA 20-Inch Fan Blade Interference Diagram.

# REFERENCES

1. Erwin, J. R., N. G. Vitale, T. C. Ware, and L. C. Wright, "High-Tip-Speed, Low-Loading Transonic Fan Stage (Part I - Aerodynamic and Mechanical Design)," NASA CR-121095, AiResearch Report 72-8421, April 1973.

2. Jackson, R. J., R. J. Kobayashi, and T. C. Ware, "High-Tip-Speed, Low-Loading Transonic Fan Stage (Final Report)," NASA CR-121263, AiResearch Report 73-9488, February 1974.